

MAY 2020

Ph.D. in Mechanical Engineering

AHMET ŞUMNU

**REPUBLIC OF TURKEY
GAZİANTEP UNIVERSITY
GRADUATE SCHOOL OF NATURAL & APPLIED SCIENCES**

AERODYNAMIC SHAPE OPTIMIZATION FOR MISSILE

**Ph.D. THESIS
IN
MECHANICAL ENGINEERING**

**BY
AHMET ŞUMNU
MAY 2020**

AERODYNAMIC SHAPE OPTIMIZATION FOR MISSILE

Ph.D. Thesis

in

Mechanical Engineering

Gaziantep University

Supervisor

Prof. Dr. İbrahim Halil GÜZELBEY

by

Ahmet ŞUMNU

May 2020



©2020[Ahmet ŞUMNU]

REPUBLIC OF TURKEY
GAZIANTEP UNIVERSITY
GRADUATE SCHOOL OF NATURAL & APPLIED SCIENCES
MECHANICAL ENGINEERING

Name of the Thesis : Aerodynamic Shape Optimization for Missile

Name of the Student : Ahmet ŞUMNU

Exam Date : 08.05.2020

Approval of the Graduate School of Natural and Applied Sciences

Prof. Dr. A. Necmeddin YAZICI
Director

I certify that this thesis satisfies all the requirements as a thesis for the degree of Doctor of Philosophy.

Prof. Dr. Melda ÇARPINLIOĞLU
Head of Department

This is to certify that we have read this thesis and that in our consensus opinion it is fully adequate, in scope and quality, as a thesis for the degree of Doctor of Philosophy.

Prof. Dr. İbrahim Halil GÜZELBEY
Supervisor

Examining Committee Members

Signature

Prof. Dr. Naki TÛTÛNCÛ

.....

Prof. Dr. Selçuk MISTIKOĞLU

.....

Prof. Dr. İbrahim Halil GÜZELBEY

.....

Prof. Dr. Abdulkadir ÇEVİK

.....

Assoc. Prof. Dr. Emrah ÖZAHİ

.....

I hereby declare that all information in this document has been obtained and presented in accordance with academic rules and ethical conduct. I also declare that, as required by these rules and conduct, I have fully cited and referenced all material and results that are not original to this work.

Ahmet ŞUMNU

ABSTRACT

AERODYNAMIC SHAPE OPTIMIZATION FOR MISSILE

ŞUMNU, Ahmet

Ph.D. in Mechanical Engineering

Supervisor: Prof. Dr. İbrahim Halil GÜZELBEY

May 2020

106 pages

In this study, aerodynamic shape optimization is performed to improve the aerodynamic performance by changing the missile external geometry and the effects of the shape optimization on the missile performance are investigated at supersonic speeds. The N1G missile model shape variation is numerically investigated to decrease its aerodynamic drag and increase its aerodynamic lift under determined constraints. Missile geometry was selected from previous study which contains experimental results. Missile aerodynamic coefficients prediction is performed using SST $k-\omega$, Realizable $k-\epsilon$ and Spalart-Allmaras turbulence models at supersonic Mach numbers and at 4° and 6° angles of attack. The prediction results of aerodynamic coefficients are in good agreement with each other for selected missile geometry. In the beginning of the optimization process, the missile body and fin parameters need to be estimated in order to design optimum missile geometry. Lift and drag coefficients are considered as objective functions. Input (design variables) and output (objective functions) parameters are collected to obtain design points. Multi-Objective Genetic Algorithm (MOGA) is used to optimize missile geometry. Nose, main body and tailfins are improved to find optimum missile model. The optimization results show that the aerodynamic performance of missile is improved about 11-17 per cent at specified Mach numbers and angles of attack.

Key Words: Shape Optimization, Missile Aerodynamic, Turbulence Models

ÖZET

FÜZE İÇİN AERODİNAMİK ŞEKİL OPTİMİZASYONU

ŞUMNU, Ahmet

Doktora Tezi, Makine Mühendisliği

Danışman: Prof. Dr. İbrahim Halil GÜZELBEY

Mayıs 2020

106 sayfa

Bu çalışmada, füze dış geometrisini değiştirerek aerodinamik performansı iyileştirmek ve süpersonik hızlarda şekil optimizasyonunun füze performansı üzerindeki etkilerini araştırmak için aerodinamik şekil optimizasyonu yapılmaktadır. Belirlenen kısıtlamalar altında aerodinamik sürükleme katsayısını azalmak ve aerodinamik kaldırma katsayısını artırmak için N1G füze modeli şekil değişimi sayısal olarak incelenmektedir. Füze geometrisi deneysel sonuçları olan bir çalışmadan seçilmiştir. Füze aerodinamik katsayılarının tahmini, 4° ve 6° hücum açılarında, süpersonik Mach sayılarında SST k- ω , Realizable k- ϵ ve Spalart-Allmaras türbülans modelleri kullanılarak gerçekleştirilmektedir. Seçilen füze geometrisi için aerodinamik katsayıların sonuçları birbiriyle eşleşmektedir. Optimizasyon işleminde, optimum füze geometrisi tasarlamak için füze gövdesinin ve kanat parametrelerinin belirlenmesi gerekir. Kaldırma ve sürükleme katsayıları objektif fonksiyon olarak belirlenmiştir. Tasarım noktaları elde etmek için girdi (tasarım değişkenleri) ve çıktı (objektif fonksiyonlar) parametreleri birleştirilir. Çok Amaçlı Genetik Algoritma (MOGA), füze geometrisini optimize etmek için kullanılmaktadır. Gövdenin ön kısmı ve ana gövde ve kuyruk yüzleri, optimum füze modelini bulmak üzere geliştirilmiştir. Optimizasyon sonuçları, füzenin aerodinamik performansının, belirtilen Mach sayıları ve hücum açılarında yaklaşık yüzde 11-17 oranında iyileştirildiğini göstermektedir.

Anahtar Kelimeler: Şekil Optimizasyonu, Füze Aerodinamiği, Türbülans Modelleri



“Dedicated to my Parents and fiancée”

ACKNOWLEDGEMENTS

I would like to thank my supervisor, Prof. Dr. İbrahim Halil GÜZELBEY for his guidance and support throughout the study. I am thankful for his encouragement and motivation. I would like to thank Asst. Prof. Dr. Orkun ÖĞÜCÜ who helped me with the optimization algorithm.

This work has been supported by the Scientific Research Projects Governing Unit of Gaziantep University (Project No. HUBF.17.04). I would like to thank the Scientific Research Projects Governing Unit for providing work station which was enormously important for this study.

Lastly, I would like to express my love and gratitude to my parents and fiancée for their support, always best wishes.

TABLE OF CONTENTS

	Page
ABSTRACT	v
ÖZET	vi
ACKNOWLEDGEMENTS	viii
TABLE OF CONTENTS	ix
LIST OF TABLES	xii
LIST OF FIGURES	xiii
LIST OF SYMBOLS	xvi
LIST OF ABBREVIATIONS	xix
CHAPTER I: INTRODUCTION	1
1.1. General Concept of Missile	1
1.2. Scope of Thesis	5
CHAPTER II: LITRATURE REVIEW	7
2.1. Missile Aerodynamics	7
2.1.1. Prediction of Aerodynamic Coefficients	7
2.2. Aerodynamic Shape Optimization	13
2.2.1. The Type of Evolutionary Algorithm Based Methods	13
2.2.2. Genetic Algorithm	14
2.2.3. Adjoint Method.....	19
2.2.4. Particle Swarm Optimization Method	21
2.2.5. Squential Quadratic Programming and Multidisciplinary Optimization	23
2.2.6. Decision of the Optimization Method	26
2.3. Motivation of the Study.....	26
CHAPTER III: MATERIAL AND METHOD	27
3.1. Introduction	27
3.2. Aerodynamic Background.....	28
3.2.1. Supersonic Flow	28
3.2.2. Viscous Interactions.....	29
3.2.3. Navier-Stokes Equations	29

3.2.4. Boundary Layer Equations	31
3.3. Computational Approach	32
3.3.1. CFD Software and Finite Volume Method.....	33
3.3.2. Fluent Software.....	36
3.3.3. Mesh Generation.....	37
3.3.4. Viscous Mesh Characteristic	37
3.3.5. Inviscid Mesh Characteristic	39
3.4. Mesh Generation of the Missile Geometry	39
3.5. Flow Solver	43
3.5.1. Turbulence Models	45
3.5.1.1. Spalart-Allmaras Turbulence Model.....	46
3.5.1.2. Standard and Realizable k- ϵ Turbulence Model.....	46
3.5.1.3. Standard and SST k- ω Turbulence Model	47
3.5.2. Setup and Solver Properties.....	48
3.6. Mesh Dependency/Sensitivity	49
3.7. Validation Study.....	53
CHAPTER IV: OPTIMIZATION.....	65
4.1. Definition of Optimization	65
4.1.1. Aerodynamic Shape Optimization.....	66
4.2. Definition of Genetic Algorithm	67
4.3. Multi-Objective Optimization Design.....	69
4.4. Multi-Objective Genetic Algorithm (MOGA)	70
4.5. Optimization Studies Using Ansys in DesignXplorer.....	70
4.5.1. Response Surface Optimization.....	71
4.5.1.1. Design Space.....	72
4.5.1.2. Design of Experiments.....	72
4.5.1.3. Response Surface	73
4.5.1.4. Optimization	73
4.5.2. Parameter Correlation.....	74
4.6. Case Studies for Missile Aerodynamic Shape Optimization	74

4.6.1. Objective Functions	75
4.6.2. Design Variables.....	75
4.6.3. Constraints	76
4.6.4. Optimization Algorithm	77
4.6.5. Optimization Problem Solution	78
4.6.6. Optimization Results	79
CHAPTER V: CONCLUSION.....	90
5.1. Recommendation for the Future Work.....	91
REFERENCES.....	92
CIRRICULUM VITAE (CV).....	104

LIST OF TABLES

	Page
Table 3.1 Differences between the experimental and numerical results	53
Table 4.1 Baseline, lower and upper values of the design variables	77
Table 4.2 Optimization results.....	79
Table 4.3 Optimum shape size at 1.4, 2, and 2.5 Mach number	80



LIST OF FIGURES

		Page
Figure 1.1	Major components of missile.....	2
Figure 1.2	Three main categories of missile flight controls	2
Figure 2.1	Crossover process.....	15
Figure 2.2	Sub-modules of EXCON.....	17
Figure 2.3	Range maximization system for a guided missile.....	17
Figure 2.4	Design cycle	20
Figure 2.5	Flowchart of PSO.....	22
Figure 2.6	Flowchart of evolutionary algorithm.....	23
Figure 3.1	Viscous shock layer.....	28
Figure 3.2	Effects of viscous interactions on boundary layer.....	29
Figure 3.3	Normal and shear stresses on a fluid elements.....	30
Figure 3.4	Thin boundary layer	32
Figure 3.5	Continuous and discrete domain.....	34
Figure 3.6	Control volume element	35
Figure 3.7	Viscous mesh for a missile body section.....	38
Figure 3.8	N1G missile configuration	40
Figure 3.9	N1G missile solid model.....	40
Figure 3.10	Three dimensional view of the fluid domain.....	41
Figure 3.11	Missile view in fluid domain.....	41
Figure 3.12	Mesh generation in fluid domain.....	42
Figure 3.13	Mesh generation on missile body.....	42
Figure 3.14	Mesh generation on missile tailfins.....	42
Figure 3.15	Solution methods.....	44
Figure 3.16	Solution controls.....	45
Figure 3.17	C_D and C_L values with respect to number of mesh elements for 1.4 Mach number.....	51
Figure 3.18	C_D and C_L values with respect to number of mesh elements for 2 Mach number.....	51

Figure 3.19	C_D and C_L values with respect to number of mesh elements for 2.5 Mach number.....	52
Figure 3.20	C_D and C_L values with respect to number of mesh elements for 4 Mach number.....	53
Figure 3.21	Drag coefficient versus Mach number at 4° AoA.....	54
Figure 3.22	Lift coefficient versus Mach number at 4° AoA.....	55
Figure 3.23	Drag coefficient versus Mach number at 6° AoA.....	55
Figure 3.24	Lift coefficient versus Mach number at 6° AoA.....	55
Figure 3.25	Lift to drag ratio versus AoA at supersonic Mach numbers.....	56
Figure 3.26	Pressure contour of baseline missile model at 4° AoA (a: 1.4 Ma, b: 2 Ma, c: 2.5 Ma, d: 4 Ma).....	58
Figure 3.27	Pressure contour of baseline missile model at 6° AoA (a: 1.4 Ma, b: 2 Ma, c: 2.5 Ma, d: 4 Ma).....	59
Figure 3.28	Pressure contour for 1.4 Mach number (a: 4° AoA, b: 8° AoA, c: 12° AoA, d: 16° AoA, e: 20° AoA, f: 24° AoA).....	61
Figure 3.29	Streamline for missile at 1.4 Mach number (a: 4° AoA, b: 6° AoA).....	62
Figure 3.30	Streamline for missile at 2 Mach number (a: 4° AoA, b: 6° AoA).....	63
Figure 3.31	Streamline for missile at 2.5 Mach number (a: 4° AoA, b: 6° AoA).....	64
Figure 3.32	Streamline for missile at 4 Mach number (a: 4° AoA, b: 6° AoA).....	64
Figure 4.1	Genetic algorithm process chart.....	68
Figure 4.2	General RSO procedures.....	71
Figure 4.3	Ansys workbench optimization set.....	74
Figure 4.4	Design variables of the missile body and nose.....	75
Figure 4.5	Design variables of missile tailfin.....	76
Figure 4.6	Optimization processes.....	78
Figure 4.7	Pressure contours optimum and baseline missile model at 1.4 Mach number and 4° AoA (a: baseline model, b: optimum model).....	81
Figure 4.8	Pressure contours optimum and baseline missile model at 2 Mach number and 4° AoA (a: baseline model, b: optimum model).....	82

Figure 4.9	Pressure contours optimum and baseline missile model at 2.5 Mach number and 4° AoA (a: baseline model, b: optimum model).....	83
Figure 4.10	Response surface for drag force with body length and nose curve radius at 1.4 Mach number and 4° AoA	84
Figure 4.11	Response surface for drag force with root thickness of tailfin and body radius 1.4 Mach number and 4° AoA.....	84
Figure 4.12	Response surface for lift force with tip and root chords of tailfin at 1.4 Mach number and 4° AoA	85
Figure 4.13	Response surface for lift force with fin span and tailfin position at 1.4 Mach number and 4° AoA.....	85
Figure 4.14	Local sensitivity chart.....	86
Figure 4.15	Pressure coefficient distribution for base and optimum missile body at 4° AoA (a: 1.4 Ma, b: 2 Ma, c: 2.5 Ma).....	88
Figure 4.16	Pressure coefficient distribution for base and optimum missile fin at 4° AoA (a: 1.4 Ma, b: 2 Ma, c: 2.5 Ma).....	89

LIST OF SYMBOLS

c	Wing chord
c_{b1}, c_{b2}	Empirical constants in the turbulence model
$c_{\epsilon1}, c_{\epsilon2}$	Adjustable constants
C_D	Drag coefficient
C_L	Lift coefficient
C_M	Moment coefficient
d	Distance to the wall
D	Drag force
E	Total energy
f_{t1}, f_{t2}	Empirical functions in the turbulence model
$f(\mathbf{x})$	Multi-objective vector
$f_n(\mathbf{x})$	Objective function
\vec{F}	Force vector
$g_i(\mathbf{x})$	Constraints
k	Kinetic energy
L	Lift force
L_b	Missile body length
L_{FS}	Fin span
L_{FR}	Root chords of tailfin
L_{FT}	Tip chords of tailfin
L_{tot}	Total length of missile
M	Moment
\hat{n}	Unit vector
\bar{p}	Average pressure
p'	Fluctuating pressure
P	Pressure
P_k	Production of turbulence

q	Heat flux
\dot{Q}	Heat transfer rate
R_b	Missile body radius
R_N	Nose curve radius
R_F	Nose front radius
S	Surface area
\tilde{S}	Intermediate variables
t	Time
T	Temperature
T_r	Root thickness of tailfin
T_t	Tip thickness of tailfin
u^*	Friction velocity
\bar{u}_i	Average velocity
u'_i	Fluctuating velocity
u	Velocity in x-direction
v	Velocity in y-direction
\vec{V}	Velocity vector
V_∞	Freestream velocity
w	Velocity in z-direction
\dot{W}	Work per unit time
x_i^l	Lower bounds value
x_i^u	Upper bounds value
X_F	Tailfin position
x, y, z	Cartesian coordinate axes
y	Normal distance from wall to first mesh center
y^+	Non-dimensional distance from wall to first mesh Center
β	Turbulence model coefficient
γ_{le}	Leading edge sweepbacks
γ_{te}	Trailing edge sweepbacks

δ_{ij}	Kronecker's delta
ε	Turbulent dissipation
κ	Von Karman constant
μ	Dynamic viscosity of the fluid
μ_t	Eddy viscosity
ν	Kinematic viscosity of the fluid
ν_t	Turbulent viscosity
$\tilde{\nu}$	Working variable of the turbulence model
ρ	Density of the fluid
$-\rho \overline{u'_i u'_j}$	Reynolds stress tensor
σ	Turbulent Prandtl number
$\sigma_k, \sigma_\varepsilon$	Turbulence model coefficients
τ	Viscous stress tensor
ω	Turbulent frequency
Ω	Vorticity
$\overline{\nabla}$	Divergence operator

LIST OF ABBREVIATIONS

AoA	Angle of Attack
AUSM	Advection Upstream Splitting Method
CFD	Computational Fluid Dynamics
DNS	Direct Numerical Solution
GA	Genetic Algorithm
LES	Large Eddy Simulation
Ma	Mach Number
MOGA	Multi-Objective Genetic Algorithm
RANS	Reynolds Average Navier-Stokes

CHAPTER I

INTRODUCTION

1.1 General Concept of Missile

Missile and rocket are crucial for the defense and aeronautical industry and nowadays, there are lots of studies to improve missile technology and aerodynamics. Missile is a rocket-guided weapon that is designed to carry a specific payload as an explosive warhead. They have various guiding systems (Image sensors, thermal sensors, radar, inertial sensors, GPS, etc.) operating in the atmosphere, and the main purpose is to carry ammunition and strike static or moving enemy positions by the way of explosion of a warhead with great precision at high speed. Missiles are increasingly preferred since they can reach the target in a timely, faster, and accurately with the development of technology. They have been used for short, medium and long distances depending to the missions.

Missile produces thrust with the burning of the solid / liquid fuel it carries. It should have good maneuvers ability in order to reach the desired targets in the right way and to shoot the movements systems. This can be done either by controlling the wings, and/or by controlling the movements of the small fins in the tail and the canard, or by controlling all of them (canard, fin, and wing). Missiles are generally steadied to fly by stabilizing fins. Moreover, guided missiles can adjust flight paths by using their control systems. The main control systems are operated by aerodynamic control surfaces and devices which are performed using of movable flaps that change the flow of air past the fins. The canards are placed near the nose and tail fins are placed near the tail of missile. Hence the wings have large span and area. They are mounted between canards and tailfins. Canard control missile is preferred for low angle of attack and low velocity since flow separation may occur and it can cause stall. However, canard control missiles provide good maneuverability and produce an additional lift. In addition, the response time is fast. Wing control missiles provide very fast response and good maneuverability, so it can lock on the target and track

with very small tracking errors. However, wing can generate strong vortices which may affect the tail of the missile, and may cause to roll the missile. If this effect is very strong, the control system may not be able to compensate. Wing location is also a very important issue due to the fact that the position of the center of gravity is not constant. Tail control missiles are used for longer ranges since they provide good maneuverability at high angles of attack. The pitch-yaw coupling and hinge moment are small. In addition to this, sometimes non-movable wings are used to provide lift and improve range. However, the response time of a tail-fin control missile is slow and the tail surface may cause a loss in lift due to an opposite force to the desired direction of missile flight (Lacau, 1988). Moreover, the nose and body of a missile are important in terms of aerodynamics and design to minimize drag and increase efficiency.

Figure 1.1 shows the missile that has canard, wing and tail control. Figure 1.2 shows the missiles which have tail control, canard control, and wing control, separately.

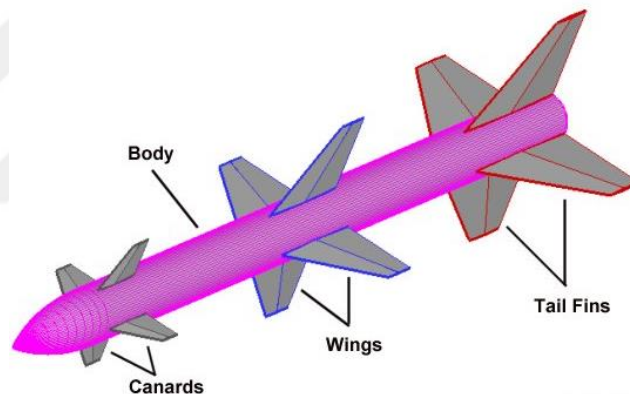


Figure 1.1 Major components of missile (<http://www.aerospaceweb.org>)

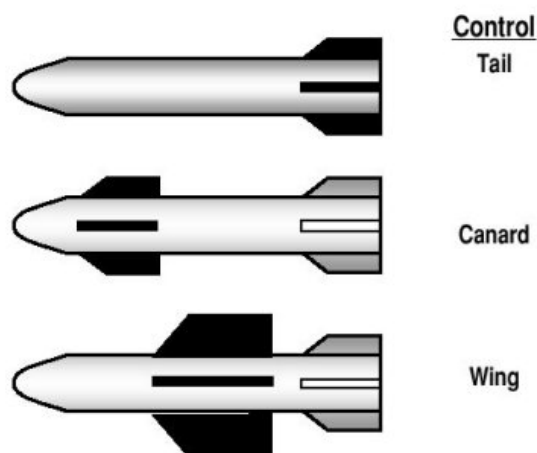


Figure 1.2 Three main categories of missile flight controls (Fleeman, 2001)

Although there are many variants of missiles specialized for different purposes from short-range cruise types to intercontinental ballistic ones, the flight performance criteria used to measure their effectiveness are common; Range, Speed and Maneuverability. The primary factors affecting the range and speed of a missile can be specified as design, operating and environmental conditions. On the other hand, the main considerations affecting the maneuverability can be indicated as stability, change in stability over time and aerodynamic properties. Hence, the aerodynamic characteristics affect all the three-flight performance criteria of a missile either directly or indirectly. Therefore, a progress in aerodynamic attributes leads to improvements in all these performance specifications. Doubtlessly, the major goal in aerodynamic design of a missile is catching a large lift coefficient and a small drag coefficient or as an equivalent description a high lift-to-drag ratio which is determined by the shape and size of the nose and body, as well as the shape, size and location of the canard, wing and tailfin (Cronvich, 1983). Once these structural features are identified and the configuration is emerged, then the numerical value of the lift-to-drag ratio can be decided by real flight tests data, wind-tunnel tests data or calculations.

Obviously, the first two approaches have high operational costs due to the consecutive reproduction requirements in actual flight tests and supersonic flow rate requirements in wind-tunnel tests (Versteeg and Malalasekera, 2007). Conversely, the third approach has high computational complexity due to the requirements to solve the coupled non-linear partial differential equations resulting from the interactions of fluid with surfaces. Fortunately, advanced computer programs such as Computational Fluid Dynamics (CFD) software packages make it possible to solve fluid flow problems in complex geometries within a reasonable time. In some engineering fields where CFD is applied, it can be assumed that the flow is inviscid and it may be sufficient to solve only main stream that is governed by Navier-Stokes Equation. However, in aerospace engineering field where shaped surfaces are investigated at subsonic or supersonic flow rates, the laminar flow assumption loses its validity due to the separation, reattachment, eddies, viscous dissipation, vortex formation and vortex shedding phenomenon arising from adverse pressure gradient, boundary-layer growth, thermal convection and atmospheric circulation. Therefore, the effects of turbulent fluctuations on the main stream should be taken into

considerations and Reynolds stresses have to be connected with the mean rate of deformation. Actually, direct realization of fluctuated values into the Navier-Stokes equation without using a turbulence model is possible which is called Direct Numerical Solution (DNS). However, in addition to being computationally expensive, the main problem is that the Navier-Stokes equation is not stable for higher values of Reynolds number. Even, a small perturbation in a parameter, or a slight variation in an initial/boundary conditions may lead to a completely different solution. Although, these kinds of problems can be overcome by introducing an appropriate turbulence model, the accurateness of the results heavily depend on the value of the turbulent viscosity. Hence, there is no universally accepted and consistently admitted turbulence model. At that point, the selection of the turbulence model is extremely important to accurately predict the boundary flow separation and shock boundary layer interaction (Deck et al., 2002). All those explanations are some difficulties of numerical solution.

In a turbulent regime, the swirling flows, or in other words, the eddies repeatedly split into smaller eddies. As a result, many sizes of them are generated in a turbulent flow field. Larger eddies have more energy than smaller ones and have more effect on main stream. In fact, differences between various turbulence models depend on how eddies are treated with different scales. In the field of interest, the most studied turbulence models can be grouped under two main headings; Large-Eddy Simulation (LES) model and Reynolds-Averaged Navier-Stokes (RANS) model. In LES model, the governing equations are filtered according to the eddy size. As the name suggests, eddies larger than the filtering threshold are directly solved, whereas, eddies smaller than the filtering threshold are modelled. It is obvious that complexity and instability, which are the problems of direct method, may or may not be solved according to the selection of the filter size (mesh width). If it is too small that is an inevitable requirement for aerospace engineering applications with complex geometries, most of the eddies are solved directly and LES becomes to suffer from same problems with DNS. However, using Reynolds decomposition assumption on Navier-Stokes equations, which is the key idea behind the RANS models family (Spalart-Allmaras, SST $k-\omega$, and Realizable $k-\epsilon$, etc.), the time-dependent chaotic velocity fluctuations can be separated from the mean flow velocity. Solving the decomposed RANS equations reduce the computational requirements efforts and

provides to simulate practical engineering flows for complex models (Lopez et al., 2014). As noticed that there is a trade-off between accuracy and complexity; faster outcomes in exchange for compromising coarser results. The question is to be asked here that whether these less accurate solutions are satisfactory or not for the studied subject. The comparative studies from the related literature that utilize the experimental data and simulations results show that the solutions obtained by RANS models are appropriate to use in a shape optimization process of a missile.

Energy is the most important key factor of development of society. Efficiency of production or systems are constantly being challenged to increase their operational limit. Therefore, optimization is crucial issue for a design problem to find the best possible engineering system under determined constraints, time limits and performance requirements. In optimization problem, initially, inputs (design variables) and output (objective functions) should be determined. Input variables may be body length, missile diameter, size of the fins, position of the fins, number of fin sets etc. and objective functions may represent aerodynamic performance which may be drag and lift coefficients. The complexity of optimization problem solution increases with increasing input variables and objective functions. Consequently, designer should have enough computational sources to search and compute the whole design space. Gradient-based optimization method which decides the maxima or minima of the objective functions is commonly used in engineering design problems. However, this method may not give reasonable results because engineering design optimization problems are discontinuous and highly nonlinear. Stochastic optimization methods don't need gradient information and cope with negative effects of gradient base methods. Genetic algorithm, Random Search methods can be given as examples of stochastic optimization methods (Arslan, 2014).

1.2 Scope of Thesis

The objective of this study is to increase the performance of missile. For this purpose, lift to drag ratio is the most important concept. Furthermore, a selected missile geometry is optimized to increase the lift to drag ratio. Initially, CFD solutions are performed and results are validated. Design parameters are then specified for selected missile and optimization process are implemented. The

obtained results are compared to how much improvement is achieved and they are presented as graphically and a table.

This thesis has been organized in five chapters. Chapter 1 presents the area of research work to be undertaken, the objectives and the work plan are discussed. In chapter 2, previous studies are presented for aerodynamic shape optimization. Material method and CFD solution results are presented in the third chapter. Optimization of the external missile and results are given in the fourth chapter. The conclusion drawn from the work and proposed the future work plan are given in the fifth chapter.



CHAPTER II

LITRATURE REVIEW

2.1 Missile Aerodynamics

Missile aerodynamics concerns the air flows through the missile and investigates how the air flow effects on it in terms of drag, lift and stability. The nose, body, wing, canard and fin of missiles are designated to provide high lift to drag ratio and control. Aerodynamic shape optimization can be performed in order to find optimum shape in terms of flight performance (Range, Maneuverability, Speed) for parts of the missile (Nose, Wing, Canard, Fin, and Body) (Cronvich, 1983).

2.1.1 Prediction of Aerodynamic Coefficients

The prediction of a missile aerodynamic is essential assignment to design external geometry of missile. This issue has been performed for many years by scientists. In order to predict flight performance accurately, computations, simulations and wind tunnel test data are compared and validated each other. Aerodynamic coefficients specify the performance and stability of a missile or a moveable vehicle. For a missile, the most important aerodynamic coefficients are drag, lift, pitching moment, yawing moment, and rolling moment. In this section, previous studies related with prediction of aerodynamic coefficient are presented.

Aerodynamic prediction is carried out using software package for validating and comparing. Teo (2008) studied the missile aerodynamic validation using missile DATCOM. Aerodynamic data was taken from wind tunnel test which provided by MSIC. Axial force and skin friction coefficients were compared with experimental results and reasonable agreement was provided. Maurice (2009) presented aerodynamic performance analysis for SA-2 type missile using Missile DATCOM. The study was carried out different Mach number and angles of attack. Performance data was provided by the project sponsor to compare the missile DATCOM results. It was concluded that the results were good agreement with each other. Ryan (2011) performed aerodynamic analysis and optimization for morphing guided unpowered

projectiles. The results of the study showed that optimal geometry provided more range than baseline geometry. Smith (2009) studied the external ballistic problem at supersonic speed for an axi-symmetric shape. In this study, two Euler solutions were used to solve projectile aerodynamics. The first method is Method of Characteristic (MoC) and second is Finite Volume Method (FVM). It was concluded that MoC solution did not show vorticity while FVM indicated the vorticity and shock wave on the nose and expansion region adjacent to the projectile. Sahu (2017) studied the flow control of the finned projectile to generate asymmetric pressure distribution and provide aerodynamic control changing the flow field in the aft finned region of the projectile. Using different geometric parameters, CFD analysis were performed to observe flow field and maximize the control of the projectile in terms of aerodynamics drag, lift, moment, pressure and pressure loss, turbulence, separation and vortices.

Guy et al. (1999) proposed an experimental study to investigate effect of canard shape on aerodynamic performance for Mach number of 0.5. The efficiency of the canards assessed based on pitching moments. It was concluded that static stability is reversely effected high aspect ratio, unswept, and untapered canards. Dillenius et al. (1999) presented engineering, intermediate and high-level aerodynamic prediction methods to design missile fin, canard and body using an experimental data-based code, and enhanced panel method-based code, and a space-marching Euler flow solver like time marching, respectively. Eventually, a fin planform optimization was conducted using the SUBDL/SUPDL method linked with an optimization code. Furthermore, Oktay et al. (2000) studied the two different missile geometries which are conventional and unconventional at 2 Mach number and at different angles of attack up to 20°. In order to obtain aerodynamic coefficients, Euler solver code was developed and it enables to reduce time cost. This developed unstructured 3D Euler flow solver compared with experimental data and Euler solver, FLU3M of ONERA for selected geometries. Hence, Champigny et al. (2003) proposed numerical simulation for missile configuration to analyze vortex flow. In order to solve flow of missile, both Euler and Navier-Stokes computations were used. It was concluded that Navier-Stokes computations was convenient to investigate wakes and vortex. In addition, Baldwin-Lomax turbulence model gave accurate results for rolling moment coefficients. Lesieutre et al. (2002, a) focused on aerodynamic prediction of missile.

In this study, prediction code MISDL was used to obtain aerodynamic coefficients for Penguin MK2 MOD7 missile configuration and the results were then compared to verify wind tunnel data for different geometric conditions. Lesieutre et al. (2002, b) proposed a study to improve aerodynamic prediction code MISL3 for missiles. Two fins set with free rolling tail fins were tested at NASA Langley Research Center. It was inferred that the experimental results matched with suggested code results for different missile geometry. Lesieutre and Quijano (2014) proposed aerodynamic prediction codes that is called MISL3 and MISDL for the engineering and intermediate level. These codes can be used to observe canard/wing vortex induced effects on tail fins. The proposed codes were verified by performing experimental study at Sandia National Laboratories. This study enabled to understand nonlinear aerodynamic characteristic of missile fins and configuration. DeSpirito et al. (2003) carried out to predict aerodynamic coefficients and flowfield a generic canard-controlled for missile configuration using viscous CFD simulations. In addition to this, wind tunnel experiment was conducted to verify the computational results. In order to improve canard and tail fin designs, flow physics were tried to understand using flow visualizations. The study showed that the canard control effectiveness was not improved using grid fins at subsonic and low supersonic speed. Sooy and Schmidt (2005) studied the aerodynamic prediction of missile using Missile DATCOM (97) and Aeroprediction 98 (AP98) which are generally used semi-empirical derivation and component build-up method for the preliminary design and analysis of missile aerodynamics and performance and commonly used prediction codes respectively.

In order to evaluate accuracy of the study, experimental wind tunnel data test was performed for different flight conditions. The results were shown that prediction error of axial force using AP98 was about 10% and DATCOM was 12%. The missile configurations were investigated axisymmetric body alone, body tail and body wing tail. Normal force, pitching moment, axial force, and center of pressure location were then investigated in this study.

Abney and McDaniel (2005) examined the accuracy of the missile DATCOM results at high angles of attack values. For this purpose, the outcomes taken from the missile DATCOM were compared with wind-tunnel data up to 20° degrees angle of attack and at subsonic Mach numbers. Normal force and longitudinal center of pressure location also matched with the experimental data up to 45 degrees angles of attack. It

was observed that missile DATCOM is able to obtain the aerodynamic coefficients of body, fin, and body-fin configurations up to 90° degrees angles of attack. Another study was presented by AL-Doulaimi et al. (2006) for predicting the aerodynamic coefficients of missile. Normal force curve slope, the pitching moments and the load distribution of missile was found using panel method with Neumann boundary. These coefficients were also predicted using DATCOM technique. The results of the study were observed that panel method have low computing cost when compared with CFD. Another similar study was presented using panel method to find aerodynamic coefficient for design missile geometry by Pankkonen (2011). In order to represent missile aerodynamics, a curve-fit scheme was developed across the entire Mach number range. The proposed method was observed that it was useable as a rapid modelling tool and compatible with panel method.

Silton (2005) focused on Navier-Stokes flow solver to predict the aerodynamic coefficients of a standard spinning projectile at different Mach numbers that start from subsonic to supersonic flow. The result of the study showed good agreement with the experimental results and semi-empirical aero prediction code. The study related with computations of complex elliptical missile both body alone and body-wing-tail configurations for supersonic flow was carried out by Sahu and Heavey (2009). In this work, using Navier-Stokes computations with a two equation k- ϵ turbulence model, numerical solution was performed to find aerodynamic coefficients and flow field for various angle of attack and side-slip angles. The solutions of the study were compared with experiential data to verify for used configuration. McDaniel et al. (2010) proposed canard controlled missiles to predict adverse rolling moment. A semi-empirical aerodynamic prediction code was then used to consider the effect of on rolling moment at different area and span of the tail fin and subsonic and supersonic Mach numbers. Bak (2010) performed both experimental study using wind tunnel and CFD solution for the missile with grid fin in subsonic flow. The results were showed that axial force coefficient of the grid fin was about 0.8 times greater than planar fin for the specified missile. Li et al. (2014) analyzed the aerodynamics and simulated the tail fin stabilized projectile using wind tunnel, CFD solution and MATLAB/Simulink. In order to convert the air compressibility into 0.6 Mach data that is performed wind tunnel, Karman-Tsien rule was used. The results were observed that the aerodynamic coefficients were good agreement with computational and experimental data between -8 and +8 degrees

angles of attack. It was concluded that improved model range increased about 26.83%.

Gülay et al. (2011) presented computational and experimental study to investigate wrap-around and flat fins of the missile rolling moment coefficients. The CFD calculation was carried out to find rolling moments and computational results were matched with experimental data. In supersonic region, the calculated and measured results were closer than subsonic region. It was concluded that rolling moment coefficient of missiles with wrap-around-fins is equal to the sum of the rolling moment coefficient of the flat-fins.

The wind tunnel experiments and CFD simulation of a generic split-canard missile were carried out to determine longitudinal aerodynamic characteristics by Honkanen et al. (2011). For the same geometry, CFD solution and experimental results were compared at angle of attack up to 60° in subsonic turbulent flow. It concluded that experimental and simulation results matched with each other.

Vidanovic et al. (2014) focused on aerodynamics of non-standard AGARD-B model which is a standard wind tunnel model. This study was implemented in two steps. In the first step, CFD simulation results were obtained for AGARD-B model with a generic-shaped nose and the results were validated by using experimental data attained from the model with the same structure. In the second step, the simulation model was introduced to acquire numerical predictions for a non-generic nose configuration. This two-step study revealed that the effects of different nose configurations are small and noticeable in the pitching moment coefficient whereas the effect of nose shape variation was negligible small on the drag and lift coefficients.

Taş et al. (2015) studied missile aerodynamics at high angles of attack values and supersonic flow regimes by applying pressure based coupled solver. In this study, $k-\omega$ SST, realizable $k-\varepsilon$ and Spalarat-Allmaras methods were used for computation. These three methods and experimental results compared each other. The results showed that the investigated solver is appropriate for cylindrical body simulations in the supersonic flows. In addition, it was observed that ANSYS Fluent solution was matched with experimental results. El-Mahdy et al. (2016) implemented study to compare computational and experimental and empirical techniques for aerodynamic coefficients of supersonic missile. In this study, CFD simulation and DATCOM code

were presented and compared experimental data at Mach number changing 1.5 to 4 at angle of attack up to 18°. It was concluded that the experimental results and computational results values were quite closer each other. Vidanović et al. (2017) focused on Multidisciplinary design optimization (MDO) for external missile configuration at different Mach numbers in supersonic flow. In order to predict drag and lift coefficients at different Mach numbers and angle of attack, CFD solution and experimental study which was implemented in Military Technical Institute (VTI), were carried out for N1G test model and AGARD-B model configurations. The optimization results were observed that the aerodynamic efficiency was increased about 2.18%, 5.73%, 5.69% for three different Mach number (1.4, 2.3, 4), respectively. Ageev and Pavlenko (2016) studied reduce of body of revolution aerodynamic drag using Euler and Reynolds averaged Navier-Stokes (RANS) equations. Sears-Haack body of revolution shape was improved making front part of the body blunted. The volume of the front part of body was transferred to back part and generated back face. It was concluded that aerodynamic drag decreased about 20 per cent when compared with Sears-Haack body.

Zhang et al. (2013) presented a paper to predict aerodynamic coefficients at “x±” finned configurations for theater ballistic missile target. Missile DATCOM and CFD methods were used to calculate aerodynamic coefficients and compared with experimental study. The results of the study showed that the missile maneuverability increased and the “x±” configurations provide the required stability. The another similar study was presented by Tahani et al. (2017) to improve aerodynamic performance changing geometric parameters for a canard control missile. In this study, increasing the canard taper ratio, aspect ratio and lift to drag ratio were observed to decide performance of missile. It was observed that lift to drag ratio increased with increasing taper ratio up to 0.67° at 4° angles of attack. CFD solution and experimental study results showed good agreement with each other for the developed missile design. Khanolkar et al. (2017) carried out an analysis study on missile aerodynamics using the CFD simulation and its results compared with experimental data. It is inferred from his study that the CFD outcomes are exact enough to accurately represent the real cases. Khalghani et al. (2016) examined the aerodynamic characteristics of a guided missile with deflectable nose at nine different configurations by programming a software routine to solve the Navier-

Stokes equations that incorporates the modified Baldwin-Lomax turbulence model and Finite-Volume discretization method.

2.2 Aerodynamic Shape Optimization

The aerodynamicists try to get better external geometry in terms of flight performance. Aerodynamic shape optimizations have been performed to find the shape which is optimal in that it minimizes cost function and maximize the efficiency while satisfying specified constraints. In this section, previous studies related with aerodynamic shape optimization methods are presented.

2.2.1 The Type of Evolutionary Algorithm Based Methods

Genetic Programming (GP), Evolutionary Programming (EP), Evolutions Strategy (ES) constitute Evolutionary Algorithm (AE) based methods. These methods are strongly related but they independently improved. For these methods, numerical evolution can be conducted.

Evolutionary algorithms have some advantages. One of them is the flexibility gains. This means that complex problems are easily adapted using evolutionary algorithm concepts. At same time, there are a few drawbacks related with this algorithm. The solution performed using evolutionary algorithm is only compared to known solution. This means the algorithm cannot give information that the solution exactly optimal. However, the solution results are only compared to other results.

Lee et al. (2008) carried out aerodynamic and RCS (Radar Cross Section) design optimization for UAV (Unmanned Aerial Vehicles) using robust Evolutionary Algorithm. The aim of this study was to improve aerodynamic performance and reduce Radar Cross Section designing wing plan form shape and airfoil sections. The results showed that the proposed method was efficient and obtained optimum solution. Giannakoglou (2002) presented the stochastic aerodynamic optimization methods, in particular, evolutionary algorithms, to show appropriate methods and reduce computational costs for design of optimal aerodynamic shapes. In this study, the population-based optimization method was used in order to eliminate the number of desperate calculations. Tianyuan and Xiongqing (2009) also focused on optimization design for unmanned combat air vehicle. In this work, there are two levels which are system level optimization and subsystem level optimization, to perform optimization process. The aerodynamic design optimization aim was to

reduce the drag coefficient and the structural weight. It was concluded that surrogate-based two level optimization can be applied and given reasonable results.

2.2.2 Genetic Algorithm

Genetic algorithm is a type of Evolutionary Algorithm (EA) which is commonly used to generate optimum solution and search problems. The concept of Genetic algorithm was defined by Holland (1975) in 1960s and it was described and developed by Goldberg (1989). The Genetic Algorithm is easily implemented to solve optimization problem and commonly used in the industry and academia. It has ability to solve highly nonlinear and mixed integer optimization problems (Hassan et al., 2005). Genetic algorithm has some features that provide some advantages to obtain optimum solution, for example, it solves lots of parameters, and it is suitable for parameterization to reduce solution time. It also works together with different type of optimization variable at same the time. Irregular, continuous, and independent solution set can be used (Oktay et al., 2009).

Many decision of genetic algorithm is probabilistic and random. These mean that the new generations may not always be better than previous generations. There are some members that are at least as good as previous members, we take best elements from the parent generation and put them in the new generation. The best n members of the previous generation can be taken and formed new members. In order to find convenient and fast optimization solution, we should take the best n members neither too large nor too small. Enough number of generations should be formed to approach optimum solution. The algorithm is terminated as the maximum number of generation is obtained. In order to qualify the individual solutions in a population, the GA uses a feasibility measure that is called fitness function. The fitness function shows how much it satisfies the required conditions. Every chromosome has a fitness function in the population. If the fitness is maximizing, the cost is minimizing. In addition, crossover process is performed to combine two chromosomes to produce a new chromosome. The aim of this process is that the new chromosome can be better both of the parents. Figure 2.1 shows crossover process. The other process in the genetic algorithm is mutation. Genetic algorithm tries to keep the best individual of the population. This can cause increase the genetic diversity and after some time all population may become same. Mutation induces a random walk through the search space which yields a new candidate solution (Gültekin et al., 2012).

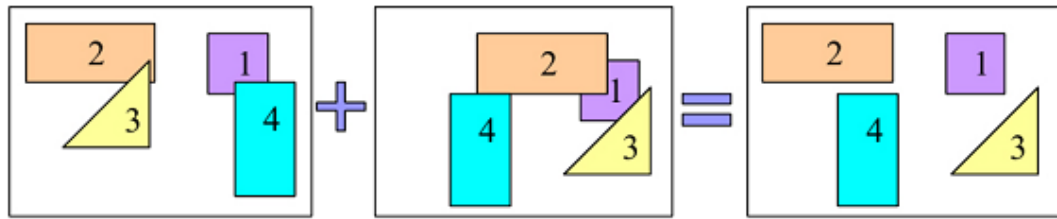


Figure 2.1 Crossover process (Gültekin et al., 2012).

Foster and Dulikravich (1997) presented two hybrid optimization methods, which are a gradient method based upon Rosen's projection and genetic algorithm using elements of the Nelder-Mead simplex method, to apply three-dimensional aerodynamic shape optimization. These methods were applied to different shapes that are ogive-shaped, star-shaped, spiked projectiles and lifting body. Using Newtonian flow theory, flowfield analysis was performed. The results showed that the hybrid genetic algorithm was able to achieve impressive convergence according to the gradient based method.

Nobahari et al. (2006) proposed aerodynamic shape optimization for unguided projectiles. They used two stochastic optimization methods which are Continuous Ant Colony System (CACS) and Genetic Algorithm (GA). In addition to this, Engineering code (EC) which combined with CACS and GA in this study, was utilized in order to compute the normal force coefficient over flight conditions. It was observed that CACS+EC gives good results compared with GA.

Nikbay et al. (2009) presented an analysis and design work of an AGARD 445.6 wing to maximize the lift-to-drag ratio and to minimize the total weight. Accordingly, modeFRONTIER software package was used as an optimization tool for implementing a genetic algorithm routine and ANSYS Fluent was used as a flow analysis tool for evaluating the configured geometry. It was concluded that the Pareto-optimal solutions match with experimental data. Another work which was performed by Vytla et al. (2010) was carried out to optimize a high speed train nose using a combined GA-PSO (Genetic Algorithm and Particle Swarm Optimization) algorithm. This hybrid algorithm was then linked with a kriging based surrogate model to obtain the optimum nose shape of the train. Required small number of simulation for optimization was then investigated using a surrogate model identical to the kriging model. The results of this study indicated that the nose shape should be

short in order to reduce aerodynamic drag and the nose shape should be long to get the least aerodynamic noise generated.

Multi-objective optimization of aerodynamic shape was performed for a guided rocket by Runduo and Xiaobing (2018). In their work, non-dominated sorting genetic algorithm (NSGA-II) and the real coding genetic algorithm (RGA) were used to solve multi-objective optimization problem. The results of the study which was conducted on a long-range guided missile showed that the lift-to-drag ratio, and not surprisingly the maneuverability can be improved as a result of optimization process. Optimal shape and original shape of the rocket were solved using CFD and it was concluded that the results were qualitatively correct. He and Agarwal (2014) performed shape optimization to improve lift and drag characteristic for NREL S809 airfoil using Genetic Algorithm. Fluent was used to calculate the flow field applying Reynolds-Averaged Navier Stokes (RANS) equations. The optimization results were compared with Adjoint-based optimization technique.

Anderson et al. (2000) focused on the shape optimization of missile aerodynamic and they used Pareto genetic algorithm to design missile geometries for specified design goals and constraints. Hybrid design can be implemented through Pareto genetic algorithm for single or multiple-goal problems. Fin shape optimization was conducted to minimize aerodynamic heating utilizing Genetic Algorithm by Misaghian et al. (2007). They developed a code to compute aerodynamic heating of swept isolated fins and aerodynamic coefficients. Genetic Algorithm was then used to develop an optimizing program. It was observed that the drag coefficients of fins and leading edge aerodynamic heating were significantly decreased. Tamil et al. (2009) proposed external configuration optimization for a missile design. In this study, MATLAB was utilized to carry out optimization using genetic algorithm based optimization tool. In order to consider aerodynamic coefficient of the missile, DATCOM was used. The design of the subsonic cruise missile external configuration was implemented by means of EXCON. The results of the study showed that the mass of the missile was reduced about 30% and maneuverability was also developed by 13%. Figure 2.2 shows the EXCON modules.

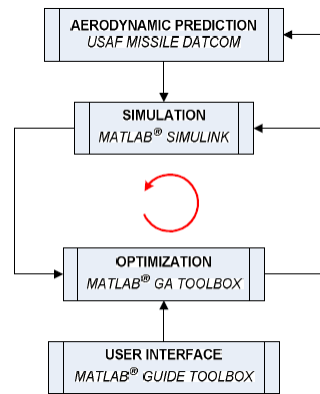


Figure 2.2 Sub-modules of EXCON (Tanıl, 2009)

In order to maximize the range of a guided missile performing aerodynamic shape optimization, trajectory analysis and real coded adaptive range genetic algorithm were interlinked by Yang et al. (2012). In this study, canards and tailfin optimization were carried out to obtain maximum range of guided missile deriving the selected optimization method and trajectory analysis. It was concluded that the range of the missile was increased about 5.8% for unguided missile and 21.4% for guided missile. Figure 2.3 represents optimization system of the proposed study.

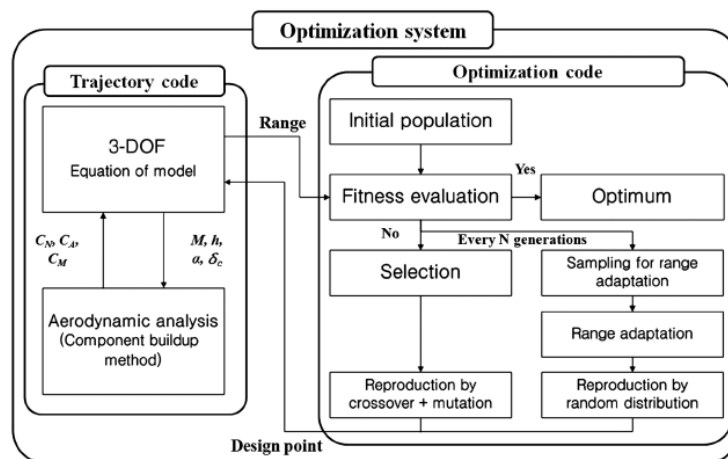


Figure 2.3 Range maximization system for a guided missile (Yang et al., 2012)

Yamazaki et al. (2008) presented the mildfield drag-decomposition method to carry out aerodynamic shape optimization. The proposed method was applied to airfoil, winglet, and planform for verification and design optimizations. Conventional genetic algorithm was used as optimizer. It was concluded that the utilized method was efficient and reliable. Gaiddon and Knight (2002) studied the flight performance of a ramjet powered missile using automated optimization loop which based on CFD

tools. In order to solve flight equilibrium, Reynolds-Averaged Navier-Stokes computations were used. In this work, global stochastic algorithms, such as Simplex, Genetic Algorithms or Evolutionary Strategies, were used to perform aerodynamic optimization of the missile. Ahuja and Hartfield (2011) used smart Panel method and modified potential theory to perform optimization of Boing-737 wing-engine. In this work, Treftz plane analysis was used to compute induced drag. In order to perform surface shape optimization, binary encoded genetic algorithm was used. Shi et al. (2011) attempted to solve the aerodynamic shape optimization problem of a missile by formulating it as a multidisciplinary design optimization (MDO) problem. The aerodynamic analysis was performed and trajectory modules were integrated by using Missile DATCOM and iSIGHT software packages, respectively. Genetic algorithm was also used to obtain optimal solution. It was concluded that the application of MDO method was good effect for missile performance. Paniagua et al. (2014) studied the aerodynamic optimization for a high-speed train entering a tunnel. In this study, they used genetic algorithm to perform optimal nose shape of the train to minimize the aerodynamic drag and pressure gradient. A multi-objective optimization was also implemented to reduce aerodynamic drag since the trains travel open air and a tunnel. Riddle et al. (2009) solved the shape optimization problem of a missile by using genetic algorithm method. The predictions of aerodynamic coefficients were obtained by using both AERODSN routine and Missile DATCOM software package. The results taken from the optimized missile geometry for each approach showed that the total weight is decreased and maximum speed is increased. However, the target offset differences are slightly diverging for these approaches; the missile optimized by using AERODSN routine and Missile DATCOM software package landed 9 [m] away and 14.3 [m] away from the target, respectively.

Dyer et al. (2012) focused on real coded Genetic algorithm to demonstrate the applicability of the aerospace engineering design. In this study, three different design studies were implemented utilizing a real coded Genetic Algorithm for single and two stage propellant missile system design and single liquid propellant missile design. For these three designs, twenty-six tests were carried out. The results of the study were observed that real coded GA is useable as compared to robust binary GA.

2.2.3 Adjoint Method

The Adjoint method is used for numerical optimization problem calculating the gradient function. Gradient-based methods depend on the Adjoint approach that is able to compute the objective function according to the design variables.

Morris et al. (2009) presented aerodynamic shape optimization depending upon a domain element approach combined with global interpolation functions. Planform parameters were used to perform shape optimization of a modern aircraft wing. Thirty parameters were used for optimization process and the results of the study, 8 per cent reduction drag was obtained. Hu et al. (2012) studied the Busemann type supersonic bi-plane at off-design conditions. In order to reduce drag force for different Mach numbers that are between 1.1 and 1.7, Adjoint based optimization method was used. Colonno et al. (2013) performed aerodynamic shape optimization using Adjoint-based method for fairing systems. Using a local spherical coordinate system, the fairing geometry was parameterized. Gradient-based optimization algorithms were used to obtain accurate sensitivities of aerodynamic performance. Zhang et al. (2012) studied the shape optimization and aerodynamic design for flying wing. They used Euler solver and gradient-based optimization to find wave-drag and induced-drag design. In order to carry out optimization, MATLAB optimization toolbox (interior-point algorithm) was used. In this study, geometry was specified and sent to CAD. Sumo that is mesh generator, and CFD computation were then performed. Azab and Ollivier-Gooch (2010) presented high order two dimensional aerodynamic optimization. The Adjoint approach was used for flow solution sensitivity. When optimization iteration was performed, the grid around the airfoil might need to be repeated. Because of this reason, they deformed the mesh in case of change the geometry. The Quasi-Newton optimization was then used with BFGS approximation of the Hessian matrix for optimization. The Adjoint method was used to perform constrained and non-constrained aerodynamic optimization of an airfoil by Hekmat et al. (2009). The results of the study showed the effect of the optimized geometry and the constraint on the optimization trend for two optimizations. It was observed that constrained optimization increased the computational costs. Figure 2.4 represents design cycle of presented study. Pape and Beaumier (2005) carried out numerical aerodynamic optimization for helicopter rotor performance. The CONMIN which is a gradient-based method was used to perform numerical optimization. 3D

Navier-Stokes solver and a lifting-line code (HOST) were then combined to implement the optimization. It was concluded that the proposed optimization method provided good performance for helicopter rotors.

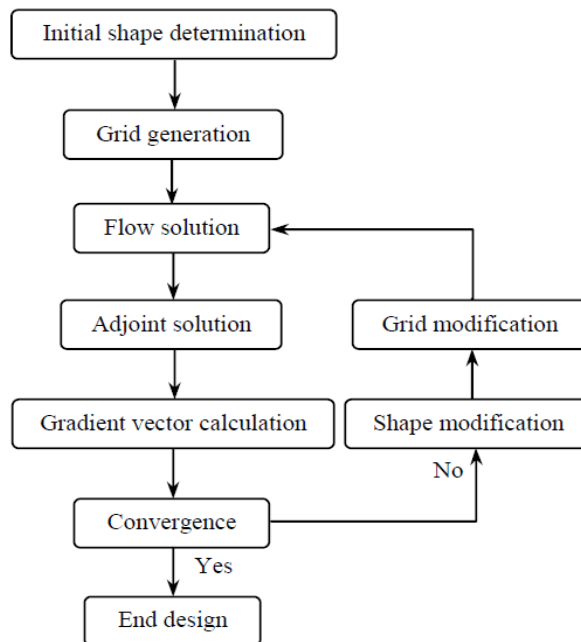


Figure 2.4 Design cycle (Hekmat et al., 2009)

Feyzioglu (2014) presented a shape optimization study for a missile that is free to rotate tail fins on canard controlled. In this study, asymmetric flows calculation was performed using Reynolds-Averaged Navier-Stokes (RANS) equations in Fluent. A gradient based planform optimization was carried out to minimize the roll rate on the free to rotate tail fins. It was concluded that roll rate of the optimized tail fin planform is reduced about 6% and increased the normal force about 4%.

Chen et al. (2015) modelled wing-body-tail configuration for aerodynamic shape optimization. In order to achieve optimization, gradient-based optimization with a Reynolds-averaged Navier-Stokes (RANS) model was used. This work was carried out two mesh levels that are 746000 and 5.97 million cells, for aerodynamic prediction. The results of the study showed that the optimization of tail and wing rotation gave good results in terms of performance. Mader et al. (2014) carried out aerodynamic shape optimization by calculating stability derivatives and their gradients. In this study, Multi-block flow solver with both Euler and Reynolds-averaged Navier-Stokes equations, and structured-grid were utilized. In addition, in order to calculate enabling gradient-based aerodynamic shape optimization and the

gradients of the stability derivatives of interest, Adjoint approach was used. Another study was presented to carry out aerodynamic shape optimization by Reuther et al. (1999). In order to compute the aerodynamic properties of complex 3-D aircraft configuration, Computational fluid dynamics (CFD) with Euler equations was used. Using control theory, the Adjoint differential equations were derived to evaluate design gradient information. Parallel computing was then carried out to increase portability and efficiency utilizing an optimization communication schedule, the Message Passing Interference (MPI) Standard, and a domain decomposition approach.

2.2.4 Particle Swarm Optimization Method

Particle Swarm optimization (PSO) was put forward by Eberhart and Kennedy (1995). It is commonly used for numerical optimization problems are reveal by social behavior of bird flocking. PSO is a swarm intelligence optimization algorithm based upon the iteration of population. PSO has some similarity with Genetic Algorithms (GA) and it is a computational method which optimizes a problem trying to develop a solution with respect to a given measure of quality. The system is started with a population of random solutions and each particle updates its own velocity and position depend on the best experience of its own and the whole population during flight. The aim of the updating process is to drive particle swarm to move toward the region with the higher objective function value. Finally, all particles are provided to gather around the point with the highest objective value (Jones, 2005).

PSO is more advantageous since it has better calculation efficiency and less number of function evaluations when compared with GA. However, GA gives more precision results than PSO with respect to accuracy of model parameters. This statement relies to the information sharing and internal velocity of algorithm of PSO. In order to compare GA and PSO and show advantages of PSO, Hassan et al. (2005) proposed a study related with design optimization problems. Kulkarni et al. (2015) proposed a review paper to explain and demonstrate PSO and some improved version of PSO applications for mechanical engineering. In this study, it was concluded that PSO is a very efficient and successfully applied optimization algorithm in mechanical engineering.

Burgreen and Baysal (1996) proposed discrete sensitivity analysis for the three-dimensional shape optimization. In this study, firstly, Euler equation was used to

predict the flow physics. Secondly, in order to carry out optimization, discrete sensitivity analysis was used. Finally, both two and three dimensional Bezier-Bernstein parameterizations were utilized to design surface geometry. Sensitivity analysis algorithm with Computational Fluid Dynamics (CFD) was proposed to carry out aerodynamic design optimization for scramjet-afterbody configuration by Baysal and Eleshaky (1992). In this work, using the quasi-analytical method, the sensitivity coefficients which are constraints and gradients of the objective function were obtained. The flow analysis was performed using first order Taylor series expansion. The results showed that the new optimum solution method quite efficient compared with the previous methods. Wei and Meijian (2013) presented a paper which was performed aerodynamic shape optimization of a wing and winglet by means of modified quantum-behaved particle swarm optimization algorithm. The results of the study showed that the shock-wave amplitude on the wing and drag was reduced and intense shock wave was eliminated. Usta et al. (2015) carried out an analysis and design work to improve the aerodynamic characteristics of missiles at supersonic Mach numbers. They used white's method, Missile DATCOM and Navier-Stokes method for prediction of aerodynamic coefficients at supersonic Mach numbers for very low aspect ratio fin configuration that is difficult to predict using linear theories because of complex nature of flow. These methods were also compared with experimental results. In this study, Particle Swarm Optimization (PSO) was used to perform optimization of the missile and mesh was generated using GAMBIT and solved using ANSYS Fluent. It was observed that after 67 iterations were performed, the optimum missile geometry was obtained.

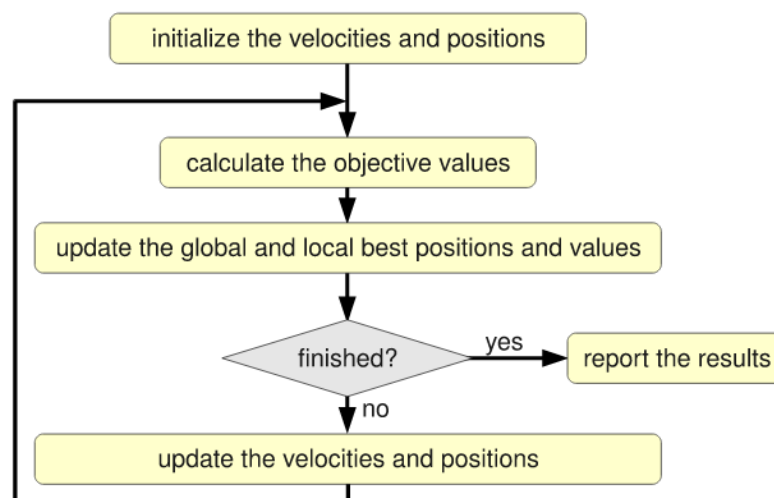


Figure 2.5 Flowchart of PSO (Schoene, 2011).

Schoene et al. (2012) proposed to Adaptive Particle Swarm Optimization (APSO) which changes its behavior operating the optimization process depend on information gathered. This method is able to solve difficult optimization problem accurately and efficiently. Figure 2.5 represents the flow chart of PSO. Xia et al. (2016) performed aerodynamic shape optimization study using PSO for supersonic launch vehicle and transonic airfoil. The results of the study were observed that the drag coefficients are reduced about % 14 and % 15 for transonic airfoil and supersonic launch vehicle, respectively. Kachitvichyanukul (2012) proposed a study to explain three evolutionary algorithms that are Genetic Algorithms, Particle Swarm Optimization, and differential algorithm. In this study, similarities and differences of these three optimization algorithms were observed and discussed. Figure 2.6 represents the flowchart of evolutionary algorithm.

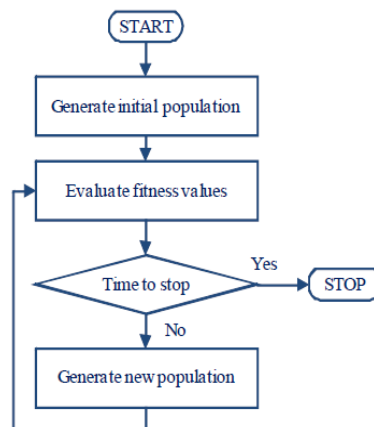


Figure 2.6 Flowchart of evolutionary algorithm (Kachitvichyanukul, 2012)

2.2.5 Sequential Quadratic Programming and Multidisciplinary Optimization

Sequential Quadratic Programming method is used for nonlinear optimization problem. Nelder-Mead Simplex Method is used to find minimum and maximum objective function and it is widely applied numerical method and nonlinear optimization problem.

To improve the aerodynamic characteristics of a missile, Nguyen et al. (2014) accomplished a two phases study composed of optimization and validation steps. In order to specify and shows effect of design variables and constraints, sensitivity analysis was implemented for missile geometry. The end of the study was observed that improvement total range of the missile was 27.8% when compared with baseline

configuration. The aerodynamic analysis was implemented using tactical missile design (TDM) and aerodynamics database (Aero DB). The experimental data and Missile DATCOM results were utilized to attain the optimum geometry, and ANSYS Fluent model was implemented to verify the optimized configuration. Körpe and Kanat (2019) proposed a study related with aerodynamic optimization of a UAV wing. Xfoil was used to predict drag and lift coefficients and the results were compared with XLFR5 and ANSYS Fluent. The sequential quadratic programming was used for optimization problem using MATLAB optimization toolbox.

Lopez et al. (2014) studied the optimization of air-ejected rocket geometries for supersonic flow field simulation that is carried out using CFD codes and simulated using OpenFOAM software. In order to perform optimization for improving suitable design, kriging based algorithms were generated. It was concluded that SST $k-\omega$ turbulence model and CDS numerical scheme provided the best accuracy for solution of the supersonic flow field when compared with Spalart-Allmaras.

Arslan (2014) focused on missile external configurations to conduct aerodynamic optimization. In order to calculate the aerodynamic coefficients, DATCOM was used. Random Search (RS) and Sequential Quadratic Programming (SQP) methods were used to perform optimization of the missile. NASA Tandem Control Missile (TCM) configurations were utilized to show whether the proposed optimization design method improved the TCM configuration in terms of aerodynamic performance. Finally, it was observed that missile external configurations could be determined by using developed optimization design method for pre-defined aerodynamic performance parameters.

Doyle et al. (2011) presented Integrated Multidisciplinary Optimization Object (IMOO) system improving aerodynamic module. The IMOO was utilized to generate geometry and grid using Geometry Manipulation by Automatic Parameterization (GMAP) and RapidFEM. The developed system was used to compute the aerodynamic performance of any vehicle design. Another shape optimization study was proposed by Cui and Yang (2010) for hypersonic arc-wing missile. They used Nelder-Mead simplex method with CFD to optimize the arc-wing and Navier-Stokes equation was used to calculate the aerodynamic performance. It was concluded that Navier-Stokes and Euler solver combination showed good performance in terms of reduction of the computational cost. Another study was presented to carry out for

wing optimization by Hutchison et al. (1994). The new method was performed combining conceptual and preliminary design techniques. Combining planform and airfoil design variable, procedure of a wing shape parameterization was improved. In order to estimate aircraft weight, friction drag, drag due to lift, and supersonic wave drag, conceptual design level algebraic equations were utilized.

Lesieutre et al. (1998) conducted shape optimization to improve missile fin in terms of aerodynamic performance. In order to design fin planform, the developed software was used. Wind tunnel test was then performed for several missile fin planforms and the results of this study, fin hinge moments were minimized by means of planform optimization. An aerodynamic optimization of nose section of missile with supersonic flow was conducted by Kaleeswaran et al. (2013). Both Spherical nose cone model and Spherical model with a parabolic nose cavity were tested at same Mach speed. It was observed that temperature, surface pressure effects and aerodynamic drag were reduced at the end of study. In this study, GAMBIT was used to design and Fluent was used to analyze for both models. In order to decrease time of computation, Design of Experiment method was then utilized.

Ocokoljić et al. (2017) performed a comparative study on a guided missile that intends to modify the front part and aims to improve the aerodynamic attributes. The outcomes revealed that experimentally obtained aerodynamic loads are in compliance with CFD-simulated aerodynamic coefficients. In order to consider optimum aerodynamic shape, the T-35 wind tunnel test was used and the tests were performed changing and improving the front part of the guided missile while the other parts of the missile remained same. The aerodynamic loads of the missile were obtained through three-dimensional Reynolds Averaged Navier-Stokes numerical simulations. The end of the study was observed that optimized configuration showed good flight performance. Öztürk (2009) was presented multi-objective design optimization for missile and rocket. DATCOM was used in order to predict aerodynamic coefficients, and Simulated Annealing (SA) was applied to find optimization design. In this study, 40 design variables were carried out to optimize the missile. The result of the study was observed that the applied algorithm gave reasonable results for highly nonlinear optimization problems.

2.2.6 Decision of the Optimization Method

Some problems may have infinite number of solutions, but we need to find the most appropriate and fast solution. In the literature survey, Genetic algorithm and Adjoint method are commonly used to solve the optimization problem since they are very fast and give more accurate results. However, optimization solution is mostly performed with single objective function. In this study, multi objective functions are used. **Multi Objective Genetic Algorithm (MOGA)** is used to find optimum geometry for selected missile model.

2.3 Motivation of the Study

Missiles have been widely used to strike enemy positions which may be movable position. In this respect, missiles have been improved in terms of aerodynamic performance and stability to strike the positions correctly. In the literature, it can be observed that multi objective optimization problem and the number of the examined design parameters are few. Therefore, in this thesis, Multi Objective Genetic Algorithm (MOGA) is decided to use. The aim of study is to increase C_L/C_D ratio at specified angles of attack and Mach number by examining more design parameters. The optimized models are then compared with base model to see how much improvement is achieved.

CHAPTER III

MATERIAL AND METHOD

In the aerodynamic shape design, the main characteristic of missile geometry is lift and drag forces or lift to drag ratio. The aerodynamic performance of missile is affected from body size, nose shape, wing or fin position and size. In other words, design variables or input parameters of the missile are crucial to optimize the geometry. Therefore, the beginning of the study, aerodynamic prediction of selected missile is performed for base geometry to obtain aerodynamic coefficients. After providing validation of aerodynamic analysis, optimization process is implemented specified design variables. In this section, methodology and results of missile aerodynamics are presented.

3.1 Introduction

Computational Fluid Dynamics (CFD) is used to evaluate and investigate flow field. It is also utilized when the scenario cannot be performed experimentally. Hence, CFD is useful, economic and efficient option to assess flow field (Vidonovic, 2014). Since 1983, it has been used in many industries around the world and has grown day by day. As commercial software with the most advanced technology, it offers easy and quick solutions for the most difficult problems of its users. ANSYS can be used to solve mechanical, fluid mechanics and heat transfer problems in many different industrial such as aviation industry, automotive industry, white goods industry, turbo machinery industry, chemical industry, food industry etc. CFD provides crucial advantages in case of economic limitation, complex model geometry design, measurement limitations and unavailability of appropriate test model geometry. CFD allows you to examine flow properties without disturbing the flow (Duygu, 2014). In addition, ANSYS enables simulation working conditions without producing prototypes. The ANSYS software allows both external CAD data and geometry to be

created with preprocessing capabilities. ANSYS Workbench is a platform that integrates parametric CAD systems with simulation technologies and unique automation. The purpose of ANSYS Workbench is to ensure that the product is validated and improved in a virtual environment.

In this study, CFD method that works based on the finite volume method is performed to simulate the fluid flow. ANSYS Fluent is used for CFD calculation to obtain aerodynamic coefficients at different Mach numbers and angles of attack.

3.2 Aerodynamic Background

Aerodynamics examines how the objects behave in the air. There are rules of aerodynamics explaining how to be able to fly an air vehicle. Aerodynamic affects all vehicle that move in the air such as from a missile to a kite.

3.2.1 Supersonic Flow

Supersonic flows can be defined as flows exceeding speeds of Mach 1. Additional complexity can occur when the flight reaches at supersonic flow. The physical phenomena take place at supersonic speeds, such as shockwaves and aerodynamic heating on the vehicle surface (Bes, 2006). Figure 3.1 represents a supersonic flow over a pointed-nose body viscous shock layer.

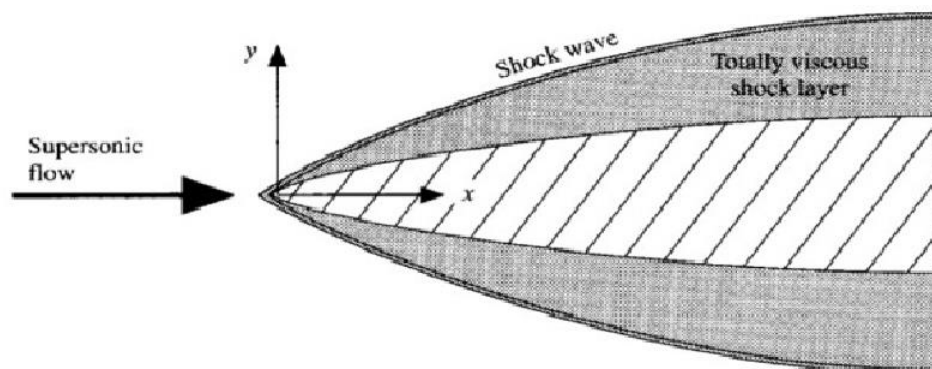


Figure 3.1 Viscous shock layer (Anderson, 1995).

Shockwaves do not occur in areas where the flow is completely subsonic. However, it is usually not possible to avoid shockwaves for transonic and supersonic flows. In subsonic flow, the drag coefficient increases since the Reynolds number increases along the missile body because of thickening of the boundary layer and eventual flow

separation. When supersonic flow occurs, stern and bow shocks attach to the body. Oblique shocks also occur in places where the supersonic flow returns into itself. Although the Mach number decreases after the oblique shock wave, the flow does not go into the subsonic regime. Pressure, temperature and density increase.

3.2.2 Viscous Interactions

Viscous interaction can be defined as; major interactions between the boundary layer and the external inviscid flow behind the shock occur as a consequence of thin shock layers. Some of the kinetic energy converted into internal energy in the form of heating that raises the temperature of the boundary layer because of viscous effects of the boundary layer (Bes, 2006). Figure 3.2 represents the effect of viscous interactions on boundary layer.

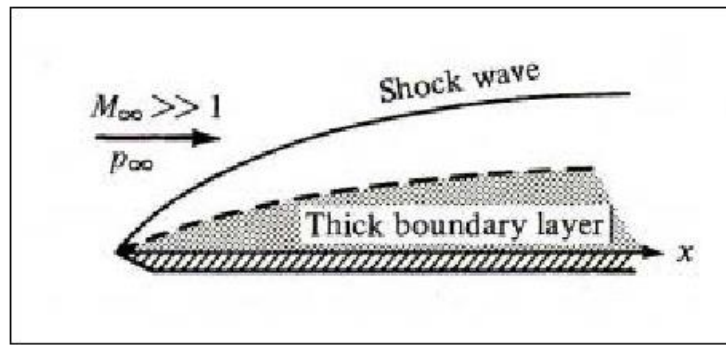


Figure 3.2 Effects of viscous interactions on boundary layer (Bes, 2006).

3.2.3 Navier-Stokes Equations

Navier-Stokes equations which represent motion of a fluid element are the general governing equations of the fluid dynamics. The equation consists of the momentum equations, the energy equation and the continuity equation. Navier-Stokes equations can be written for a laminar, viscous, unsteady, compressible, three-dimensional flow in Cartesian coordinates of equations (3.1) to (3.5). Figure 3.3 shows normal and shear stresses on a fluid element.

$$\text{Continuity Equation: } \frac{\partial \rho}{\partial t} + \vec{\nabla}(\rho \vec{V}) = 0 \quad (3.1)$$

$$X - \text{Momentum Equation: } \rho \frac{Du}{Dt} = -\frac{\partial P}{\partial x} + \frac{\partial \tau_{xx}}{\partial x} + \frac{\partial \tau_{yx}}{\partial y} + \frac{\partial \tau_{zx}}{\partial z} \quad (3.2)$$

$$Y - \text{Momentum Equation: } \rho \frac{Dv}{Dt} = -\frac{\partial P}{\partial y} + \frac{\partial \tau_{xy}}{\partial y} + \frac{\partial \tau_{yy}}{\partial y} + \frac{\partial \tau_{zy}}{\partial z} \quad (3.3)$$

$$Z - \text{Momentum Equation: } \rho \frac{Dw}{Dt} = -\frac{\partial P}{\partial z} + \frac{\partial \tau_{xz}}{\partial z} + \frac{\partial \tau_{yz}}{\partial y} + \frac{\partial \tau_{zz}}{\partial z} \quad (3.4)$$

$$\begin{aligned} \text{Energy Equation: } \rho \frac{D(e + V^2/2)}{Dt} = \rho q + \frac{\partial}{\partial x} \left(k \frac{\partial T}{\partial x} \right) + \frac{\partial}{\partial y} \left(k \frac{\partial T}{\partial y} \right) + \frac{\partial}{\partial z} \left(k \frac{\partial T}{\partial z} \right) \\ - \vec{\nabla} \cdot p \vec{V} + \frac{\partial (u\tau_{xx})}{\partial x} + \frac{\partial (u\tau_{yx})}{\partial y} + \frac{\partial (u\tau_{zx})}{\partial z} + \frac{\partial (v\tau_{xy})}{\partial x} + \frac{\partial (v\tau_{yy})}{\partial y} + \frac{\partial (v\tau_{zy})}{\partial z} \\ + \frac{\partial (w\tau_{xz})}{\partial x} + \frac{\partial (w\tau_{yz})}{\partial y} + \frac{\partial (w\tau_{zz})}{\partial z} \end{aligned} \quad (3.5)$$

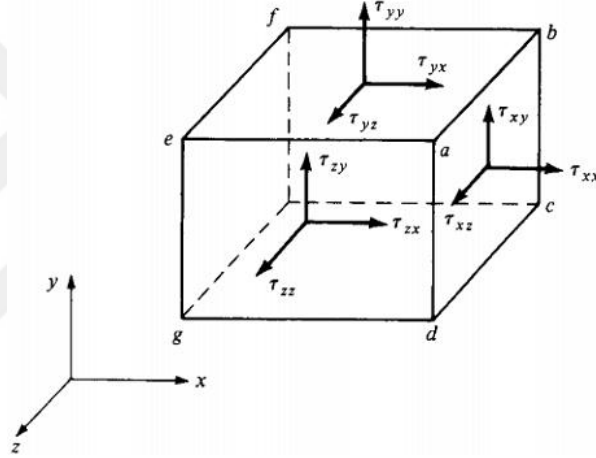


Figure 3.3 Normal and shear stresses on a fluid element

The normal and shear stresses can be defined as the following equations (3.6) to (3.11).

$$\tau_{xx} = -\frac{2}{3}\mu(\vec{\nabla} \cdot \vec{V}) + 2\mu \frac{\partial u}{\partial x} \quad (3.6)$$

$$\tau_{yy} = -\frac{2}{3}\mu(\vec{\nabla} \cdot \vec{V}) + 2\mu \frac{\partial v}{\partial y} \quad (3.7)$$

$$\tau_{zz} = -\frac{2}{3}\mu(\vec{\nabla} \cdot \vec{V}) + 2\mu \frac{\partial w}{\partial z} \quad (3.8)$$

$$\tau_{xy} = \tau_{yx} = \mu \left(\frac{\partial v}{\partial x} + \frac{\partial u}{\partial y} \right) \quad (3.9)$$

$$\tau_{yz} = \tau_{zy} = \mu \left(\frac{\partial w}{\partial y} + \frac{\partial v}{\partial z} \right) \quad (3.10)$$

$$\tau_{xz} = \tau_{zx} = \mu \left(\frac{\partial u}{\partial z} + \frac{\partial w}{\partial x} \right) \quad (3.11)$$

Reynolds Average Navier-Stokes (RANS) equations can be written for a turbulent, viscous, unsteady, compressible flow in x-direction as the following equations (3.12) to (3.15) (Ansys inc, 2011).

The time averaging is expressed as

$$\bar{f} = \lim_{T \rightarrow \infty} \frac{1}{T} \int_0^T f(x_i, t) dt \quad (3.12)$$

The sum of the mean and fluctuating components can be expressed as

$$p = \bar{p} + p' \quad u_i = \bar{u}_i + u'_i \quad (3.13)$$

Reynolds Averaged Navier-Stokes equations are defined as

$$\frac{\partial \rho}{\partial t} + \frac{\partial(\rho \bar{u}_i)}{\partial x_i} = 0 \quad (3.14)$$

$$\begin{aligned} & \frac{\partial(\rho \bar{u}_i)}{\partial t} + \frac{\partial(\rho \bar{u}_i \bar{u}_i)}{\partial x_j} \\ &= -\frac{\partial \bar{p}}{\partial x_i} + \frac{\partial}{\partial x_j} \left[\mu \left(\frac{\partial \bar{u}_i}{\partial x_j} + \frac{\partial \bar{u}_j}{\partial x_i} - \frac{2}{3} \delta_{ij} \frac{\partial \bar{u}_m}{\partial x_m} \right) \right] + \frac{\partial}{\partial x_j} (-\rho \overline{u'_i u'_j}) \end{aligned} \quad (3.15)$$

Analytic solution does not exist for the full (3-D) Navier-Stokes equations until now because of the complexity of the system of partial differential equations. In order to achieve the approximate numerical and viscous flow solution, some assumptions is made.

3.2.4 Boundary Layer Equations

The Navier-Stokes equations can be solved to obtain the closest to exact possible answer using computer source with high capacity. However, the equations can be simplified to obtain solution for viscous flow. The first assumption is that the boundary layer thickness is decided very small when compared with the body length. Figure 3.4 represents thin body layer versus length of the body (Bes, 2006). The

other assumption can be made from boundary layer theory. Reynolds number is determined large for this assumption.

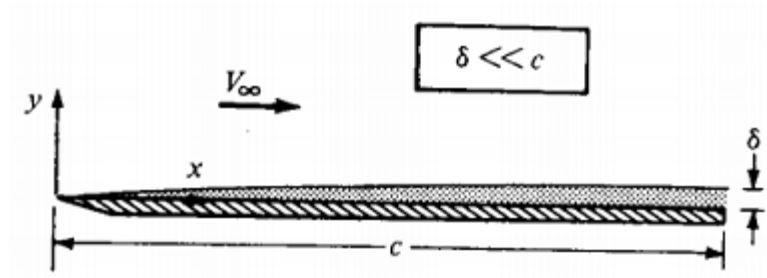


Figure 3.4 Thin boundary layer (Bes, 2006)

After some simplification, the new equations which based on the boundary layer theory assumptions are obtained. This is called boundary layer equations which are presented the following equations (3.16) to (3.19).

$$\text{Continuity Equation: } \frac{\partial(\rho u)}{\partial x} + \frac{\partial(\rho v)}{\partial y} = 0 \quad (3.16)$$

$$X - \text{Momentum Equation: } \rho u \frac{\partial u}{\partial x} + \rho v \frac{\partial u}{\partial y} = -\frac{dP_e}{dx} + \frac{\partial}{\partial y} \left(\mu \frac{\partial u}{\partial y} \right) \quad (3.17)$$

$$Y - \text{Momentum Equation: } \frac{\partial P}{\partial y} = 0 \quad (3.18)$$

$$\text{Energy Equation: } \rho u \frac{\partial h}{\partial x} + \rho v \frac{\partial h}{\partial y} = \frac{\partial}{\partial y} \left(k \frac{\partial T}{\partial y} \right) + u \frac{dp_e}{dx} + \mu \left(\frac{\partial u}{\partial y} \right)^2 \quad (3.19)$$

3.3 Computational Approach

Traditional CFD software packages provide quickly estimation a convenient design in terms of aerodynamic performance. CFD has become commonly used tool for improving, optimizing, supporting, validating and verifying procedures.

A general three-dimensional flow requires considerations of mathematical complexity and solution of strong equations when considering phenomena such as friction, heat transfer, shocks. For this reason, it is more appropriate to utilize the simpler models with respect to problem features for solutions instead of getting the general equations for every problem.

Lift, drag and moments are major and important characteristics in aerodynamic design of a missile. The axial and normal force coefficients are used to calculation of the drag and lift coefficients. Equations (3.20) and (3.21) represent relation between the body coordinate system of the forces, lift and drag. Equations (3.22) to (3.24) also represent aerodynamic coefficients of the lift, drag and moment.

$$C_D = C_A \cos \alpha + C_N \sin \alpha \quad (3.20)$$

$$C_L = C_N \cos \alpha - C_A \sin \alpha \quad (3.21)$$

$$C_D = \frac{D}{\frac{1}{2} \rho V_\infty^2 S} \quad (3.22)$$

$$C_L = \frac{L}{\frac{1}{2} \rho V_\infty^2 S} \quad (3.23)$$

$$C_M = \frac{M}{\frac{1}{2} \rho V_\infty^2 S c} \quad (3.24)$$

3.3.1 CFD Software and Finite Volume Method

Accuracy of a CFD simulation can be performed by means of verification and validation efforts. CFD results can be compared with experimental results. In computational simulation, a particular problem which occurs in nature can be simulated using computers. In order to perform simulation, computational domain is generated for a fluid dynamic problem. Computational domain involves volume of space where we can observe the physical phenomena. In addition, space of time which represent a continuum, can be interested for computational domain (Chakravarthy and Akdag, 2015).

In this thesis, the supersonic flow of missile is analyzed numerically through the use of Computational Fluid Dynamics methods. The Navier-Stokes equations that are governing equations of fluid dynamics and presented in section 3.2.3, are utilized for analyzing the motion of fluid element. The solution is performed using computer methods which give rise to Computational Fluid Dynamics. CFD idea is to take continuous domain in which the flow variables are defined for problem and change over it with a discretized domain using a mesh. If flow variable value is outside the

mesh points, it can be computed interpolating the values at the mesh point. Partial differential equations are then acquired in a continuous domain using a discrete domain. These equations are then turned into a system algebraic equation (Bes, 2006). In summary of this paragraph, the mathematical model is applied to the discretized computational domain. The results of this process, algebraic equations are formed and these equations must be solved using suitable techniques on the computers. Figure 3.5 represents differences of the continuous and discrete domain.

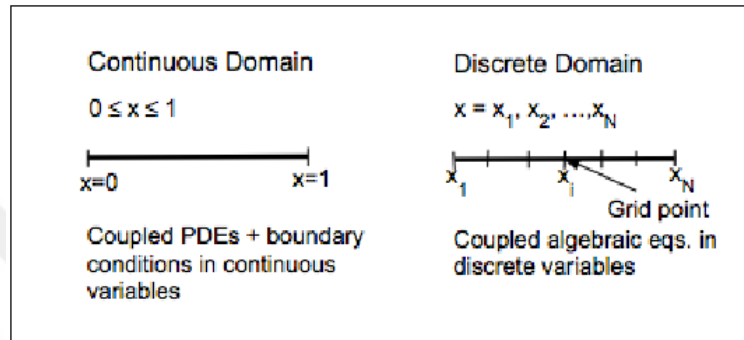


Figure 3.5 Continuous and discrete domain (Bes, 2006)

The finite volume method (FVM) evaluates partial differential equations in the form of algebraic equations (LeVeque, 2002). The values are computed on a meshed geometry at discrete places. In finite volume method, the computation is performed in a small volume which surrounds each node point on a grid. Mesh can be generated 2D which contains quadrilateral and triangular, and 3D which contains hexahedral, tetrahedral. Volume integrals are converted into the surface integrals in a partial differential equation using the divergence theorem. The obtained terms are calculated as fluxes at the surfaces of each finite volume since the flux which enters a volume is equal to leaving the adjacent volume. Figure 3.6 presents a typical infinitesimal fluid element (dV) contained in a control volume moving along a streamline. \vec{V} , ρ and \hat{n} are velocity vector, fluid density and unit vector, respectively.

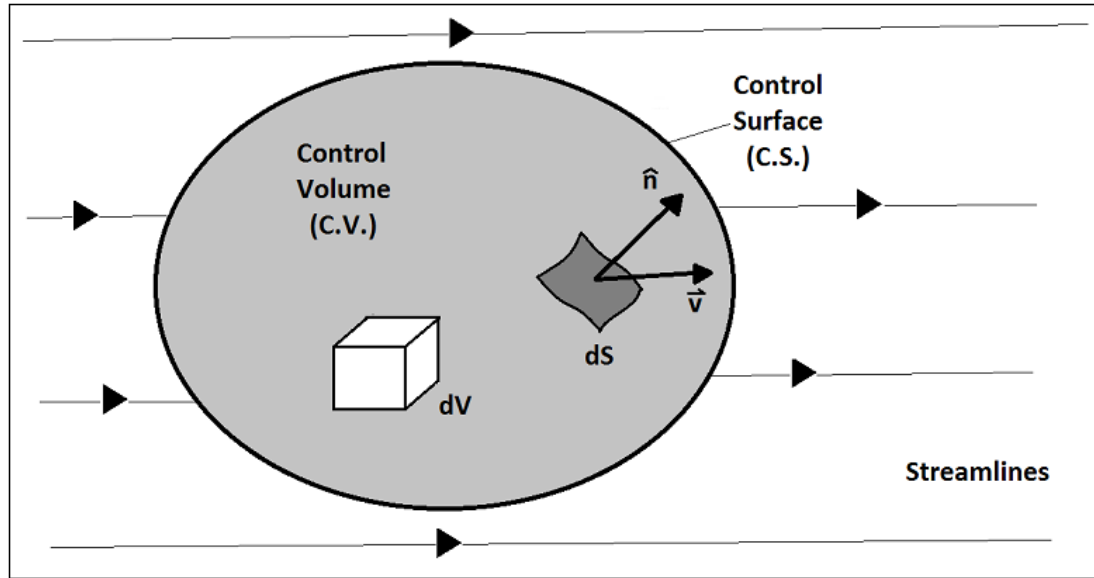


Figure 3.6 Control volume element (Bes, 2006)

Using transport equation, the governing equations of fluid motion can be obtained in the integral forms which is given in equation (3.25)

$$\frac{D\Phi}{dt} = \frac{\partial}{\partial t} \int \varphi \rho \, dVol + \int \varphi (\rho \vec{V} \cdot \hat{n}) dS \quad (3.25)$$

The transfer of mass, momentum and energy which are transferred by molecules from one location to another location by means of diffusion and convection are represented by the transport equation. When the conservation laws are applied to equation (3.25), the following equations (3.26) to (3.28) can be obtained.

$$\text{Conservation of Mass} \quad \frac{\partial}{\partial t} \int \rho dV + \int \rho \vec{V} \cdot \vec{n} dS = 0 \quad (3.26)$$

$$\text{Conservation of Momentum} \quad \sum \vec{F} = \frac{\partial}{\partial t} \int \rho \vec{V} \, dV + \int \vec{V} (\rho \vec{V} \cdot \vec{n}) \, dS \quad (3.27)$$

$$\text{Conservation of Energy} \quad \frac{\partial}{\partial t} \int \rho E \, dV + \int E (\rho \vec{V} \cdot \vec{n}) dS = \dot{Q} + \dot{W} \quad (3.28)$$

The finite volume method can be applied for unstructured meshes. This method can be used for many computational fluid dynamic problems.

3.3.2 Fluent Software

The Fluent code uses finite volume method to solve the conservation equations. The conservation of mass, momentum and energy can be rearranged to use solving problem for CFD in Fluent. Equation (3.29) represents the summarized equation for using CFD solution.

$$\frac{\partial}{\partial t} \vec{U} + \frac{\partial}{\partial x} \vec{F} + \frac{\partial}{\partial y} \vec{G} + \frac{\partial}{\partial z} \vec{H} = 0 \quad (3.29)$$

The terms of entire system of governing equations are represented by following equations (Anderson, 1995).

$$\vec{U} = \begin{Bmatrix} \rho \\ \rho u \\ \rho v \\ \rho w \\ \rho E \end{Bmatrix},$$

$$\vec{F} = \begin{Bmatrix} \rho u \\ \rho u^2 + p - \tau_{xx} \\ \rho uv - \tau_{xy} \\ \rho wu - \tau_{xz} \\ \rho uE + pu - q_x - u\tau_{xx} - v\tau_{xy} - w\tau_{xz} \end{Bmatrix}$$

$$\vec{G} = \begin{Bmatrix} \rho v \\ \rho uv - \tau_{yx} \\ \rho v^2 + p - \tau_{yy} \\ \rho vw - \tau_{yz} \\ \rho vE + pv - q_y - u\tau_{yx} - v\tau_{yy} - w\tau_{yz} \end{Bmatrix}$$

$$\vec{H} = \begin{Bmatrix} \rho w \\ \rho uw - \tau_{zx} \\ \rho vw - \tau_{zy} \\ \rho w^2 + p - \tau_{zz} \\ \rho wE + pw - q_z - u\tau_{zx} - v\tau_{zy} - w\tau_{zz} \end{Bmatrix}$$

\vec{F} , \vec{G} and \vec{H} are the called the flux terms. The solution vector is called \vec{U} since the elements in \vec{U} (ρ , ρu , ρv , ρw , ρE) are dependent variables that are acquired in steps of time. τ is the viscous stress tensor and ρ , E and p are the density, total energy and pressure, respectively. q is the heat flux vector.

3.3.3 Mesh Generation

Mesh or grid generation is a crucial issue to solve flow field or an aerodynamic engineering problem. Mesh/grid is a collection of multiple discrete points. In order to solve the problem, CFD solvers need a discrete representation of the geometry. The number of mesh elements is important for obtaining accurate result. In addition to this, boundary layer of the geometry may be critical in terms of results of the problem. Therefore, the density of the mesh generation may change regionally or the mesh structures can change according to geometry.

Mesh generation can be performed in two ways that are structured and unstructured. The structured mesh is applied for simple geometry as quadrilateral elements in a 2D and hexahedral elements in a 3D model. The structured mesh provides advantages in terms of computational time. The computer transforms the curvilinear mesh into a uniform Cartesian mesh to solve the problem easily. The unstructured mesh which available irregular connectivity between the mesh points; can be applied for complex geometries which contain sharp edges or angles or indentations. Triangular elements and tetrahedral elements are formed for 2D and 3D geometries, respectively. This mesh type provides advantages for mesh adaptation and flexibility and meshing process is faster when compared with structured mesh generation. However, the unstructured grids require larger storage and more computational time according to structured grids.

For decreasing the numerical error and obtaining accurate results, the number of mesh elements may be increased or the more discrete point can be generated around geometry and denser the grids. Therefore, finer mesh is generated in order to capture fluid flow closer to the area of interest. In addition, coarser elements can be generated to decrease computational time consuming and avoid unnecessary calculations further away from the area of interest. In this study, mesh is generated using Mesh ANSYS. The following sections mention related with viscous and inviscid mesh characteristic.

3.3.4 Viscous Mesh Characteristic

Structured mesh is properly generated close to the walls with much finer elements to capture physical phenomena and observe the effects of the boundary layer when

viscous effects are considered. In order to obtain accurate result, hybrid mesh which contains structured and unstructured grid can be generated. Figure 3.7 shows viscous mesh generation that is proper to solve viscous flow for missile geometry. In this figure, the prismatic layer is generated around the body in order to capture effects of boundary layer and tetrahedral mesh is generated fluid domain to compute flow field. Boundary layer is especially important for solving and capturing the turbulent boundary layer.

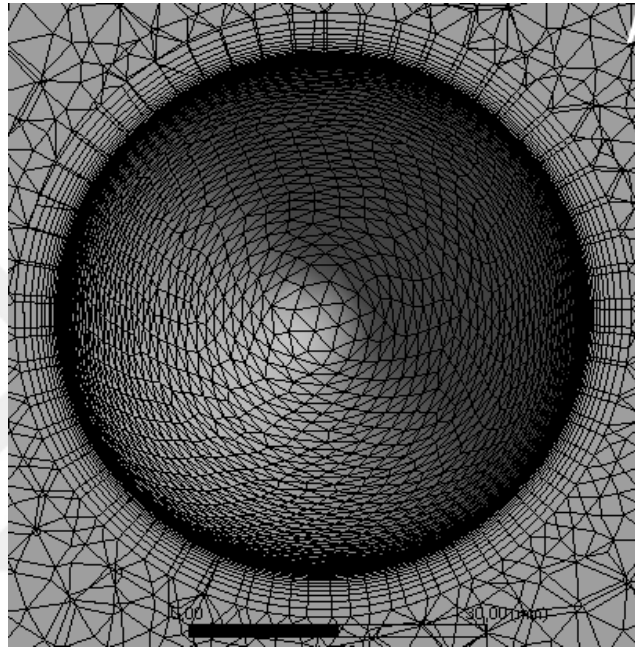


Figure 3.7 Viscous mesh for a missile body section

The value of y^+ is examining in boundary layers and it depends on Reynolds number and the mesh structure. The value of y^+ is used to compute wall shear stress in the wall-adjacent cells. Turbulent boundary layer can be separated as inner and outer regions. These regions are called viscous sublayer (inner region), fully turbulent layer (outer region). In viscous sublayer, the flow is laminar in very close the wall and molecular viscosity is essential to driver momentum transfer in this region. The turbulent boundary layer is further away from the wall however it is still within the boundary layer. In this region, the velocity profile is driven by turbulent viscosity. In addition, the blending region called the buffer layer occurs between the viscous sublayer and fully turbulent layer. Turbulent and molecular viscosities affect the flow equality. The non-dimensional parameter y^+ represents the division of turbulent boundary layer (Bes, 2006). The equation (3.30) represents y^+ formulation.

$$y^+ = y \frac{u^*}{\nu} \quad (3.30)$$

The equation (3.6) where y is the normal distance from the wall to the center point of the nearest element, ν is the kinetic viscosity and u^* is friction velocity.

Viscous effects become dominant such as in the vertical flow region around the missile geometries at high angle of attacks. Euler computations cannot predict the viscous effects in separated flow regions. In these regions, Navier-Stokes equations should be solved to predict the complete physics of the flow field and to determine accurately the aerodynamic coefficients. However, for Navier-Stokes solver applications appropriate turbulence model pertaining to the physics of the particular problem is a major issue. Besides, the grid generated for a Navier-Stokes solver that is in general much finer than Euler grid, must be suitable for the turbulence model (Oktay et al., 2000).

3.3.5 Inviscid Mesh Characteristic

The mesh generation process for the inviscid mesh characteristic does not require to account for the turbulent boundary (Bes, 2006). Therefore, the mesh may be formed less dense in proximity of the walls. Euler computations can be applied to predict for inviscid flow characteristic. In high speed, boundary layer is very thin so, inviscid method can be used to obtain solution. This provides saving computational time in solution of the problem and obtaining the results easily since the number of mesh is less than viscous problem solution.

3.4 Mesh Generation of the Missile Geometry

In this study, the investigated missile geometry was selected as N1G model which is body-tail-fins configuration. The referenced geometry is only controlled tail due to high speed. In high Mach number or high speed, stall may occur on the wing and canard. This situation may cause to lose motion control and maneuverability.

The solid model of the selected missile geometry was formed in Design Modeler in ANSYS. The dimension of the missile is given as in seen Figure 3.8. The solid model of missile geometry represents in Figure 3.9. Three-dimensional computational domain and mesh generation was formed using Design Modeler and Mesh in ANSYS, respectively. The three-dimensional mesh generation was required

because the use of periodicity was not suitable due to four fins arrangement and angle of attack. The computational domain was formed as a cylinder. The radius of the cylinder is 10 body lengths. The dimension of computational domain is 10 body lengths upstream from the tip of the missile nose and approximately 20 model body lengths downstream from the model. Fluid domain and missile view in fluid domain are represented in Figure 3.10 and Figure 3.11, respectively.

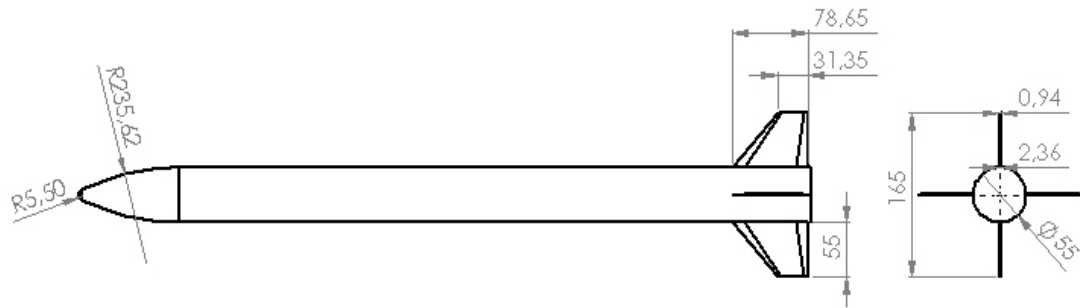


Figure 3.8 N1G missile configuration (all dimensions mm)

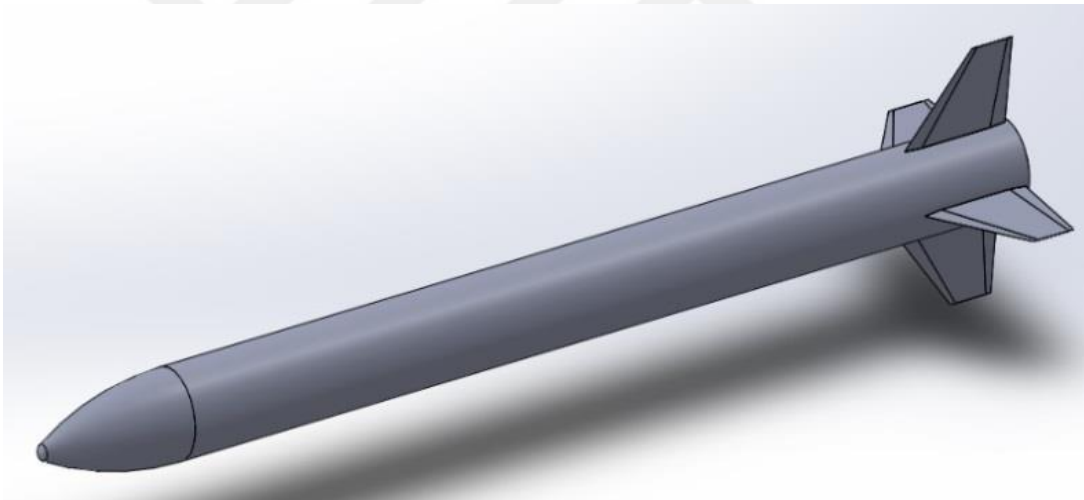


Figure 3.9 N1G missile solid model

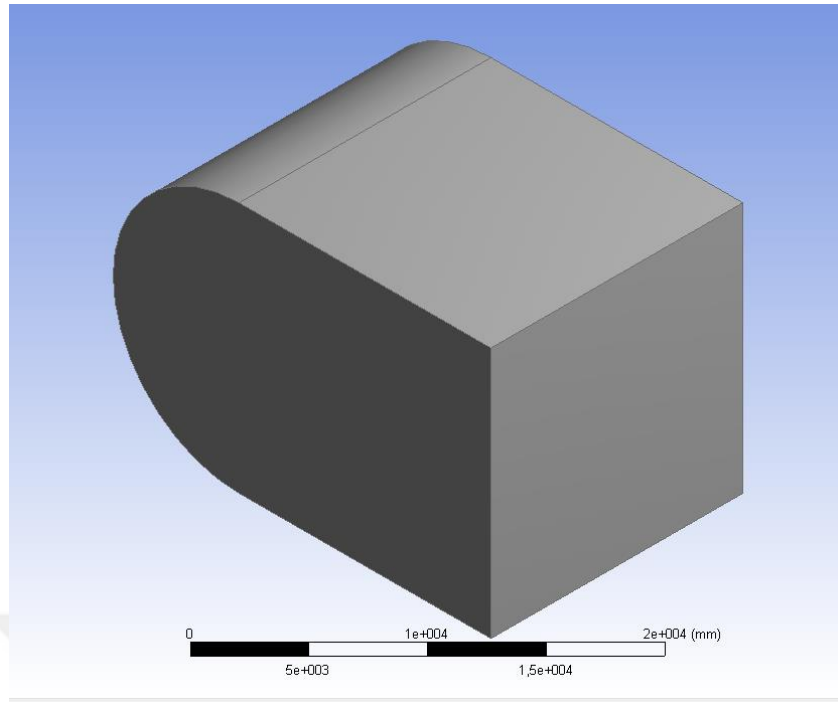


Figure 3.10 Three dimensional view of the fluid domain

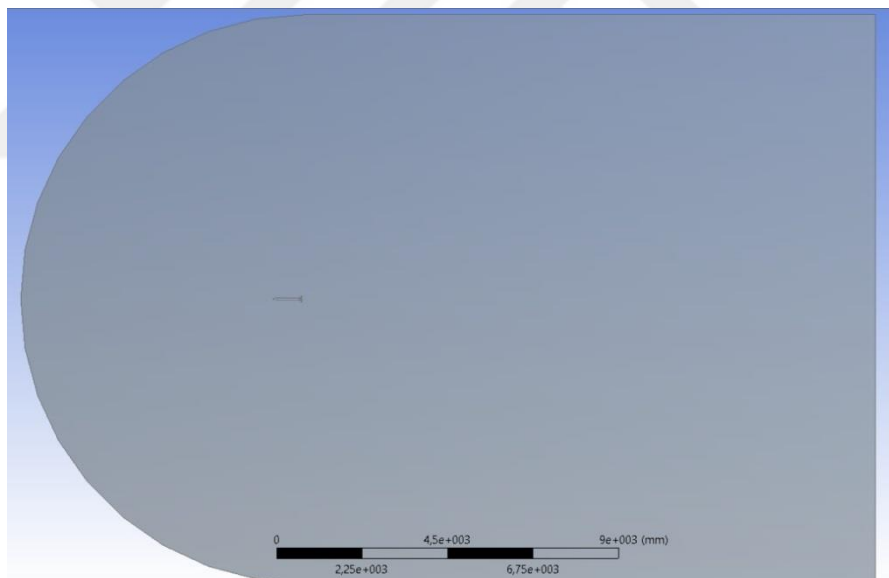


Figure 3.11 Missile view in fluid domain

The mesh generation of missile is based on capturing the shock wave since the CFD analyses have been performed at supersonic flow. So, in order to resolve the boundary layer of missile, twenty five layers of prismatic cells were formed around missile body and fins. Tetrahedral mesh elements were generated for the remaining part of computational domain. Mesh generation in fluid domain is shown in Figure

3.12. The cross-sectional views of mesh generation are presented for missile body and tail fins in Figure 3.13 and Figure 3.14, respectively.

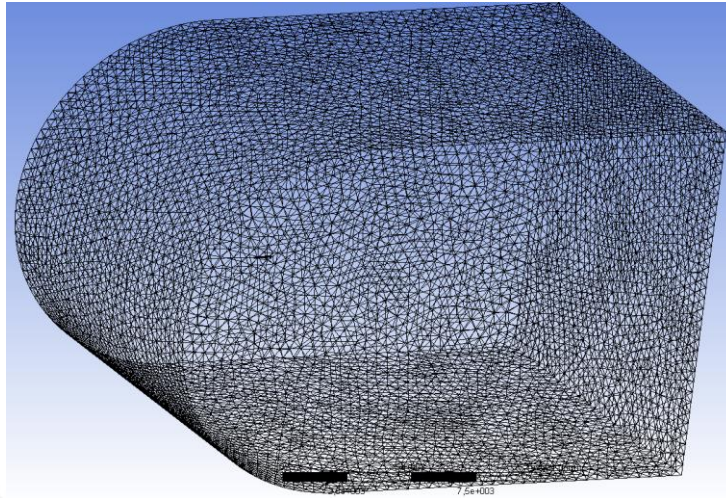


Figure 3.12 Mesh generation in fluid domain

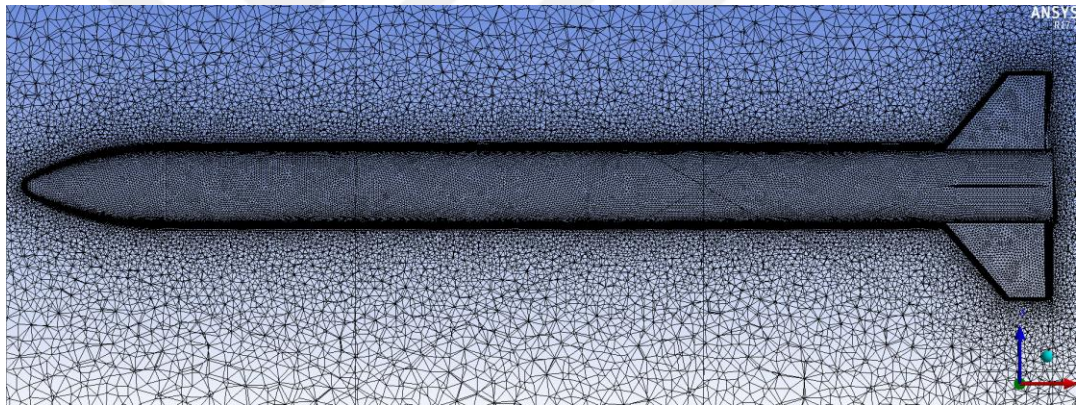


Figure 3.13 Mesh generation on missile body

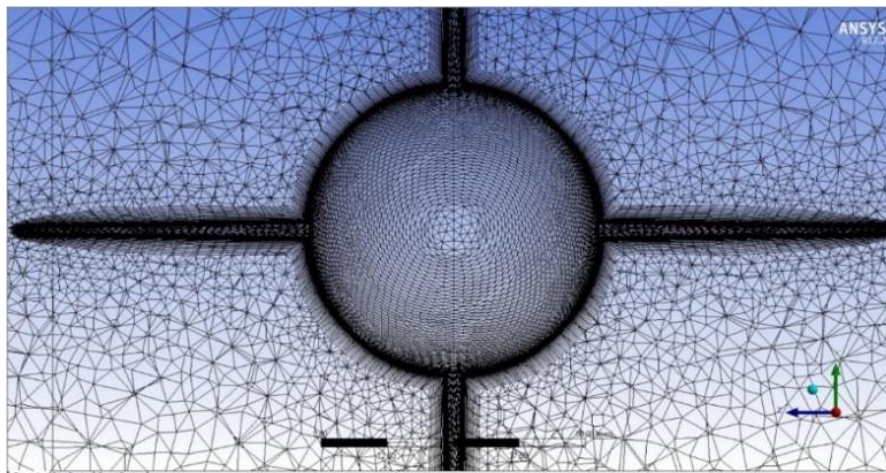


Figure 3.14 Mesh generation on missile tailfins

The mesh setting was selected proximity and curvature in order to capture flow-field around missile body. Growth rate was selected as 1.2. Patch conforming method was used to generate tetrahedral mesh for solution domain. Mesh size was formed to obtain finer mesh around the missile geometry. The non-dimensional distance from the body was $y^+ \approx 1$ for the solution. The number of generated mesh elements was about 2 millions.

3.5 Flow Solver

CFD is becoming important solvers to validate and design virtual prototyping of everything involving fluids. The solvers are computationally inexpensive, accurate and robust. In this study, the ANSYS Fluent solver was utilized to obtain drag and lift coefficients (C_D , C_L) and flow field around the missile geometry. The Fluent code that uses finite volume method solves conservation equations. A plurality of control volume elements that discretize the fluid domain are generated. The Navier-Stokes equations are used to solve the control volume elements. High computer power and time are needed to solve Navier-Stokes equations. However, Navier-Stokes equations are simplified to provide convenience. Hence, Reynolds-Averaged Navier-Stokes equations, which take into account the viscous effects in a simpler way, are used for solution of the flow. Therefore, Reynolds-Averaged Navier-Stokes (RANS) equations can be used for complex flow solution (DeSpirito et al., 2004). In addition, this method provides enough accuracy and faster processing when compared with Large Eddy Simulation (LES) method which provide high accuracy however, it takes a lot of computer power or memory and running time (Franzluebbbers, 2013).

In this study, steady-state computations were used to calculate the flowfield using Fluent 17.2 version. Density based solver was selected since the solution of problem was carried out at high speeds that are larger than 0.3 Mach so, it can be called compressible flow. The continuity equation is used to find density field in the density approach. The implicit formulation with the Green-Gauss Cell based gradient option solver was also selected. The implicit method solvers use differences between physical parameters that mean one iteration step to the next iteration as a means of determining as solution accuracy is achieved. This difference is named residual error. The change of aerodynamic coefficients and flow residuals were tracked to determine convergence during the computations. When the change of aerodynamic

coefficients value became less than 1% during 100 iterations and the flow residuals reached to 10^{-5} , the computation run was finished. The missile body surface was also selected the wall type due to no-slip condition. Solution methods scheme in Fluent represents in Figure 3.15.

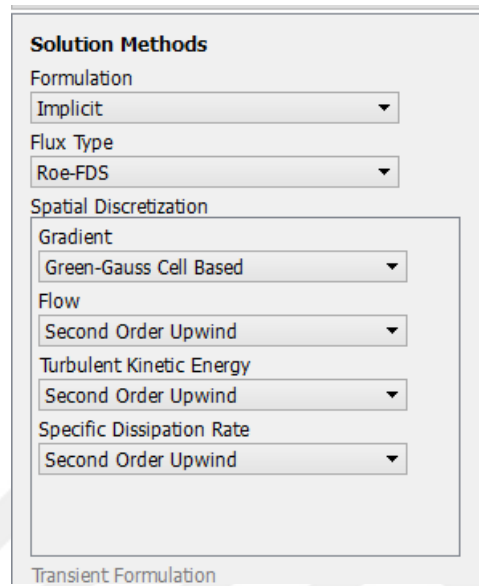


Figure 3.15 Solution methods

The standard residual error monitor that evaluates and compares continuity, velocity and total energy values for the entire mesh is available in Fluent. Second order upwind is used with tri/tet mesh or when flow is not aligned with grid. Second order upwind method (Discretization Interpolation methods) was selected for flow, turbulent kinetic energy and specific dissipation rate to obtain more precious results. The Roe Flux-Different Splitting (Roe-FDS) was used for this study due to the fact that Advection Upstream Splitting Method (AUSM) wasn't convenient for convergence of solution. Convergence is achieved overall mass, momentum, energy and scalar balances. Courant number is also important parameter for the solution. It helps to find the appropriate time step for a given mesh. Sonic and supersonic flows require to run high courant numbers since the extent of particles flowing through cells may be high and it can be caused to form shock waves. Courant number for the density based implicit formulation; it is possible to increase 20, 30, 50 or even higher according to the complexity of the problem. Figure 3.16 shows the solution control scheme.

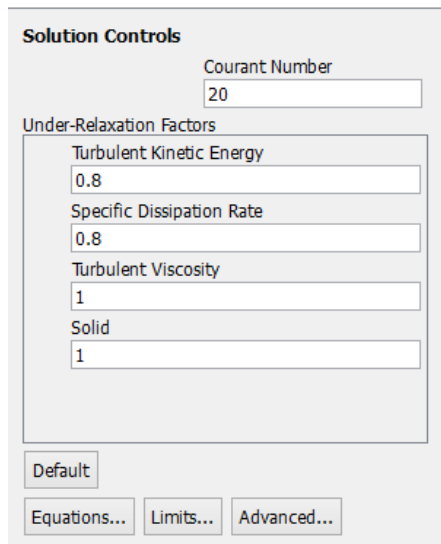


Figure 3.16 Solution controls

RANS equations require turbulence model equations in order to solve high accuracy in turbulence flow. In this thesis, three turbulence models that are SST $k-\omega$, Realizable $k-\varepsilon$ and Spalart-Allmaras, were used to solve missile aerodynamics since it is suitable to solve complex aerodynamic shape at supersonic Mach number and high angle of attack. The following sections are given turbulence models and their properties and formulations.

3.5.1 Turbulence Models

Most engineering flows are turbulent. Solution of turbulence flows needs to select a turbulence model and near-wall modeling approach providing inlet boundary conditions for the turbulence model. Fluent enable to simulate turbulent flow around the missile at supersonic flow. The 3-D, RANS (The Reynolds-averaged Navier-Stokes) equations are solved using finite volume method for complex flow solution. The choice of the turbulent model is a crucial issue to be performed simulation for turbulent flows. If the chosen of turbulence model is suitable for modeling certain physical phenomena, it will give good results when compared with natural situation or experimental results. SST $k-\omega$, Realizable $k-\varepsilon$ and Spalart-Allmaras are the most famous based turbulence models. The following subsections describe these turbulence models.

3.5.1.1 Spalart-Allmaras Turbulence Model

Spalart-Allmaras model that is commonly used is one equation model. So, it is quicker and has low computational time and power requirements. In addition, it is convenient for transonic flows and stable with good convergence. This model also gives good results for the flows with adverse pressure gradient. The transport equation can be solved by the Spalart-Allmaras model for the variable $\tilde{\nu}$ which is used to attain turbulent kinematic viscosity. The transport equation of the Spalart-Allmaras turbulence model is expressed in equation (3.31) (Spalart and Allmaras, 1992).

$$\frac{D\tilde{\nu}}{Dt} = \frac{1}{\sigma} [\nabla((\nu + \tilde{\nu})\nabla\tilde{\nu}) + c_{b2}(\nabla\tilde{\nu})^2] + c_{b1}\tilde{S}\tilde{\nu}(1 - f_{t2}) - \left[c_{w1}f_w - \frac{c_1}{\kappa^2}f_{t2} \right] \left[\frac{\tilde{\nu}}{d} \right]^2 + f_{t1}(\Delta q)^2 \quad (3.31)$$

From Equation (3.7) , $\frac{1}{\sigma} [\nabla((\nu + \tilde{\nu})\nabla\tilde{\nu}) + c_{b2}(\nabla\tilde{\nu})^2]$ is the diffusion term, and $c_{b1}\tilde{S}\tilde{\nu}(1 - f_{t2})$ is the production term and $\left[c_{w1}f_w - \frac{c_1}{\kappa^2}f_{t2} \right] \left[\frac{\tilde{\nu}}{d} \right]^2$ is the destruction term of turbulent viscosity and $f_{t1}(\Delta q)^2$ is the trip term which is generally ignored when performing fully turbulent analysis.

3.5.1.2 Standard and Realizable k-ε Turbulence Model

The Standard k-ε turbulence model (k is kinetic energy and ε is turbulent dissipation) includes two transport equations which account for diffusion of turbulent energy and convection. The k-ε turbulence model is isotropic that means the ratio between the mean rate of deformation and the Reynolds stress is the same in every direction. K-ε model gives good solution for free shear layer flows with relatively small pressure gradients. In addition, this model shows superior performance for boundary layer under strong adverse pressure gradients, recirculation and separation (Ansys inc, 2011). The enhanced wall treatment is the only viscous sublayer resolving near wall treatment when using any k-ε model. The realizable k-ε differs from k-ε in terms of C_μ calculation. The other difference is based upon ε equation that is derived from the mean-square vorticity fluctuation (Shih et al., 1995).

The turbulent kinetic energy k and the turbulent dissipation ε are defined in Equation (3.32) and Equation (3.33);

$$k = \frac{1}{2}[\bar{u}^2 + \bar{v}^2 + \bar{w}^2] \quad (3.32)$$

$$\varepsilon = v_t \overline{\frac{\partial u_i \partial u_i}{\partial x_j \partial x_j}} \quad (3.33)$$

The standard k-ε two equations turbulence model is expressed in Equation (3.34) and Equation (3.35);

$$\rho \frac{dk}{dt} = \frac{\partial}{\partial x_j} \left[\left(\mu + \frac{\mu_t}{\sigma_k} \right) \frac{\partial k}{\partial x_j} \right] + P_k - \rho \varepsilon \quad (3.34)$$

$$\rho \frac{d\varepsilon}{dt} = \frac{\partial}{\partial x_j} \left[\left(\mu + \frac{\mu_t}{\sigma_\varepsilon} \right) \frac{\partial \varepsilon}{\partial x_j} \right] + c_{\varepsilon 1} P_k \frac{\varepsilon}{k} - c_{\varepsilon 2} \rho \frac{\varepsilon^2}{k} \quad (3.35)$$

3.5.1.3 Standard and SST k-ω Turbulence Model

K-ω turbulence models (k is kinetic energy and ω is turbulent frequency) with two equations were improved to solve complex turbulent flow field which includes separation and unsteadiness. Standard k-ω model shows good performance at low Reynolds number and wall bounded. However, this model requires good mesh resolution near the wall to predict separation.

The shear stress transport (SST) k-ω turbulence model which is combination of Standard k-ω model and Standard k-ε model is two-equation model (Menter, 1994). It is convenient in terms of adverse pressure gradients and for separated flow. SST is recommended for correctly simulating the boundary layer. The combination function is used in the near wall region where Standard k-ω model operates the near wall region and Standard k-ε model operates away from the walls using a blending function (Ansys inc, 2011). Disadvantage of SST k-ω model is that it is difficult to converge and it is not convenient to use for free shear flows when compared with standard k-ω model because of dependency on wall distance of SST k-ω model.

The SST k-ω two equations model is expressed in Equation (3.36) and Equation (3.37);

$$\frac{\partial}{\partial t} (\bar{\rho} k) + \frac{\partial}{\partial x_j} (\bar{\rho} \bar{u}_j k) = \frac{\partial}{\partial x_j} \left[\left(\mu + \sigma_k \mu_t \right) \frac{\partial k}{\partial x_j} \right] + P_k - \beta \bar{\rho} \omega k \quad (3.36)$$

$$\begin{aligned}
& \frac{\partial}{\partial t}(\bar{\rho}\omega) + \frac{\partial}{\partial x_j}(\bar{\rho}\bar{u}_j\omega) \\
&= \frac{\partial}{\partial x_j} \left[(\mu + \sigma_\omega \mu_t) \frac{\partial \omega}{\partial x_j} \right] + 2(1 - F_1)\bar{\rho}\sigma_{\omega 2} \frac{1}{\omega} \frac{\partial k}{\partial x_j} \frac{\partial \omega}{\partial x_j} + \alpha \frac{\omega}{k} P_k \\
& - \beta \bar{\rho}\omega^2
\end{aligned} \tag{3.37}$$

In Equation (3.37), P_k (production of turbulence) and τ_{ij} can be defined as following Equations (3.38) and (3.39).

$$P_k = \tau_{ij} \frac{\partial u_i}{\partial x_j} \tag{3.38}$$

$$\tau_{ij} = \mu_i \left(\frac{\partial u_i}{\partial x_j} + \frac{\partial u_j}{\partial x_i} - \frac{2}{3} \delta_{ij} \frac{\partial u_i}{\partial x_j} \right) - \frac{2}{3} \rho k \delta_{ij} \tag{3.39}$$

The constant F_1 that is available in Equation (3.37) is equal to 1 for the k - ω model and it is equal to 0 for the k - ε model. Turbulent viscosity is defined as Equation (3.40) for SST k - ω model.

$$\nu_t = \frac{0.31k}{\max(0.31w, \Omega F_2)} \tag{3.40}$$

Ω and F_2 are defined by Equations (3.41) and (3.42) as follows.

$$\Omega = \left| \frac{\partial v}{\partial x} - \frac{\partial u}{\partial y} \right| \tag{3.41}$$

$$F_2 = \text{Tanh} \left\{ \left[\max \left(2 \frac{\sqrt{k}}{0.09wy}, \frac{500\nu}{wy^2} \right) \right]^2 \right\} \tag{3.42}$$

3.5.2 Setup and Solver Properties

In this study, the aerodynamic solution was carried out at between 1.4 and 4 Mach numbers that are called compressible flow. Therefore, the air was selected as ideal gas. Double precision solver was used to run the simulations and parallel processing was chosen.

In boundary condition, inlet-velocity was selected for inlet and pressure-outlet was selected for outlet and wall was selected for missile body. The other edges were chosen as symmetry. Wall indicates no-slip on the missile body. In reference value,

the missile projectile area was used as 0.002376 m^2 as specified reference article. The baseline of the missile length is 0.763 m and velocity of the air is specified between 1.4 Mach and 4 Mach. The simulation was compute from inlet. Courant-Friedrich-Lewy (CFL) number was set as default value for implicit. Solution methods were set to solve the flow as implicit, Green-Gauss cell base and second order upwind. Under-relaxation factor was also set as default value. However, it is reduced for faster convergence of the solution. The change of flow residuals and aerodynamic coefficients which are drag and lift, were tracked to determine the convergence during the solutions. The residuals were specified as 10^{-5} and convergence criteria were provided for solution of the flow. The convergence is affected Mach number, mesh numbers and size. In Fluent, the pressure and viscous forces which are computed from flowfields were integrated to calculate the aerodynamic coefficients along the missile body and fin surfaces.

Aerodynamic analysis of the missile is performed in parallel environment on Casper Workstation with 32 cores Intel Xeon E5- 2683 v4 processors and 128 GB RAM.

3.6 Mesh Dependency/Sensitivity

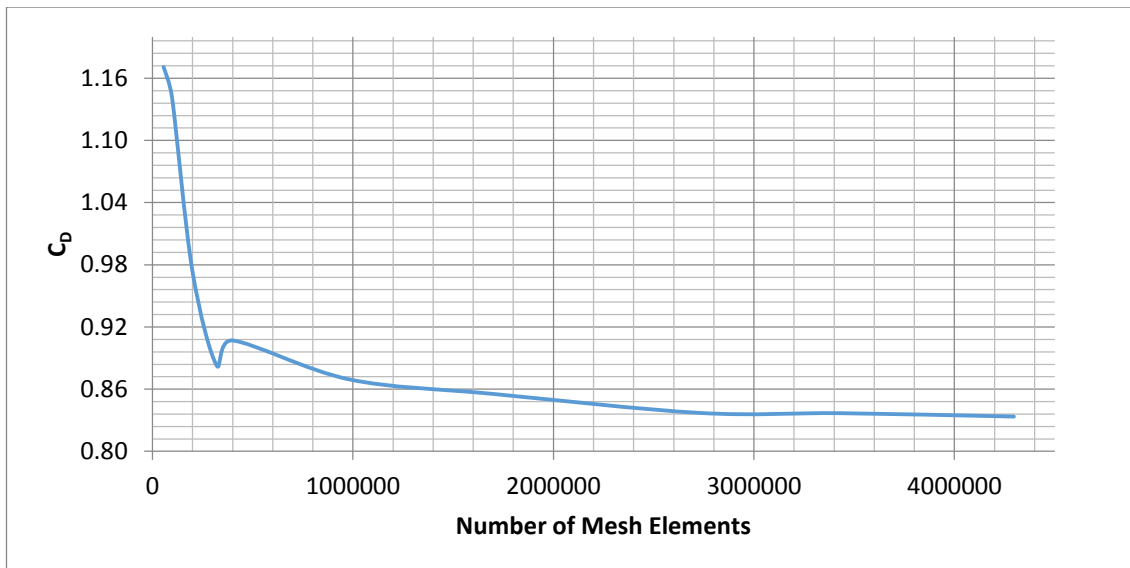
The goal of this section is to use mesh adaption to produce a finer and courser mesh and then compare the results the original mesh with adapted mesh. The number of mesh elements is determined according to convergence of the solution or grid sensitivity test in the simulation. In order to observe the mesh sensitivity and effects on the CFD simulation results, mesh independency study of missile is performed. This study was carried out using SST $k-\omega$, $k-\varepsilon$ and Spalart-Allmaras turbulence models at course, medium and finer mesh resolution. Mesh independent solution is a fundamental need for all missile or rocket designers due to obtaining accurate aerodynamic coefficients of missile.

In this study, viscous mesh characteristic was used for solution. So, mesh dependency or sensitivity is important to determine enough number of the mesh for the solution of problem in point of saving computational time. The results of the solutions are negligible change, after sufficient mesh number is attained for solution of problem.

In order to show mesh independency, the number of the mesh elements was generated between approximately 100000 to 4.2 million. Growth rates were changed with respect to mesh density. For finer mesh, the prismatic cell generated on boundary layer was formed with twenty five layers and 1.1 growth rate. The size of the mesh and its growth rate were also changed to obtain course and finer mesh. After CFD solution was performed for each case and finer mesh elements, it was observed that 2008827 elements were enough to obtain a good agreement with experimental results. It also ensured the convergence of the computed aerodynamic coefficients and residuals. The computation was initially performed on a course mesh with a non-dimensional distance from the body or model of $y^+ \approx 40$ and for finer mesh, the non-dimensional distance was $y^+ \approx 1$.

The results of the solution showed that mesh independency was ensured for finer grids that are between about 2 million and 4.2 million elements (Güzelbey et al., 2018). The same mesh structure was used for 1.4, 2, 2.5 and 4 Mach numbers at 6° AoA.

Figure 3.17 to 3.20 are represented to show mesh independency for C_D and C_L values at 1.4, 2, 2.5 and 4 Mach numbers.



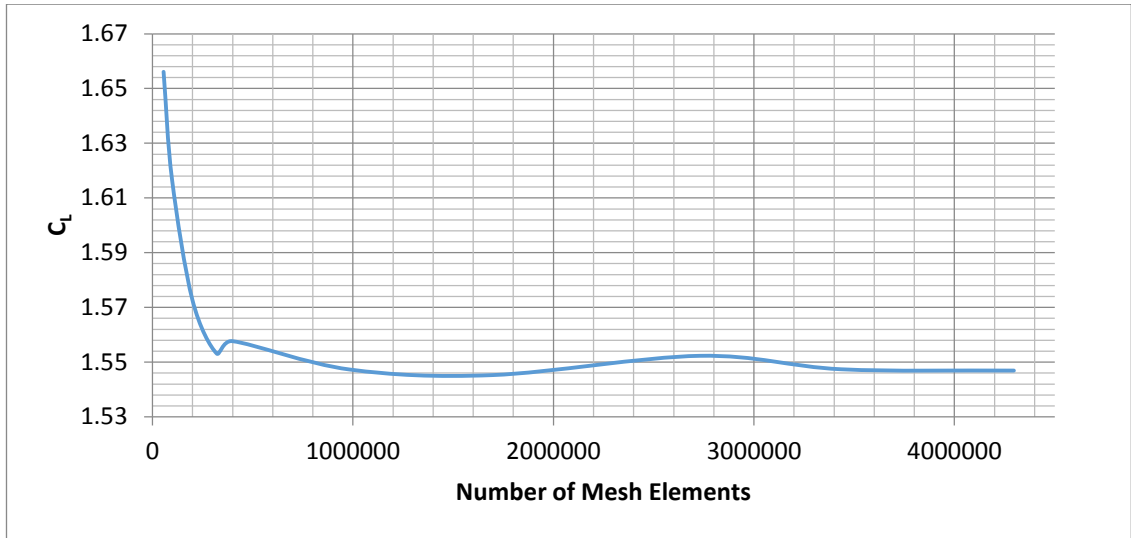


Figure 3.17 C_D and C_L values with respect to number of mesh elements for 1.4 Mach number

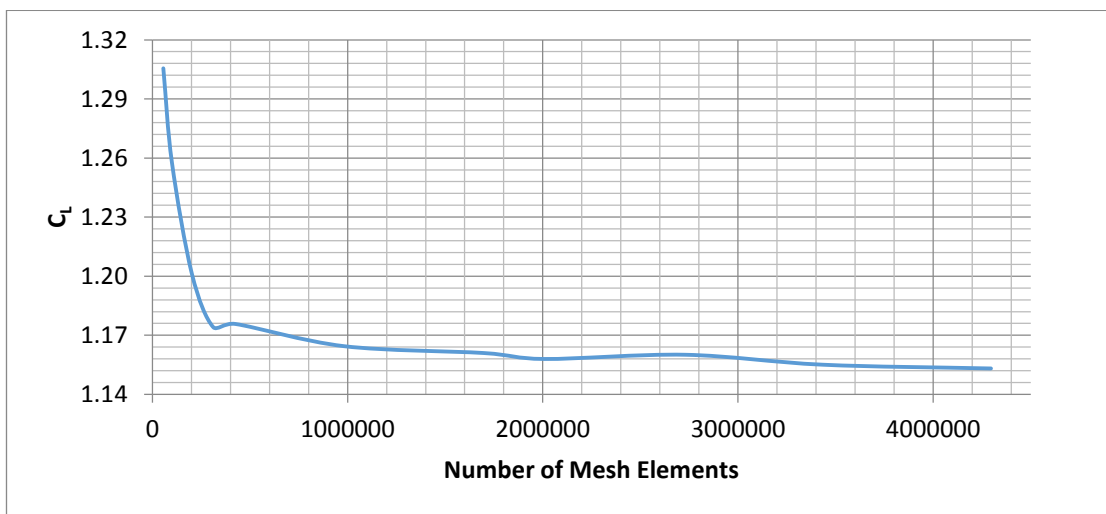
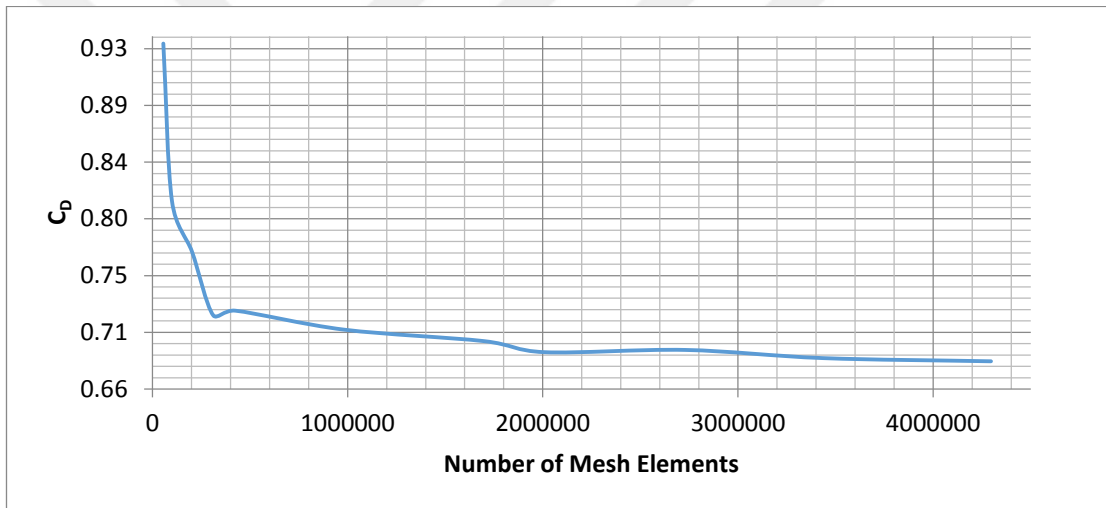


Figure 3.18 C_D and C_L values with respect to number of mesh elements for 2 Mach number

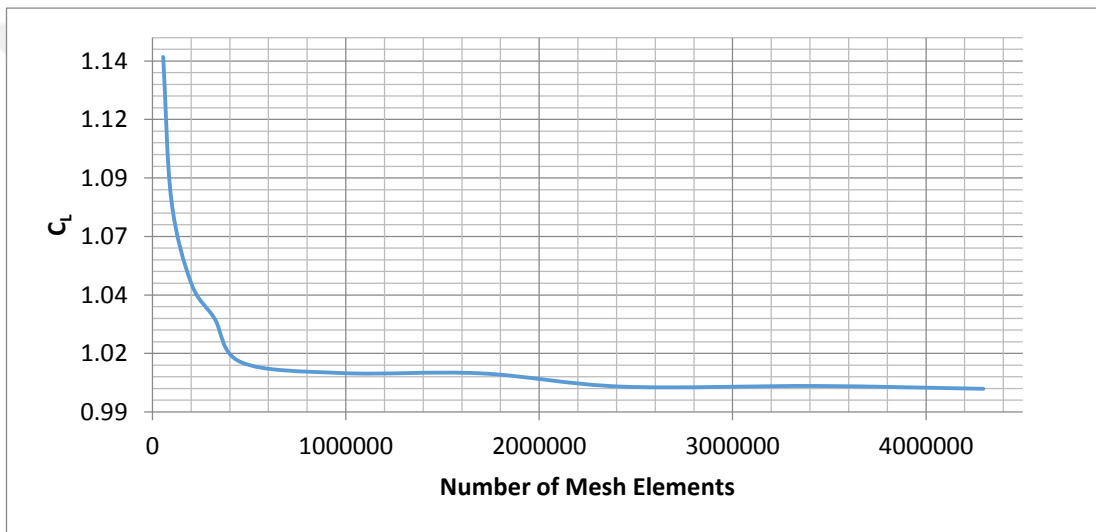
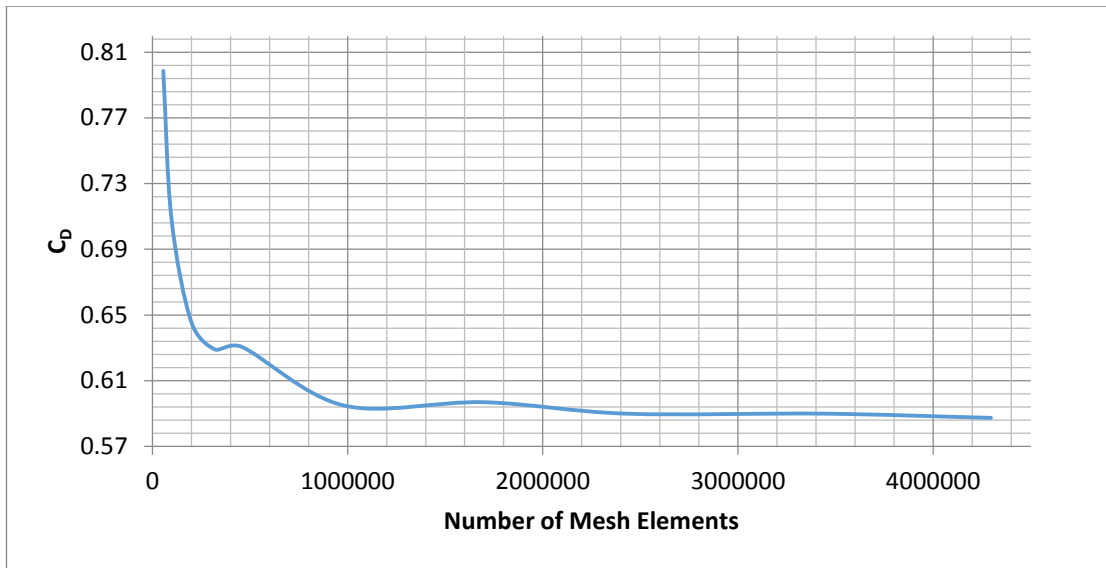
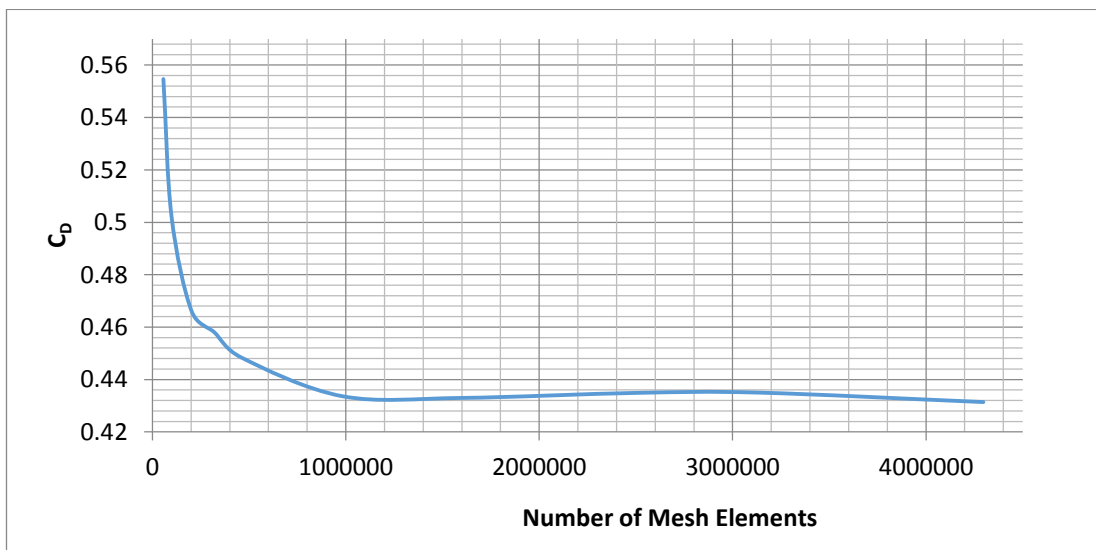


Figure 3.19 C_D and C_L values with respect to number of mesh elements for 2.5 Mach number



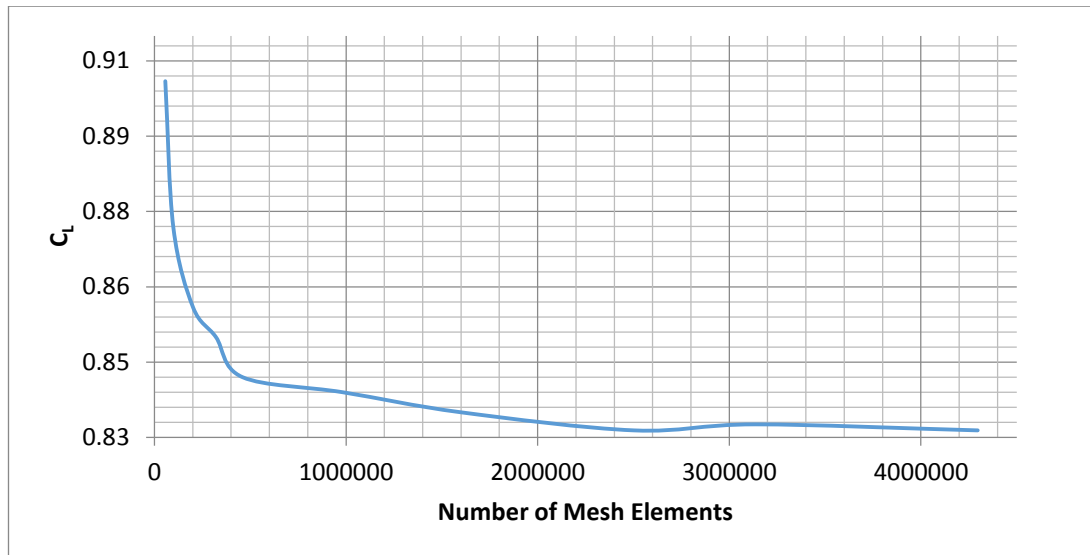


Figure 3.20 C_D and C_L values with respect to number of mesh elements for 4 Mach number

3.7 Validation Study

In this section, the comparison of three turbulence models and experimental studies which are available in literature, are presented to indicate validation of CFD solution at supersonic Mach numbers for N1G missile model.

Table 3.1 Differences between the experimental (Vidanović et al., 2017) and numerical results.

Mach number	AoA	C_D (Fluent)	C_D (Exp)	Disc. %	C_L (Fluent)	C_L (Exp)	Disc. %
1.4	3.96°	0.688	0.6971	1.3	1.024	1.067	4.02
	5.97°	0.7977	0.8068	1.12	1.547	1.609	3.85
2	3.99°	0.5834	0.5903	1.16	0.752	0.773	2.61
	6.02°	0.673	0.6831	1.47	1.148	1.184	3.01
2.5	4.01°	0.5181	0.5134	0.92	0.648	0.676	4.1
	6.05°	0.5874	0.5971	1.61	1.011	1.055	4.17
4	4.03°	0.3808	0.3931	3.12	0.502	0.532	5.49
	6.08°	0.4359	0.4539	3.95	0.829	0.881	5.88

CFD solution was carried out for Mach number 1.4 at 3.96° and 5.97° AoA, for Mach number 2 at 3.99° and 6.02° AoA, for Mach number 2.5 at 4.01° and 6.05° AoA, for Mach numbers 4 at 4.03° and 6.08° AoA, respectively. Drag and lift coefficients values were computed since these values are available in literature to compare with experimental results for the N1G missile model (Vidanović et al., 2017). Table 3.1 represents CFD and experimental results and discrepancies of the results.

The solution of CFD results show that these three turbulence models which are SST k- ω , Realizable k- ϵ and Spalart-Allmaras match well experimental results. It is concluded that SST k- ω turbulence model gave reasonable results at supersonic flow and high AoA. In addition, SST k- ω model is convenient to solve near wall region. Drag and lift coefficients versus Mach numbers at 4° AoA are given in Figure 3.21 and Figure 3.22, respectively. Drag and lift coefficients versus Mach numbers are also presented at 6° AoA in Figure 3.23 and Figure 3.24, respectively. In addition, lift to drag ratio (C_L/C_D) is presented in order to show how to change the performance of missile at high AoA. Figure 3.25 represents lift to drag ratio versus AoA at supersonic Mach numbers (1.4, 2, 2.5 and 4). From Figure 3.25, it can be observed that the performance of missile increases up to 12° AoA for each Mach number. However, after exceeding 12° AoA, lift to drag ratio decreases. Moreover, lift to drag ratio increase with increased Mach number as in seen Figure.

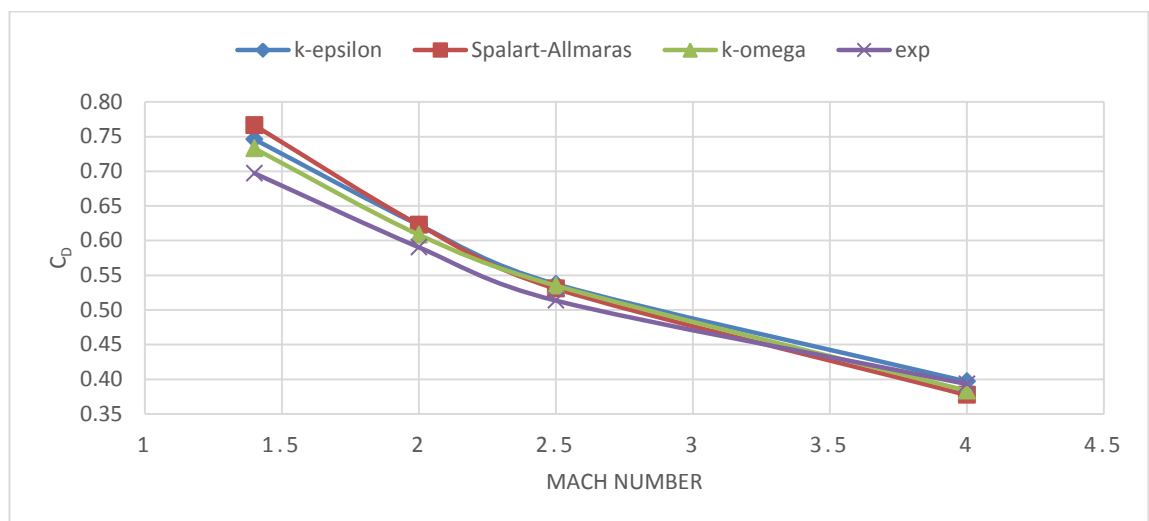


Figure 3.21 Drag coefficient versus Mach number at 4° AoA

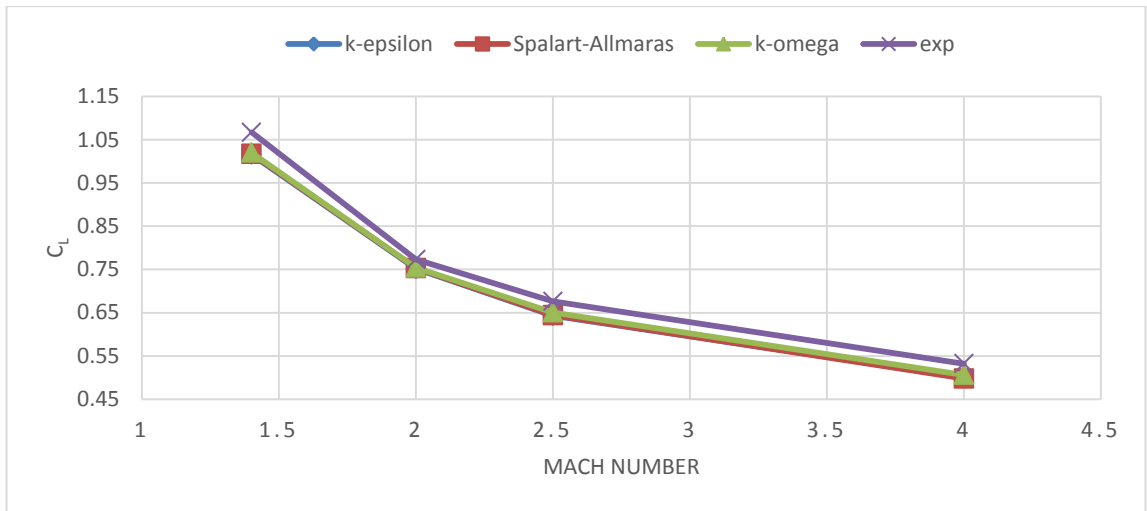


Figure 3.22 Lift coefficient versus Mach number at 4° AoA

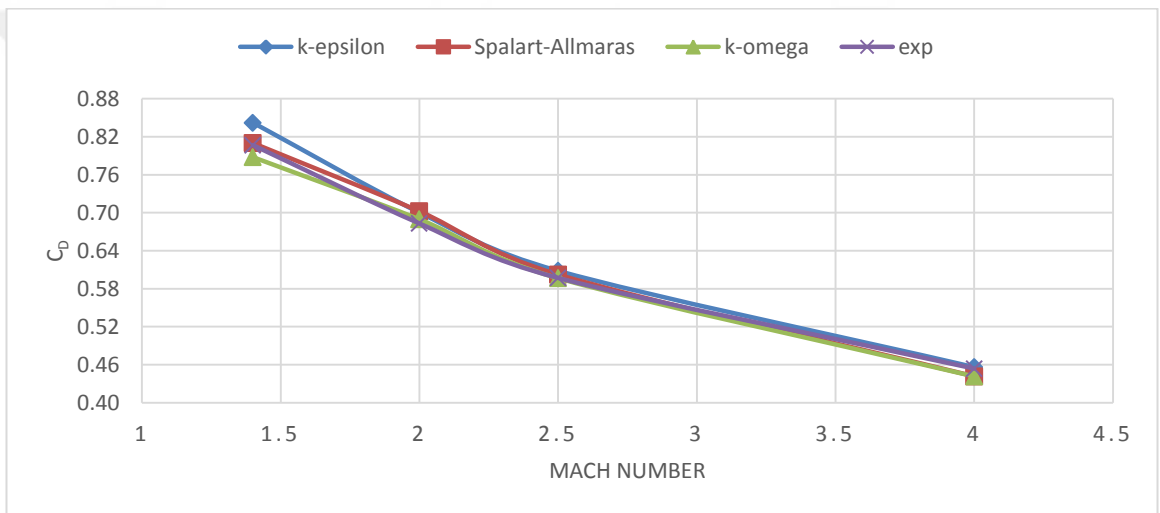


Figure 3.23 Drag coefficient versus Mach number at 6° AoA

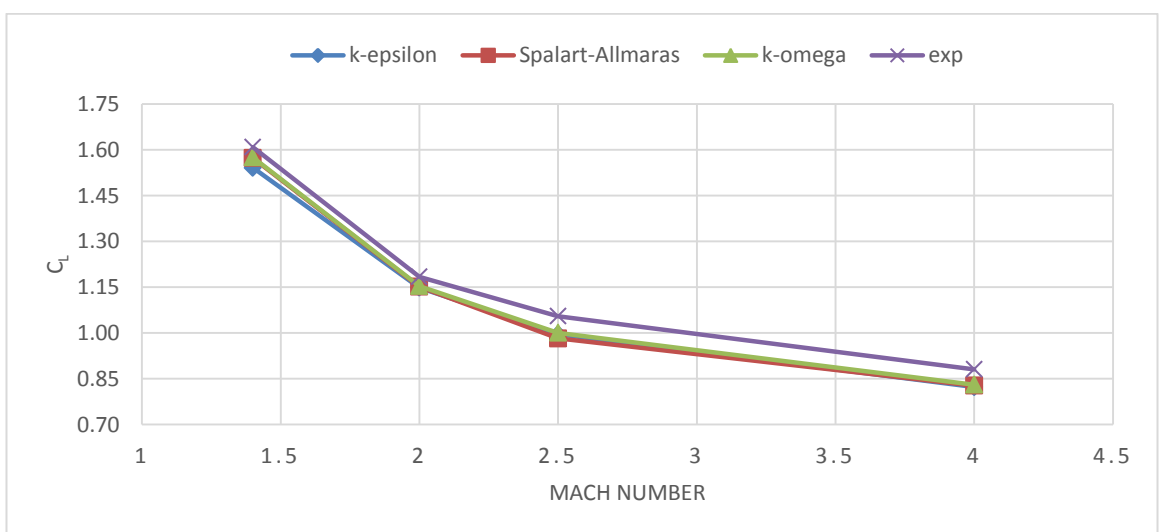


Figure 3.24 Lift coefficient versus Mach number at 6° AoA

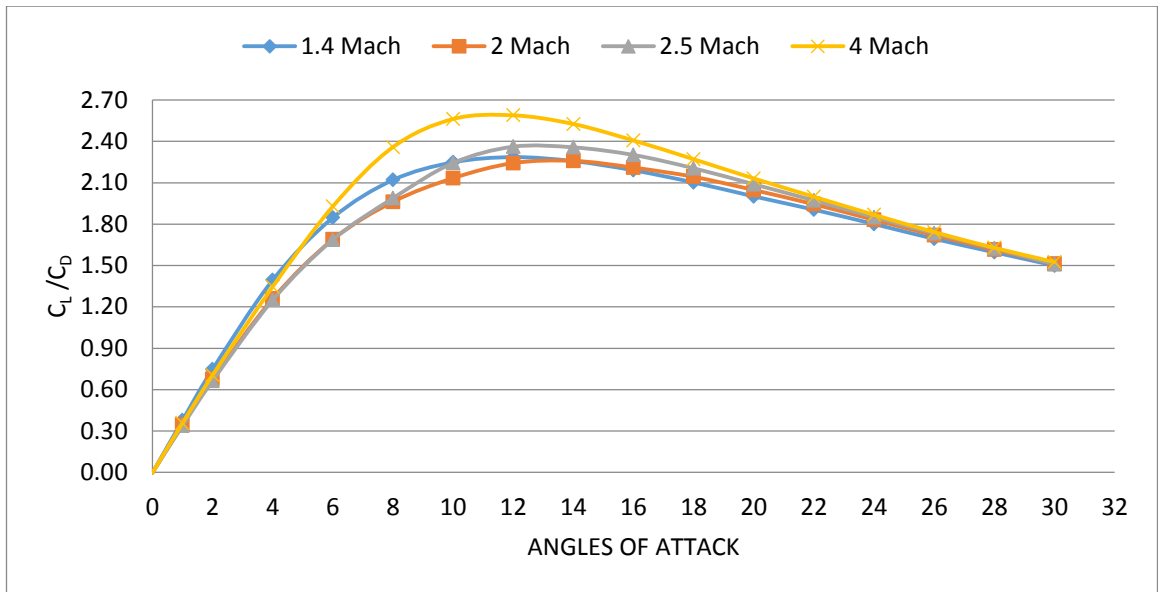


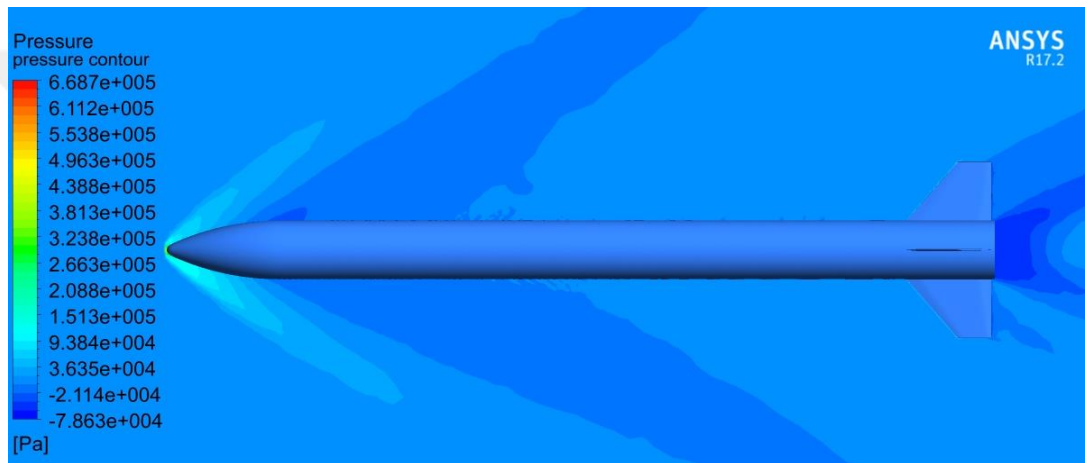
Figure 3.25 Lift to drag ratio versus AoA at supersonic Mach numbers

The pressure contours of the missile are presented to show effects of pressure on missile body and fins and separation of the flow. Pressure contours and pressure values are given in Figure 3.26 and Figure 3.27 at 4° and 6° AoA and 1.4, 2, 2.5, 4 Mach numbers, respectively.

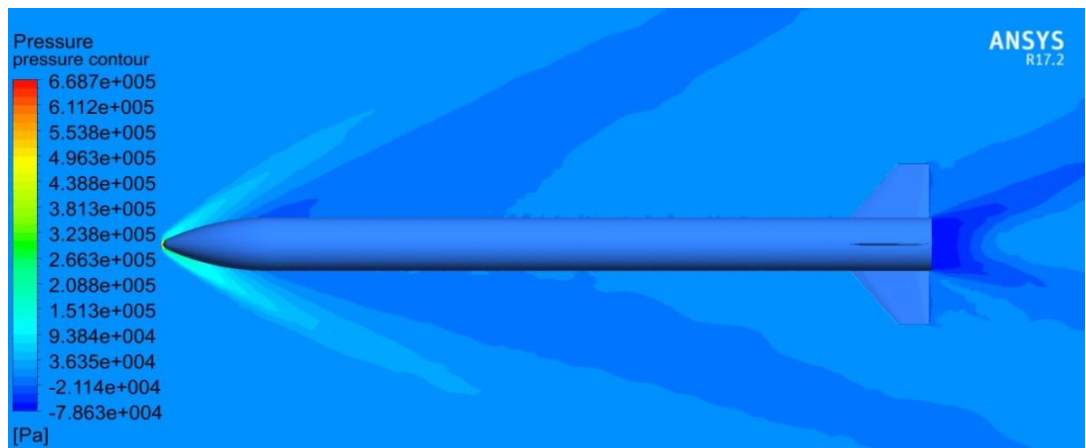
When figures are examined, minimum and maximum pressure values are same since the pressure contours are observed and commented easily. The pressure which occur on missile nose tip, increased when Mach number was increased. Low pressure area occur rear of the missile. However, the low pressure area increases with increased Mach number. This case can cause to increase drag forces but, lift force also increase with Mach number at the same time. Therefore, lift to drag ratio have high value at high Mach number. Moreover, the angle of shock waves that is between wave and missile body was decreased when Mach number was increased. It can be observed that the pressure differences between the upper and lower surface of missile nose increases with increased Mach number. Lift to drag ratio also increase when AoA is increased from 4° AoA to 6° AoA.



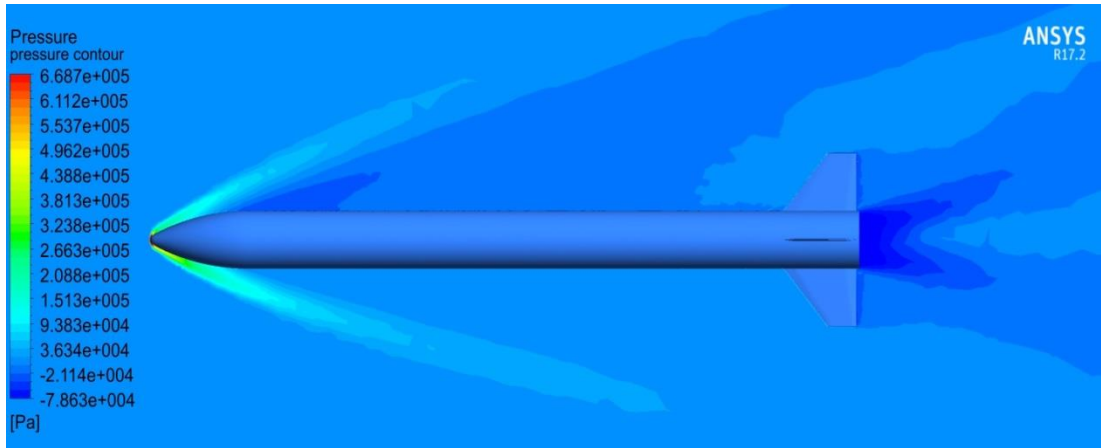
(a)



(b)



(c)

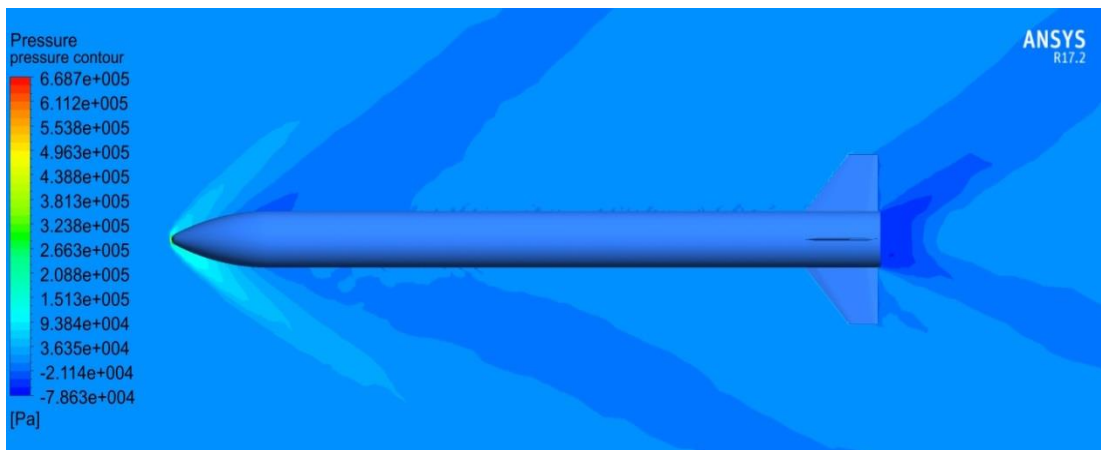


(d)

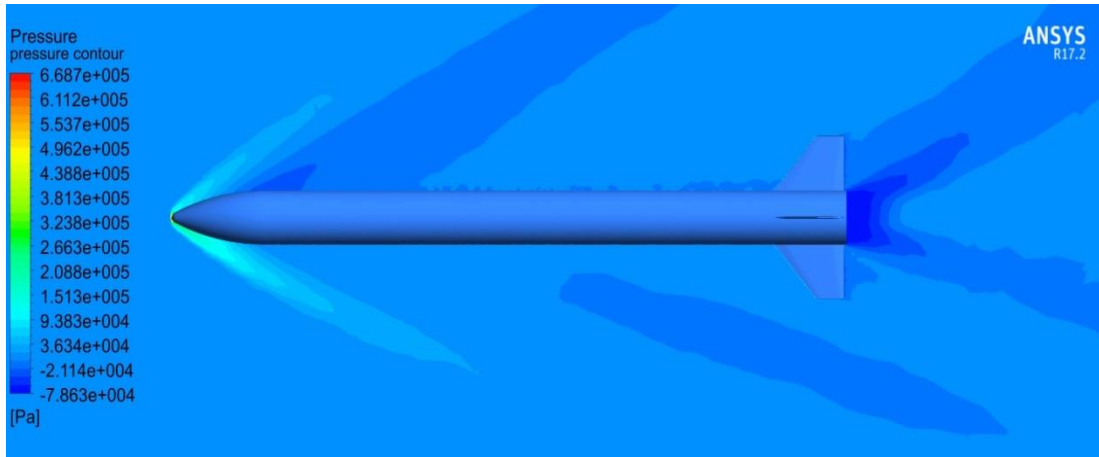
Figure 3.26 Pressure contour of baseline missile model at 4° AoA (a: 1.4 Ma, b: 2 Ma, c: 2.5 Ma, d: 4 Ma)



(a)



(b)



(c)



(d)

Figure 3.27 Pressure contour of baseline missile model at 6° AoA (a: 1.4 Ma, b: 2 Ma, c: 2.5 Ma, d: 4 Ma)

Pressure contours and pressure values are given from Figure 3.28 at 1.4 Mach numbers. There are six cases in Figure which represents AoA between 4° and 24° . It can be observed that the pressure differences between the upper and lower surface of missile nose increases with increased AoA. In addition, the pressure occurring on lower part of tail fins increase with increased AoA. Low-pressure region is observed rear of the missile. This region is shifting upward with the increase in AoA. Therefore, the pressure differences lower and upper region increase and this improves the lift to drag ratio. However, as mentioned earlier, this ratio rises up to 12° and after that point, it decreases since flow separation occurs. When flow separation occurs, drag force increase and lift force decrease. So, the performance of missile or lift to drag ratio decreased. In some cases, drag coefficients increase more

than lift coefficients at high AoA since the wake flow appears on missile body and fins so, it also causes to decrease lift to drag ratio.



(a)



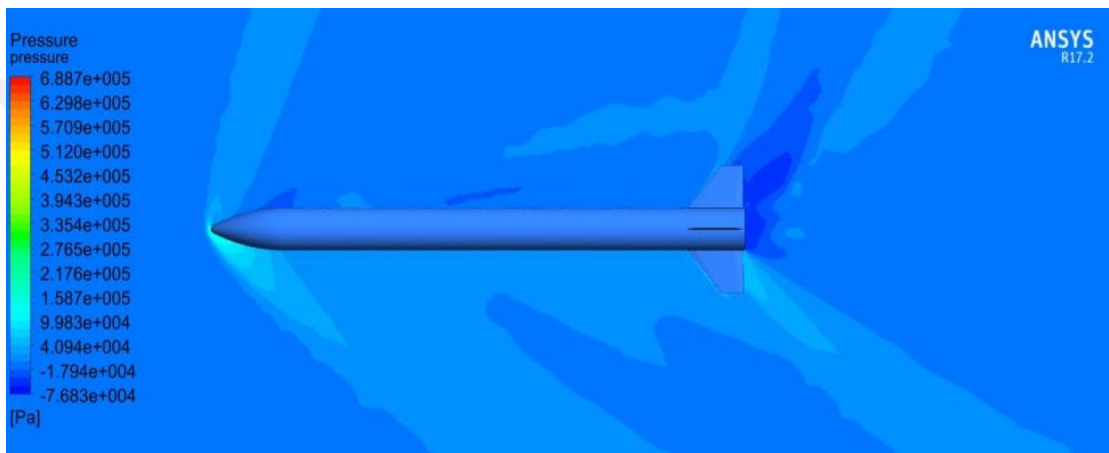
(b)



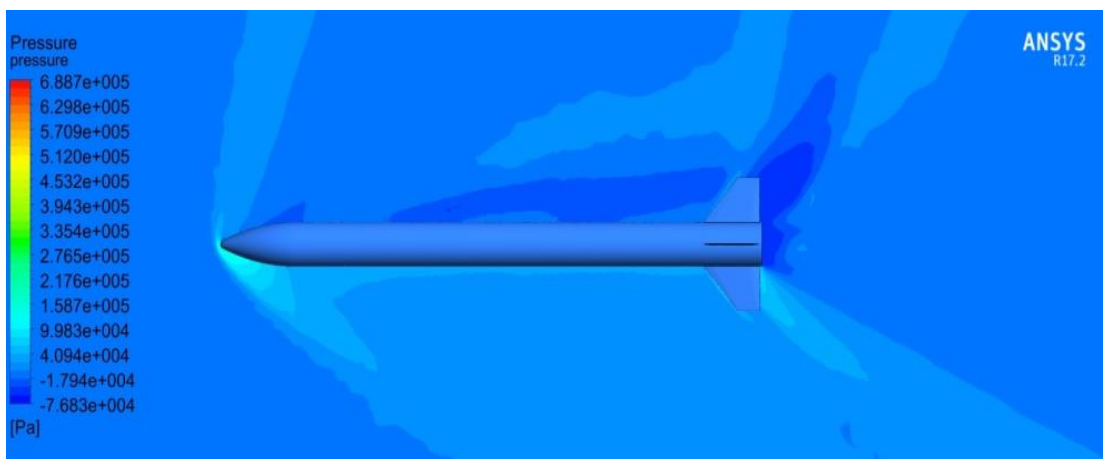
(c)



(d)



(e)

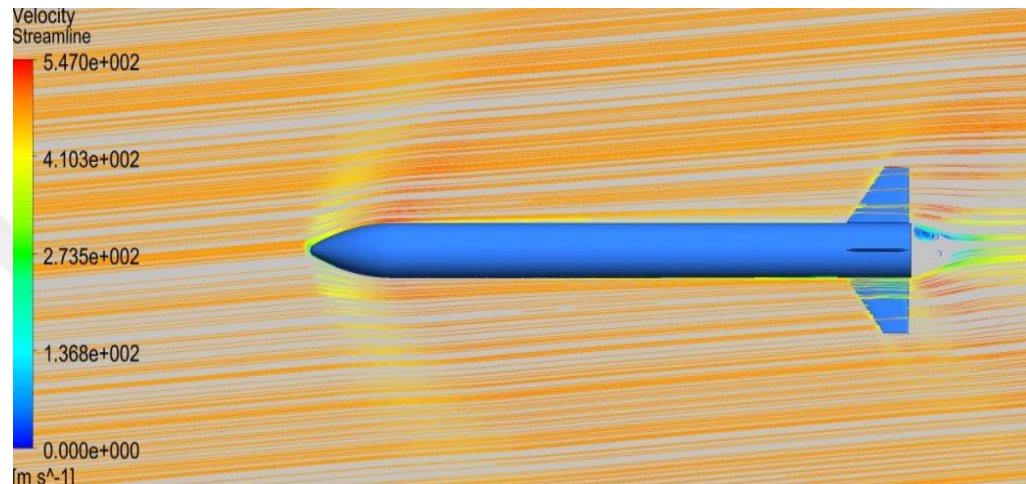


(f)

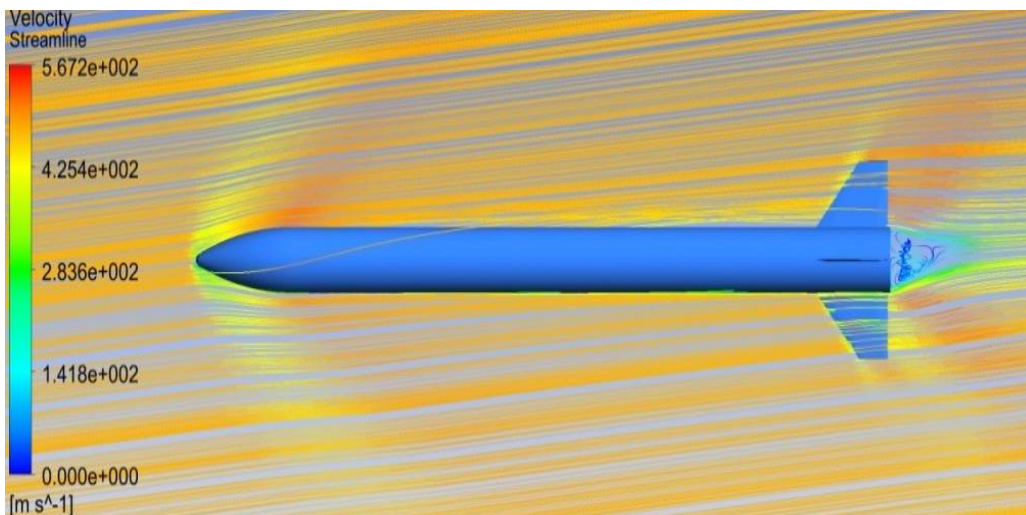
Figure 3.28 Pressure contour for 1.4 Mach number (a: 4° AoA, b: 8° AoA, c: 12° AoA, d: 16° AoA, e: 20° AoA, f: 24° AoA)

The streamlines of the missile are presented for 1.4, 2, 2.5 and 4 Mach numbers at 4° and 6° AoA in Figures 3.29, 3.30, 3.31 and 3.32, respectively. The vortex can be

observed rear of the missile. This cause increases the drag forces. So, the performance of missile or lift to drag ratio decreased due to separation of flow. Low pressure area which occur rear of the missile body can be decreased to reduce drag coefficients by means of optimizing the missile model. In addition, flow separation can be prevented as much as possible to improve aerodynamic performance. From these figures, it is observed that the low pressure area decrease with increase Mach number so, lift to drag ratio improve as mentioned previous section.

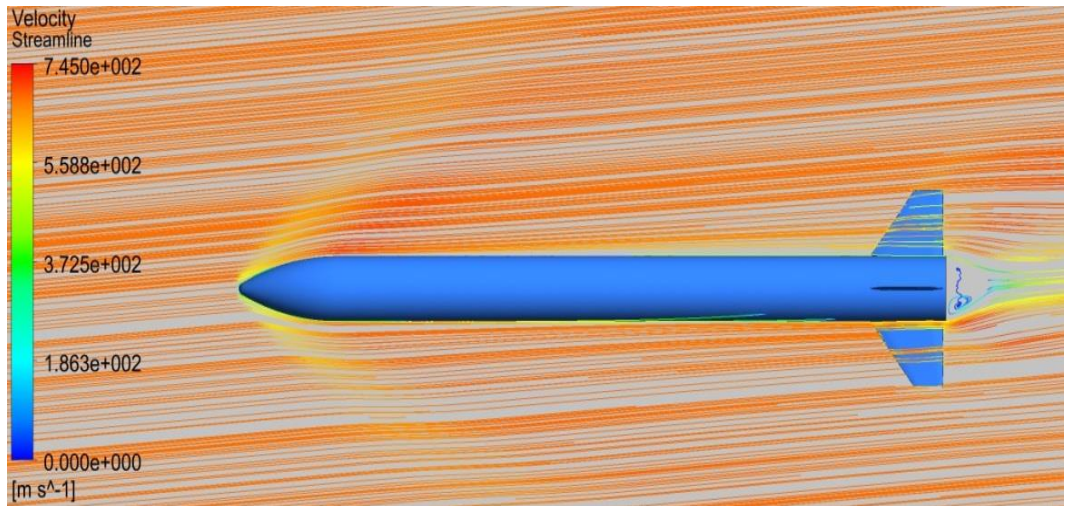


(a)

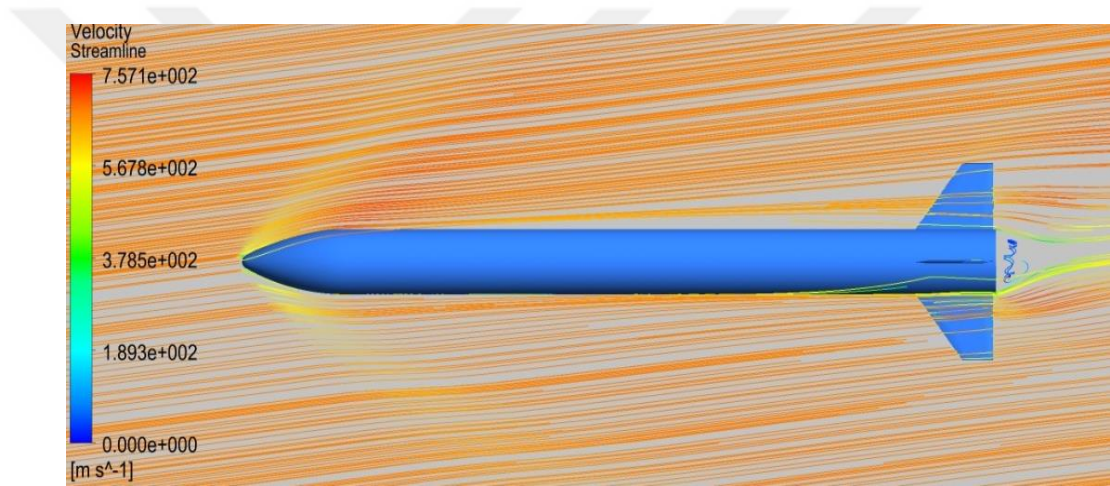


(b)

Figure 3.29 Streamline for missile at 1.4 Mach number (a: 4° AoA, b: 6° AoA)

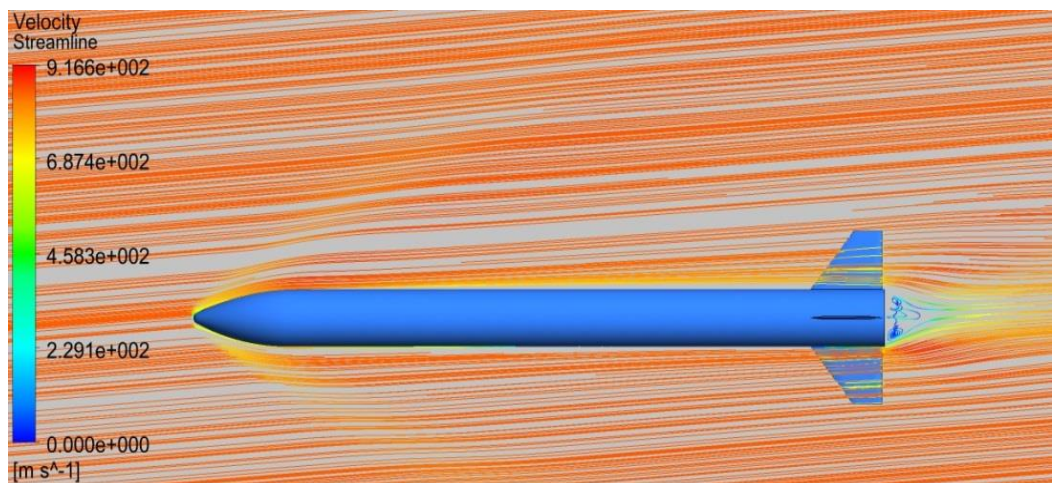


(a)

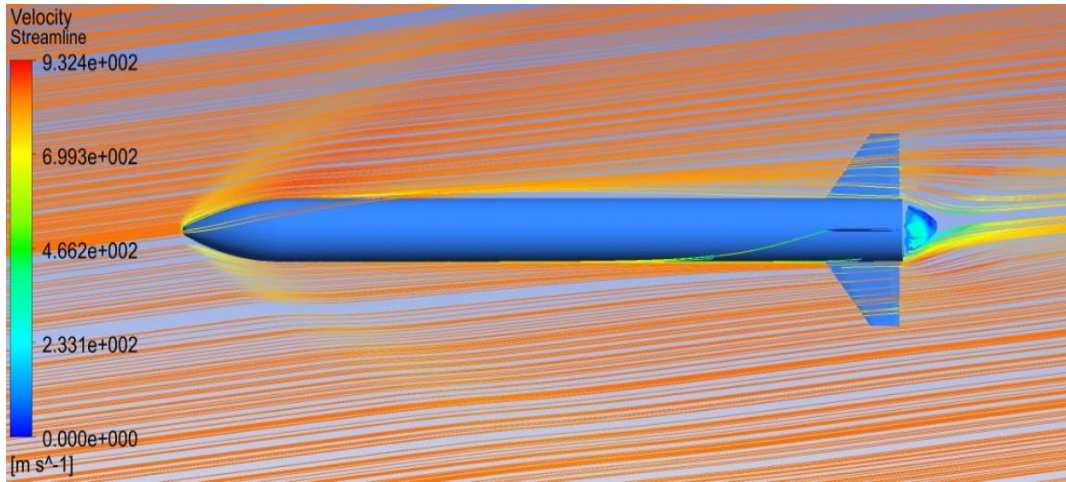


(b)

Figure 3.30 Streamline for missile at 2 Mach number (a: 4° AoA, b: 6° AoA)

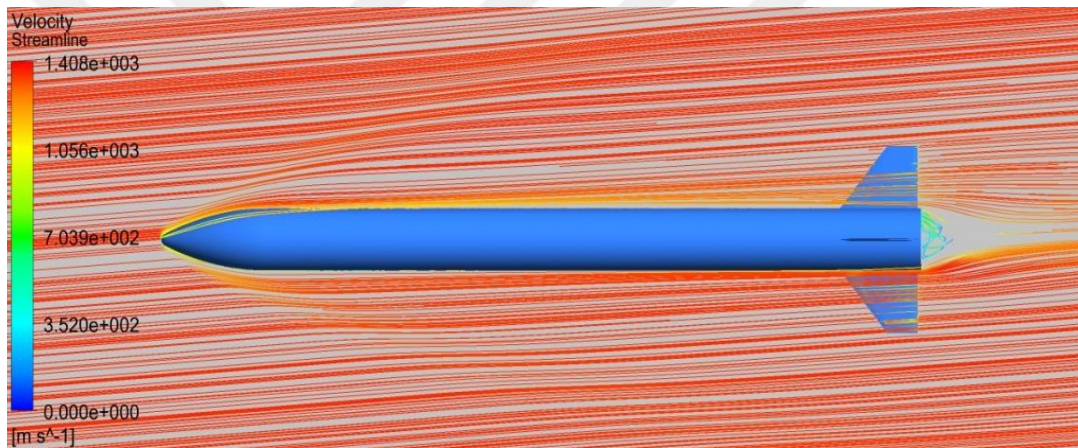


(a)

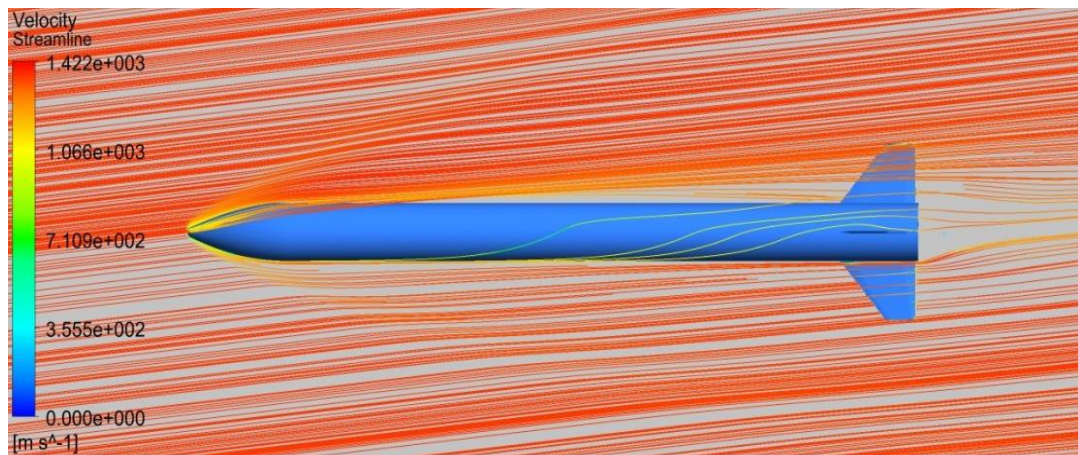


(b)

Figure 3.31 Streamline for missile at 2.5 Mach number (a: 4° AoA, b: 6° AoA)



(a)



(b)

Figure 3.32 Streamline for missile at 4 Mach number (a: 4° AoA, b: 6° AoA)

CHAPTER IV

OPTIMIZATION OF EXTERNAL MISSILE GEOMETRY

4.1 Definition of Optimization

Optimization is the process which gives the maximum or minimum of some objective function under specified constraints. It tries to perform a process, or design of system, or methodology of making decision for objective function or functions. Maximum profit is tried to be obtained for all conditions and constraints. Engineers make an optimization during design, manufacturing and maintenance phases. The importance of optimization has increased even more, as many large scale combinational optimization problems and highly constrained engineering problems can be solved by today's computer. Hence, optimization plays very important role in terms of efficiency or productivity.

There are two stages of the optimization which are modeling and analysis. Modeling can be expressed as mathematical expression for an encountered problem in real life. Analysis can be expressed as the best solution of this model is achieved.

In mathematical optimization there are two common approaches to attain optimality. The first one, starting from the first principles and knowledge of the system behavior construct a deterministic objective function that relate your output response to the input factors and generate the constraint set based on the restrictions on your input variables. The second approach, one that do not require much system knowledge a priori is the Statistical optimization methods, in particular the Response Surface Methodology (RSM), here the objective is to obtain a data driven approximate model of the true system response surface , usually a low order polynomial model, whose optimal point is a close approximation to the true system optimum point, however, this method involves a lot of sequential experimentation and data analysis but it is extremely useful when your system is extremely complex and construction of a deterministic model of output behavior is extremely difficult.

Size optimization, topology optimization and shape optimization are used to design an efficient mechanism or system in terms of mechanics, aerodynamics etc. There are some differences these optimization types. Size optimization refers to the physical size of the members within a structure such as a cross-sectional area or a distributed thickness of a truss model that can be varied. Topology optimization focuses on the internal member configuration of a structure by reducing the volume to the desired ratio without any change in the external dimensions of the part to be optimized. Shape optimization refers to the geometric layout. It tries to find the optimum shape to minimize a certain cost function under specified constraints. (Mortazavi and Toğan, 2016).

In this study, shape optimization is performed to find optimal shape of the N1G missile model in terms of aerodynamic at different supersonic speeds. The following section is presented about aerodynamic shape optimization and steps of optimization processes.

4.1.1 Aerodynamic Shape Optimization

The aim of aerodynamic shape optimization is to maximize the performance of a given body such as a wing, airfoil or whole air vehicle changing its shape under specified constraints and requirements. Aerodynamic shape optimization has some sub-problems that are geometry designation, determining aerodynamic parameters of the geometry and obtaining a better configuration in terms of aerodynamic performance. CFD is usually used to calculate aerodynamic performance and optimization can be performed using a number of algorithms. This is the iterative process which starts with an initial shape and continues to obtain optimum shape in terms of aerodynamic performance by changing given shape until specified constraints are satisfied.

In this study, we try to obtain optimum shape for N1G missile model. For this purpose, previous studies were examined to determine which methods are commonly used and appreciate for the aerodynamic shape optimization of missile. It is observed that Genetic algorithm and Adjoint methods and Particle Swarm Algorithm are used in previous studies and gives quite accurate optimum results. However, genetic algorithm gives more accurate results when compared with others. Hence, in this

study, Multi-Objective Genetic Algorithm has been used to perform in optimization processes of missile shape optimization.

4.2 Definition of Genetic Algorithm

Genetic algorithm (GA) based on principle of natural selection and genetics and uses rules with probability. It is the most popular type of Evolutionary Algorithm. Genetic Algorithms gives good results in problems where solution space is large, discontinuous and complex. In addition, it only takes into account real function and doesn't use derivative information.

In GA, genes that are discrete units form chromosomes. Chromosomes can be defined as a solution vector $x \in X$. A chromosome corresponds to a unique solution x in the solution space. A mapping mechanism that is called encoding is required between the chromosomes and the solution space. So, it can be said that GA work on the encoding of a problem. Chromosomes are collected to create population and population is randomly initialized. The population is evaluated and filtered, eventually, the search converges that means it is dominated by a single solution.

GA involves two operators which are mutation function and crossover function to generate new solution. Mutation function is an operator used to maintain genetic adaptation from one generation of a population of genetic algorithm chromosomes to the next. Crossover function is a genetic operator used to vary the programming of a chromosome. Using these operators, a new population is obtained and the new population replace with old population. It is tried to produce good generations that are more compatible with each new generation.

Hence, in crossover process, new chromosomes that are called offspring are formed by combining two chromosomes which are called parents. In cross-over process, the new chromosome occurs and if it takes the best characteristics from each of the parents, it may be better than both of the parents. Cross-over takes place with respect to a user definable cross-over probability during evolution. Therefore, in order to formed offspring which has good genes; parents are chosen among chromosomes with prefer towards fitness. The result of crossover process, genes of good chromosomes appear in the population. The mutation process is then performed randomly and changed the characteristic of chromosomes. The mutation rate that is probability of changing the properties of a gene is based on the length of the chromosome. Produced new chromosomes will not be very different when compared

original one. Crossover provides converge the population making the chromosomes. Mutation then reintroduces genetic diversity back into the population. Reproduction process involves chromosomes selection for next generation. The fitness of an individual specifies the probability of its survival for the next generation. In GA, different selection producers are available according to the fitness value.

These processes are followed to optimize parameters using Genetic Algorithms (Goldberg, 1989) and Genetic Algorithm process chart is represented in Figure 4.1.

- 1) A set of solutions from all possible solutions in the search space are encoded as arrays. In this case, random processing is generally performed. An initial population is formed.
- 2) The fitness value is calculated for each array. The obtained fitness value indicates the solution quality of the arrays.
- 3) A group of arrays is randomly selected according to a given probability value. Crossing and mutation operations are performed on selected sequences.
- 4) The new population is replaced by the old population.
- 5) The above operations are continued until the stop criterion is met. The most appropriate sequence is chosen as the solution.

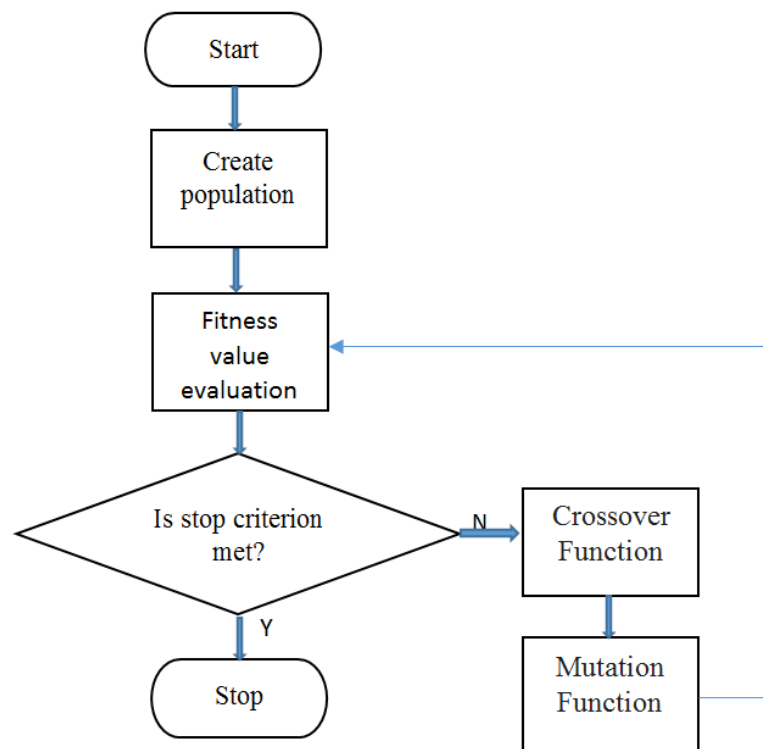


Figure 4.1 Genetic algorithm process chart

4.3 Multi-Objective Optimization Design

Aerodynamic shape optimization is a crucial task for air vehicles. All external parts of the air vehicle are important in point of aerodynamic performance. In optimization design, a single design objective is not frequently sufficient to face with the optimization problem. Therefore, the designer prefers to solve a Multi-objective optimization problem to maximize performance and reliability and minimize cost. These are difficult to perform however, it is realistic problems. Optimization problem includes objective functions, design variables and constraints. The objectives can conflict and prevent simultaneous optimization of each objective for multi-objective problems. Selection of the design variables is important task to find optimum solution and constraints should be met requirements for specified optimization problem.

There are two methods that are commonly used for multiple optimization problems. The first one is to combine the individual objective function into a single composite function. This method provides to determine as a single objective function using weighted sum method, utility theory, etc., however, the utility and weight function is crucial to obtain accurate results since these functions characterize the decision maker. The second method is to determine Pareto optimal solution set that is a set solution which is non-dominated according to each other. Pareto optimal solution sets are generally given preference for single solution since they are convenient to real life problems due to fact that decision maker is trade-off for final solution (Konak et al., 2006).

In order to explain formulation of multi objective optimization, consider a decision maker that want to optimize n objectives which are non-commensurable and the decision maker has no idea whether the objectives are relative to each other or not. Mathematical representation of multi-objective optimization problem can be expressed as follows (Kallrath et al., 2009).

General terms of the mathematical optimization is given in Equation (4.1),

$$\text{Maximize } f(x) = [f_1(x), f_2(x), \dots, f_n(x)] \in R^n \quad (4.1)$$

Subject to the constraints are given in Equation (4.2),

$$\begin{aligned}
g_i(x) &\leq 0, & i &= 1,2,\dots,m \\
h_i(x) &= 0, & i &= 1,2,\dots,q \\
x_i^l &\leq x_j \leq x_i^u & j &= 1,2,\dots,p
\end{aligned}
\tag{4.2}$$

Where $x = [x_1, x_2, \dots, x_j]^T$ is the vector of design variables, $f(x)$ is the multi-objective vector, $f_n(x)$ is the objective function, $g_i(x)$ and $h_i(x)$ are the constraints and x_i^l and x_i^u are lower and upper bounds of the design variables, respectively.

4.4 Multi-Objective Genetic Algorithm (MOGA)

Genetic Algorithms are suited to solve multi-objective optimization problems. It can support all types of input parameters. GA can research different regions of solution space and this provides to obtain a diverse set of solution for discontinuous difficult problems.

The beginning of process, MOGA is run and a new population is generated via cross-over and mutation. Each population is then run when it reaches the number of samples. In the new population, design points are updated. The convergence is validated and achieved for optimization. Optimization problem converges when the maximum allowable Pareto percentage has been reach. After validation process, if stopping criteria is not achieved, MOGA is run again to generate a new population and the process is continued until the stopping criteria have been achieved.

4.5 Optimization Studies Using Ansys in DesignXplorer

Designers or researchers need to be able to quickly predict the outcome of design changes of their product. Therefore, engineering simulation provides advantages for designers to evaluate how the designed product will carry out under specified operating conditions.

Ansys DesignXplorer is an integrated Ansys Workbench application which leverages the parametric and persistent power of workbench for parametric analyses. DesignXplorer includes correlation, design of experiments, response surface creation and optimization analysis. Optimization steps of the missile are presented in DesignXplorer as following sub-sections.

4.5.1 Response Surface Optimization

Response surface methodology analyzes the relationship between variables and one or more response variable. The main idea of response surface methodology is to utilize a sequence of designed experiments for obtaining an optimal response. Combining this methodology in design optimization is called as Response Surface Optimization (RSO) (Queipo et al., 2005). Thousands of configurations can be analyzed in a short time. Figure 4.2 represents procedure of RSO.

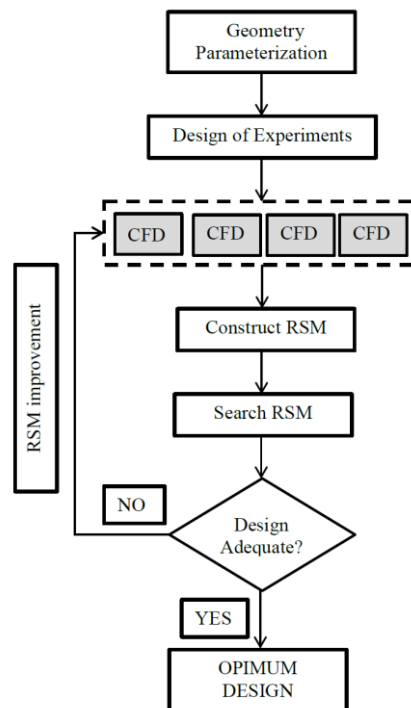


Figure 4.2 General RSO procedures (Khot, 2012)

Response surfaces are functions which describe the output parameters in terms of the input parameters. Genetic aggregation is a type of response surface. It uses genetic algorithm to obtain the best Response Surface and setting for each output parameter. Kriging is another type of response surface. Kriging model interpolates the design of experiment points. In this thesis, Kriging model is selected to obtain response surface because this model is more sensitive due to polynomial model.

RSO includes four steps. (Khot, 2012)

1. Simulations are performed for a select set of points within the design space.

2. Response Surface based on the responses attained for the sampling points. Response Surface Model (RSM) is generated. The RSM indicates an approximation of the system response.
3. The RSM is optimized using Response Surface Optimization algorithms in order to find the best operating point values.
4. The RSM approximation is improved by including additional simulated responses.

4.5.1.1 Design Space

The design space can be defined as a region that is bounded by the upper and lower limits of the design variables. This means that the design variables or input parameters are changed only within the specified limits. Structural and material constraints are also defined to obtain realistic shape or design for specified optimization problem.

4.5.1.2 Design of Experiments

The aim of a design of experiments (DoE) is to gather set of data to calculate a response surface and it is used to run an optimization for a response surface optimization.

In the DoE step, the design space is explored and generated the test matrix of design points using a technique to investigate in each computational experiment. The objective of DoE is to obtain a matrix of design variable values in a specific format. This is performed by discretizing the variation range of each design variable. (Khot, 2012).

In this study, a geometric quantity was parameterized as input parameters and the output of parameters is specified as drag and lift coefficients on the missile to investigate and improve aerodynamic performance. By computing a DoE over 281 simulation points, the response of the system is produced by means of interpolation. This enable to us predict the optimum conditions and give information showing the trade-off between the different quantities. But, it is crucial to calculate the selected optimum conditions to verify the solution in this case showing good agreement with what was expected because these predictions are depended on the interpolated response surface.

4.5.1.3 Response Surface

Response surface are functions that the output parameters are described in point of the input parameters. Response surface provide the approximated values of the output parameters which are analyzed in design space without the need to perform a complete solution. Genetic aggregation and Kriging Response Surface types are commonly used to analyze design space. Genetic Aggregation is consuming when dealing with high number of design points while Kriging type is efficient in a large number of cases. In addition, Kriging is suitable for highly nonlinear responses. Therefore, Kriging type is preferred to analyze Response Surface for this study because of gives more accurate results for nonlinear responses.

4.5.1.4 Optimization

The best possible designs are obtained for specified input parameters and under constraints using optimization technique. MOGA, NLPQL, MISQP methods are commonly used for optimization problem in DesignXplorer. MOGA is based on sampling so, the number of samples is increased for optimum results. NLPQL is a gradient based single objective optimizer that is based on quasi-Newton methods. MISQP method (Mixed-integer Sequential Quadratic Programming) solves mixed-integer nonlinear programming problems by a modified quadratic programming (SQP) method. Adaptive Multiple-Objective is an iterative method that combines MOGA algorithm and Kriging response surface. Hence, MOGA is used to optimize missile external shape in terms of aerodynamics in this thesis.

In this study, missile model is form in Designmodeler and mesh generation is performed to solve flow field using finite volume method. The solution is implemented in Fluent. Optimization process is then started using DesignXplorer in ANSYS. Parameter Correlation is also carried out for observation relationship among the design variables. ANSYS workbench optimization set is presented in Figure 4.3.

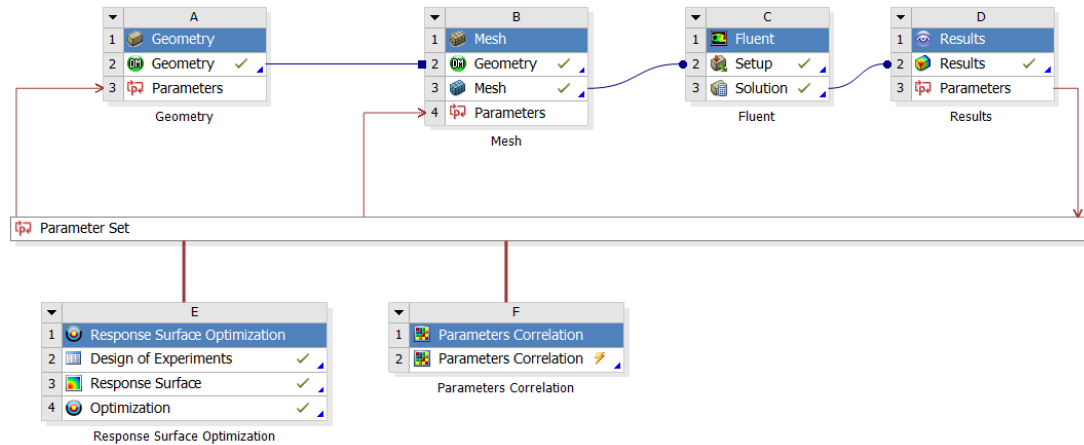


Figure 4.3 ANSYS workbench optimization set

4.5.2 Parameter Correlation

Input parameters or design variables are used to generate a set of design points. Using parameter correlation, it can be explored the degree of correlation between all parameters. It is recommended to omit unremarkable input parameters from the DoE sampling to reduce unnecessary sampling points and waste of time for solutions. In addition, correlation matrices, determination matrices, correlation scatter plots, and sensitivity chart is utilized to observe the parametric relationships. In addition, global sensitivities chart shows how to impact an input parameter to the output parameter. Positive sensitivity values occur when increasing the input increases the output. Negative sensitivity values occur when increasing the input decreases the output.

Case studies are given in the following section that involves all comments related with results and correlation charts.

4.6 Case Studies for Missile Aerodynamic Shape Optimization

In this study, aerodynamic shape optimization was presented for N1G missile model. CFD solution was performed to find aerodynamic forces occurring on missile for base dimensions. The beginning of the optimization step, design points were generated with respect to input parameters that are specified upper and lower values in design of experiment. CFD solution was performed for each design point. After this stage, response surface can be implemented to describe the output parameters in terms of the input parameters. In addition, local sensitivity chart can be obtained to observe how the input and output parameters are affected each other. Eventually,

optimization was performed and optimum result was solved again for validation. The following sub-sections mention details of missile external design optimization.

4.6.1 Objective Functions

The aerodynamic performance of the missile can be determined computing lift and drag coefficients. Lift to drag ratio is the most important characteristic for missile shape design. Therefore, in this study, the objective functions have been specified as lift and drag coefficients. The aim of the optimization study is to increase the lift coefficient and decrease the drag coefficient. Maximizing the lift to drag ratio (C_L/C_D) is crucial to improve the performance of missile and increase range of the missile.

4.6.2 Design Variables

The important task in achieving optimum solution is to select design variables. The selected missile model consists of three main parts which are nose, body and tailfins. These parts effect on the aerodynamic characteristics of the missile model. In our study, 12 parameters that are body length (L_b), body radius (R_b), nose curve radius (R_N), nose front radius (R_F), tailfin position (X_F), fin span (L_{FS}), leading-edge (γ_{le}) and trailing edge (γ_{te}) sweepbacks, root chords (L_{FR}) and tip chords (L_{FT}) of tailfin, root (T_r) and tip (T_t) thickness of tailfin were chosen to find optimum size and shape of the missile geometry. Tailfin position is influence the stability and maneuverability. Figure 4.4 and Figure 4.5 represent the design variables for missile body, nose and tailfin, respectively.

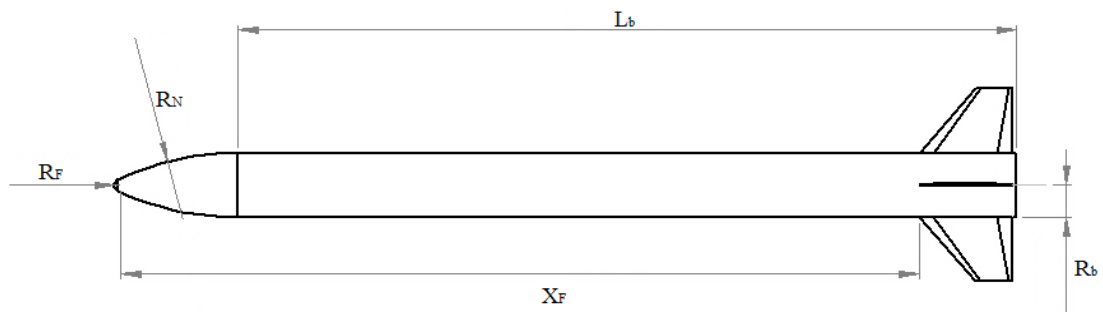


Figure 4.4 Design variables of the missile body and nose

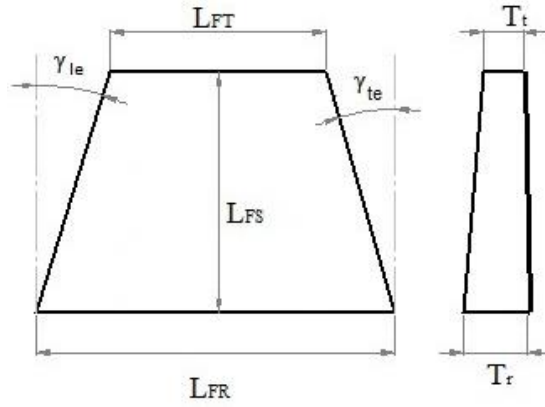


Figure 4.5 Design variables of missile tailfin

4.6.3 Constraints

There should be some constraints to meet requirement of performance and provide some shape limits during the optimization process. The first constraint is position of the tailfin. Summation of tailfin length and body length should be equal or smaller than total length. Equation (4.3) represents the constraint of the problem.

$$X_F + L_{FR} \leq L_{tot} \quad (4.3)$$

The second constraint is lift and drag coefficients. Lift coefficient of optimum missile geometry should be higher than baseline missile geometry while drag coefficient should be smaller than baseline missile geometry. The following Equations (4.4) and (4.5) show the defined constraints.

$$C_L(\text{opt.}) \geq C_L(\text{base}) \quad (4.4)$$

$$C_D(\text{opt.}) \leq C_D(\text{base}) \quad (4.5)$$

Baseline, lower and upper values of the design variables are given in Table 4.1.

Table 4.1 Baseline, lower and upper values of the design variables

Design Variables	Baseline	LB	UB
L_b [mm]	630	570	690
R_b [mm]	27.5	25	30
R_N [mm]	235.62	210	260
R_F [mm]	5.5	5	6
X_F [mm]	682.15	670	690
L_{FS} [mm]	55	50	60
γ_{te} [deg]	40.69	30	50
γ_{te} [deg]	0	0	15
L_{FR} [mm]	78.65	70.65	86.65
L_{FT} [mm]	31.35	28.35	34.35
T_r [mm]	2.36	1.8	2.8
T_t [mm]	0.94	0.82	0.104

4.6.4 Optimization Algorithm

In this study, Multi-Objective Genetic Algorithm was used to solve optimization problem. In engineering problem, GA is convenient to solve multi-objective optimization problem. It can be possible to obtain a diverse set of solution searching different regions of a solution space thanks to GA. In crossover process, GA may utilize structures of good solutions to create non-dominated solutions in undiscovered parts of the Pareto front. Hence, GA is the most popular for multi-objective optimization design (Konak et al., 2006). We generated a multi-objective optimization model using Genetic Algorithm. The optimization processes is represented in Figure 4.6.

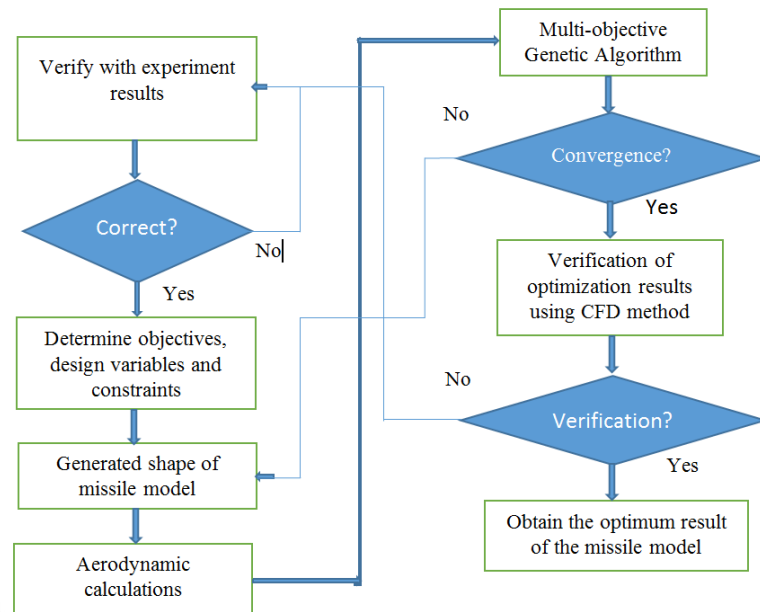


Figure 4.6 Optimization processes

4.6.5 Optimization Problem Solution

Optimization problem solution was carried out providing objective function under specified constraints and selected design variables. The calculation of the objective functions were performed at 1.4, 2, 2.5 and 4 Mach numbers and 4° AoA using RANS with the k- ω SST turbulence model in Fluent. Optimization was carried out by means of ANSYS DesignXplorer.

The geometry is formed Design Modeler and specified design variables are selected to transfer Parameter set block of the ANSYS Workbench. The formed geometry is transferred to ANSYS Mesh, where computational grid that is associated geometry, is generated at the different boundary regions. The generated computational grid was then transferred to ANSYS Fluent. The calculation is performed to obtain lift and drag coefficients with respect to preset initial and boundary conditions. These coefficients are transferred to parameter set block of the ANSYS Workbench. In this way, input and output parameters are gathered together in the Parameters set block. Input and output parameters are automatically transferred from parameter set block to ANSYS DesignXplorer. There are three steps in DesignXplorer to perform optimization process. In the first step, parametric investigation is carried out. Input data can be generated using various methods. In this study, Central Composite Design is applied. In Design of Experiments, 281 design points are generated for 12

input parameters. This means that 281 different missile models are constructed and CFD solution is performed for each design point. In the second step, Response surface (Approximating function) which depends on the obtained data is generated. Response surface construction was formed using Kriging surface that enables to best solution of the optimization problem. After these calculations, optimization is performed using MOGA.

4.6.6 Optimization Results

The aerodynamic coefficients are computed using RANS equations. After calculation, it was observed that lift to drag ratio shows satisfactory improvement. Lift to drag ratio of the optimized missile model is higher than about 11.8, 16.05 and 17.17 per cent when compared with baseline missile model at 1.4, 2 and 2.5 Mach numbers, respectively. The results of the optimization problem are given in Table 4.2. Design variables are also presented for optimum missile model in Table 4.3. It is concluded that body radius is more effective to reduce the drag coefficients with respect to nose curve radius and nose front radius. In addition, fin thickness, fin root and tip chords lengths and leading edge angle are more effective on the lift coefficient when compared with other design variables.

Table 4.2 Optimization results

Mach Number	Baseline C_L/C_D	Optimum C_L	Optimum C_D	Optimum C_L/C_D	Improvement
1.4	1.463	1.128	0.6581	1.794	17.17 %
2	1.269	0.8201	0.5568	1.475	16.05 %
2.5	1.261	0.675	0.4783	1.411	11.89 %

Table 4.3 Optimum shape size at 1.4, 2 and 2.5 Mach numbers

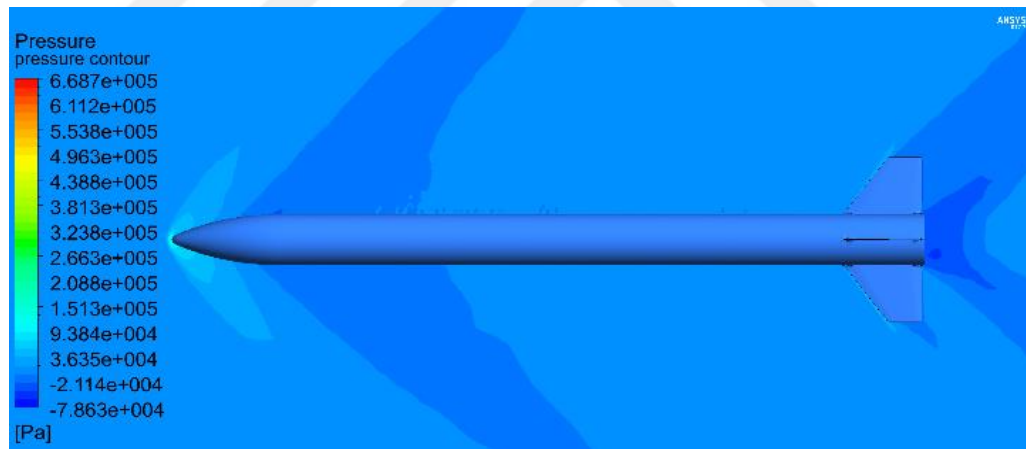
Design Variables	Mach 1.4	Mach 2	Mach 2.5
L_b [mm]	649.05	613.88	636.37
R_b [mm]	26.306	26.018	26.013
R_N [mm]	252.56	255.66	239.49
R_F [mm]	5.034	5.753	5.602
X_F [mm]	681.9	682.92	682.36
L_{FS} [mm]	58.121	58.271	57.704
γ_{le} [deg]	36.11	39.67	39.5
γ_{te} [deg]	1.959	1.277	1.105
L_{FR} [mm]	77.757	82.894	81.027
L_{FT} [mm]	33.361	33.263	32.34
T_r [mm]	1.804	1.812	1.871
T_t [mm]	0.915	0.986	0.961

Verification processes were performed for each optimization problem. The following Figures that are Figure 4.7, Figure 4.8 and Figure 4.9 show the pressure contours for baseline and optimum missile model comparison at 1.4, 2 and 2.5 Mach numbers and 4° AoA, respectively. From these Figures, it can be observed that low pressure area decrease the rear of optimum missile model when compared the baseline geometry at 1.4, 2 and 2.5 Mach numbers. This means that drag coefficient decrease for optimum model. In addition, the pressure that occurs on tailfins of leading edge of baseline model at 1.4 Mach number is higher than optimum model. This shows that tailfins of the optimum model are improved. At the same time, lower drag force and larger lift force on the tailfins represent a larger control force. The higher pressure occurs on the lower area of the nose of optimum model when compared baseline model. This result shows that after optimization, the lift force occurring lower part of the nose increases. Pressure differences between tip of the missile nose and rear of the missile

body decreases when compared with baseline missile results. This means that drag forces acting on the missile body and tailfins is decrease. In addition, it can be observed that the flow of the missile body and fins are uniform for optimum geometry and separation of flow occur later for optimized missile model. Consequently, the contribution of the optimum model to the lift force is more than baseline model after optimization processes.

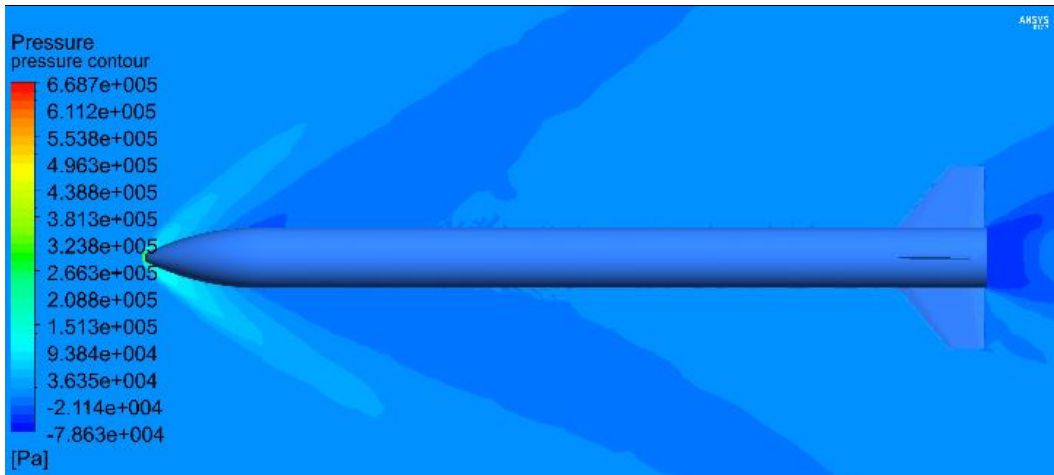


(a)

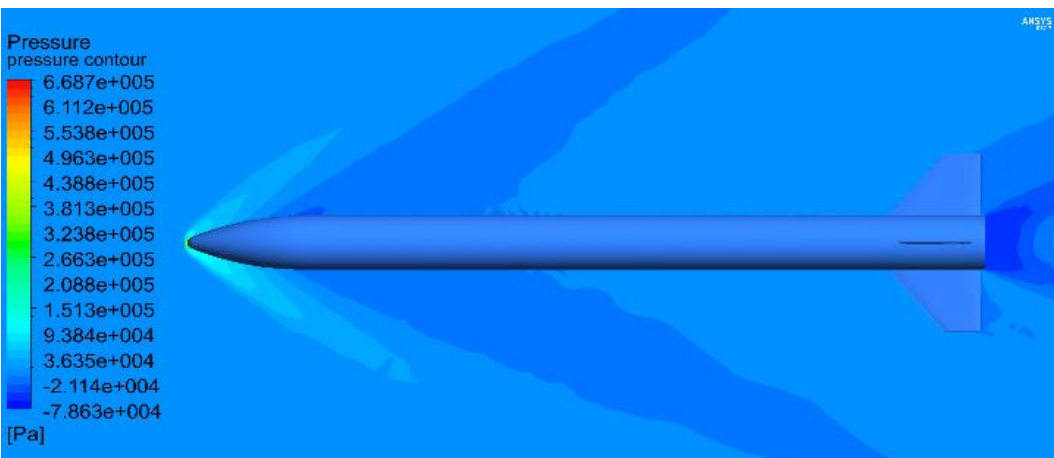


(b)

Figure 4.7 Pressure contours optimum and baseline missile model at 1.4 Mach number and 4° AoA (a: baseline model, b: optimum model)



(a)



(b)

Figure 4.8 Pressure contours optimum and baseline missile model at 2 Mach number and 4° AoA (a: baseline model, b: optimum model)



(a)



(b)

Figure 4.9 Pressure contours optimum and baseline missile model at 2.5 Mach number and 4° AoA (a: baseline model, b: optimum model)

Response surface charts are given at 1.4 Mach and 4° AoA to observe how the design variables affect the output parameters that are drag and lift forces. Response surface chart for the drag force with body length and nose curve radius is presented in Figure 4.10. It can be observed that the increased nose curve radius results in decrease the drag force and the increase in body length adversely affected the drag force. Especially drag force starts to increase suddenly when the missile body length exceeds 615 mm. This may be due to flow separation on the missile body. The other response surface chart for drag force with root thickness of tailfin and body radius is presented in Figure 4.11. From this figure, it can be seen that the radius of body has a direct effect on the drag force and root thickness of tailfin increases the drag force since the cross-sectional area is increased. However, they can provide to increase lift force. In addition, there are 12 design variables and all of them effects on drag and lift force therefore, some variables increase drag or lift forces while some variables decrease them. Eventually, lift to drag ratio determines whether the aerodynamic performance is improved or not.

Response surface charts are given for the lift force versus design variables. Figure 4.12 represents lift force versus tip and root chords of tailfin. The length of tailfin has a considerable effect on the lift force. It can be concluded that lift force increase when tip and root chords lengths are increased. Figure 4.13 represents lift force with fin span and tailfin position. Tailfin position is not more effective than fin span. However, from this figure, it can be understood that lift force suddenly increase

when the range of tailfin position is between 686 mm and 690 mm. Moreover, it can be said that the lift force increases in direct proportion to the fin span.

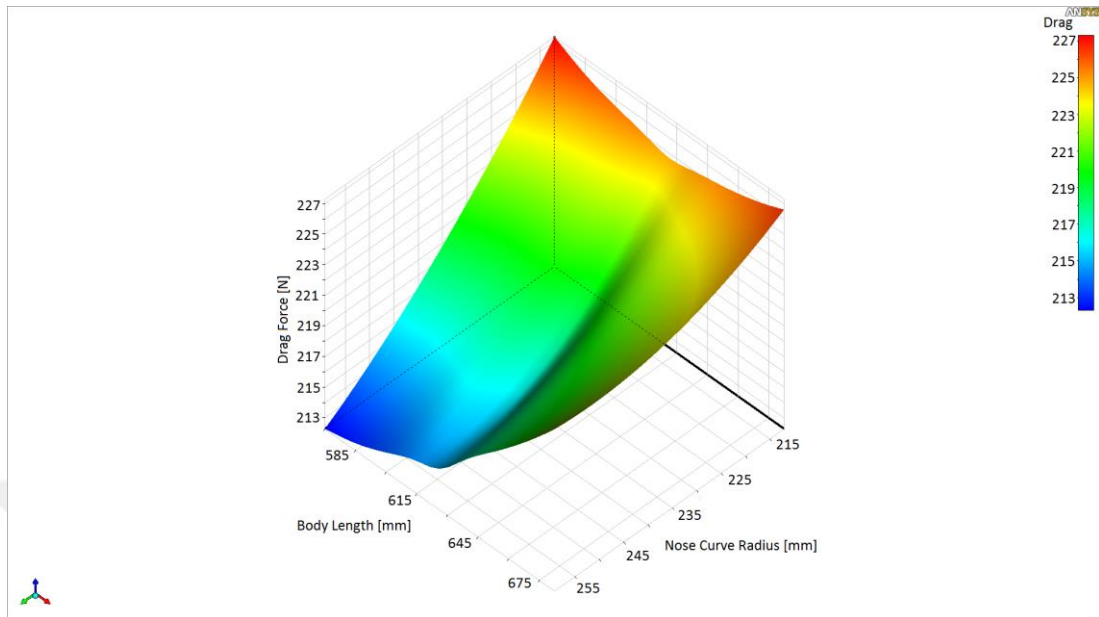


Figure 4.10 Response surface for drag force with body length and nose curve radius at 1.4 Mach number and 4° AoA

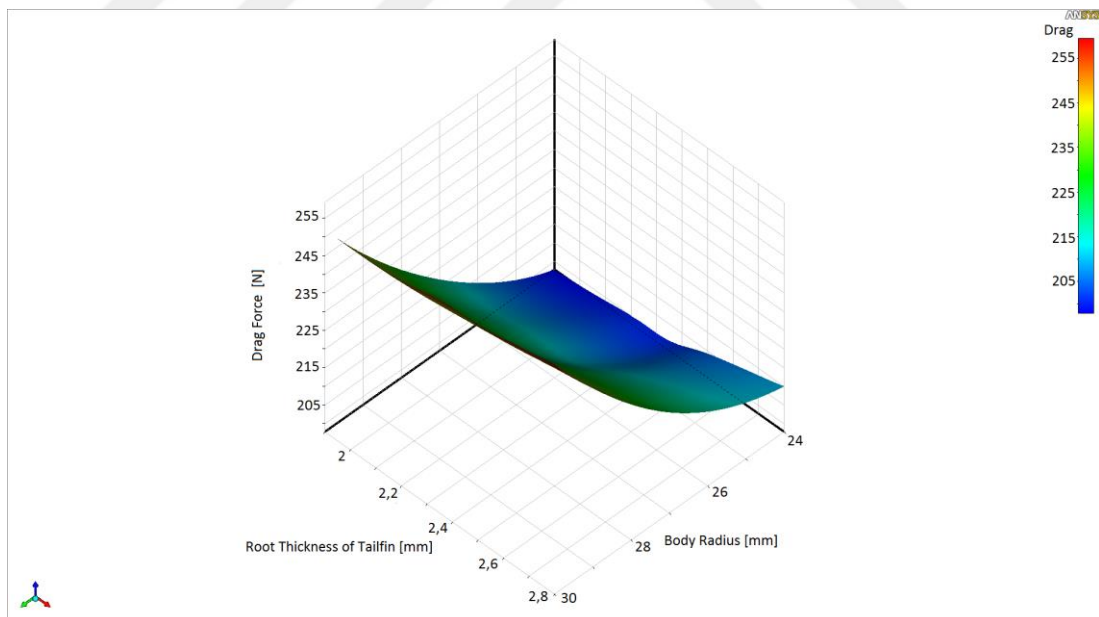


Figure 4.11 Response surface for drag force with root thickness of tailfin and body radius at 1.4 Mach number and 4° AoA

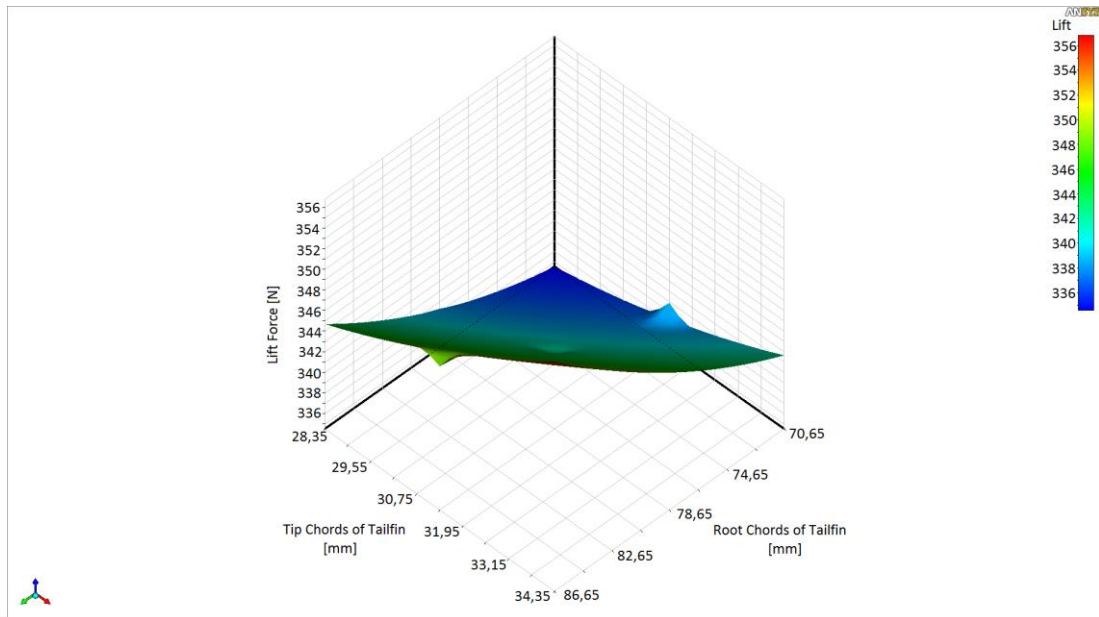


Figure 4.12 Response surface for lift force with tip and root chords of tailfin at 1.4 Mach number and 4° AoA

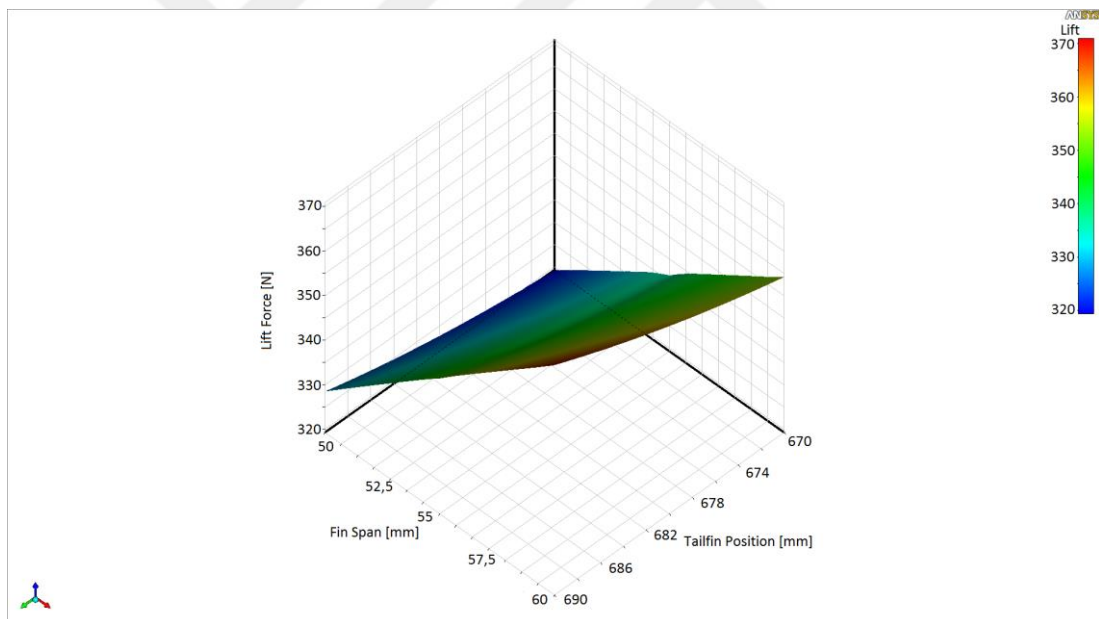


Figure 4.13 Response surface for lift force with fin span and tailfin position at 1.4 Mach number and 4° AoA

Local sensitivity chart analysis is also important to observe input and output parameters how to affect each other. The local sensitivity chart is represented in Figure 4.14. It is showed that body radius is the most effect drag force and lift force that occur on the missile body. If body radius has high value, drag force and lift force are increase. However, drag force is affected more than the lift force according to

sensitivity chart. At same time, if the nose blunt radius is increased, the drag force decrease since nose blunt radius sensitivity is mines value. In addition, nose front radius is reverse effect on the lift force but, it is quite small value.

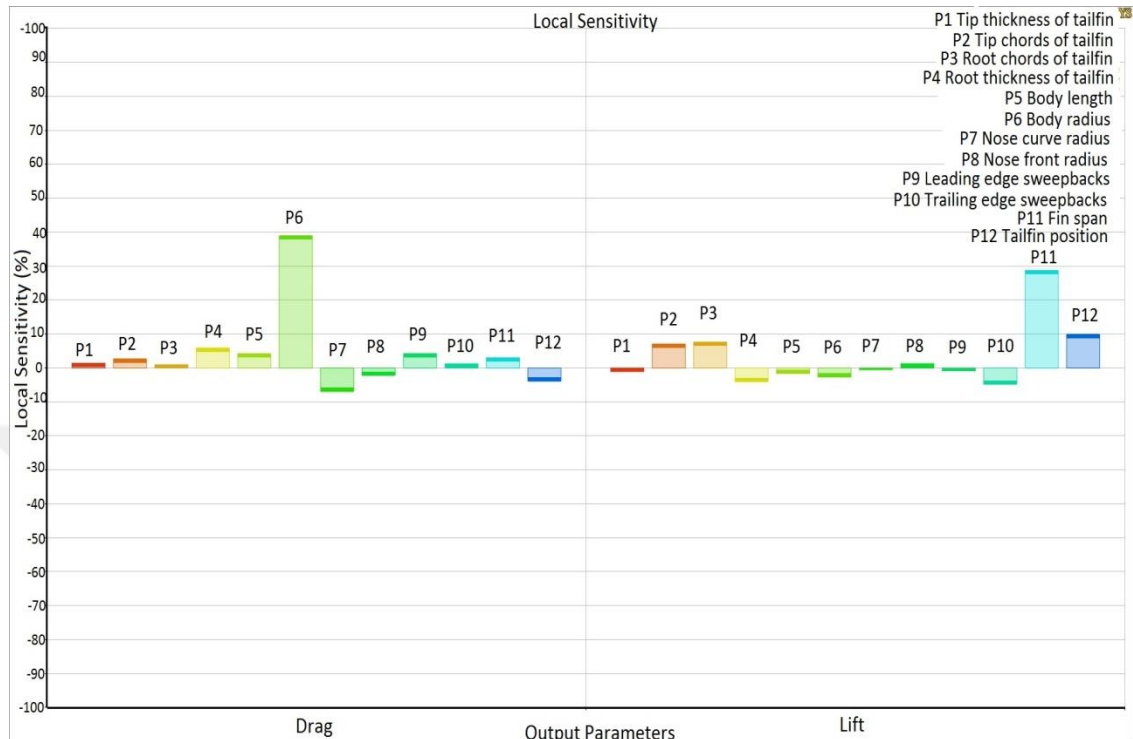
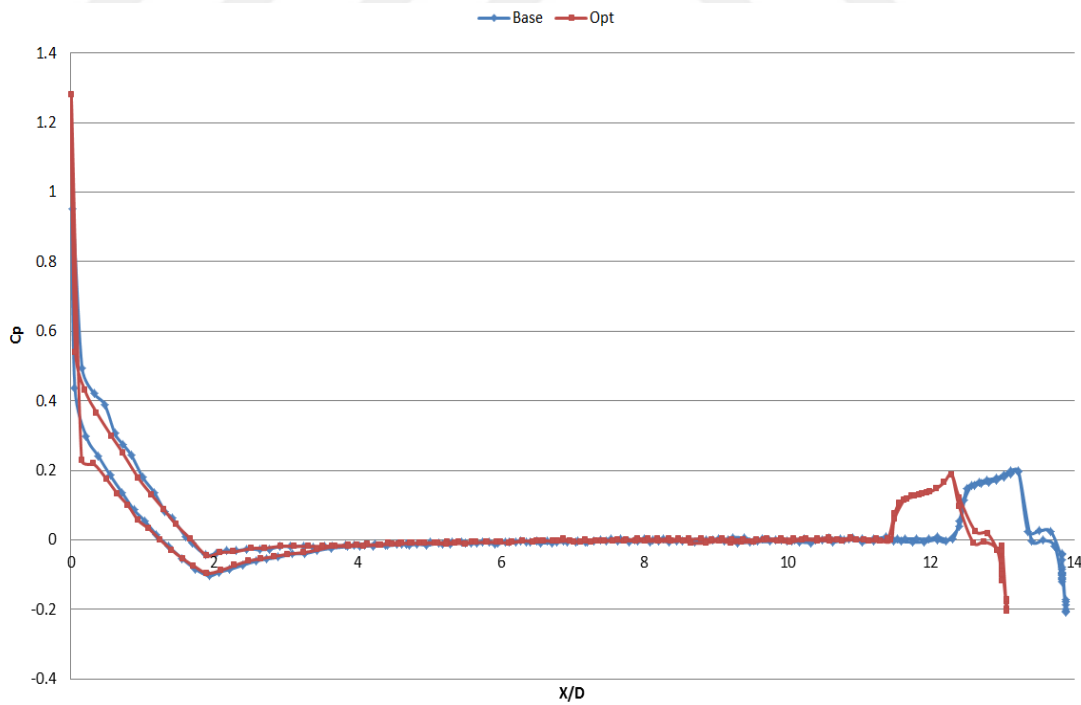
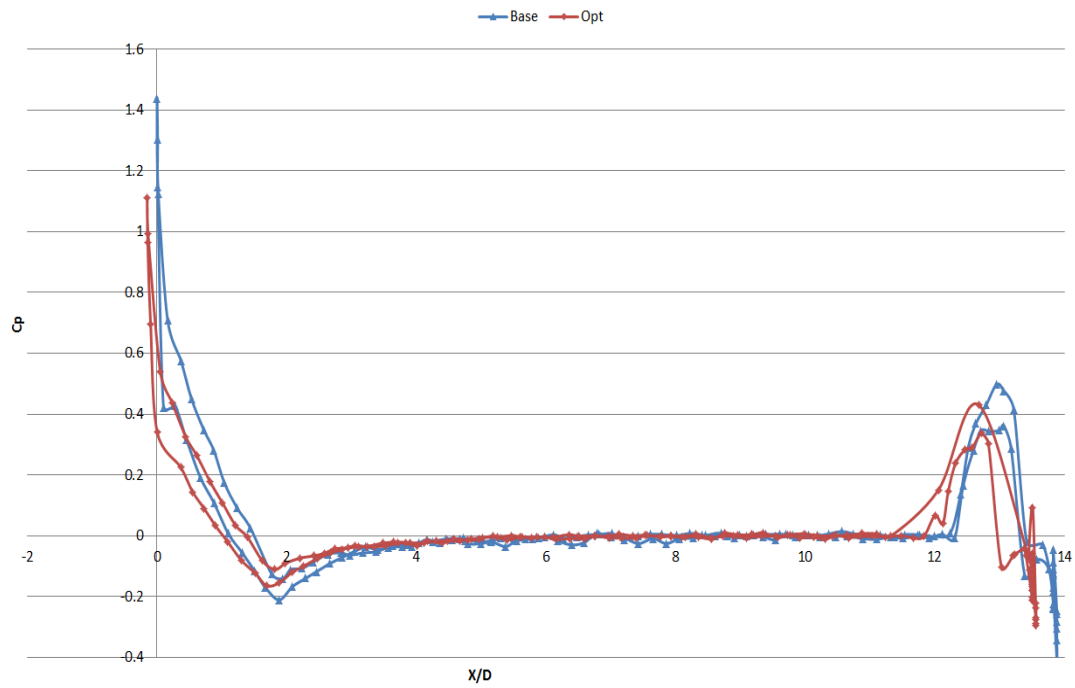


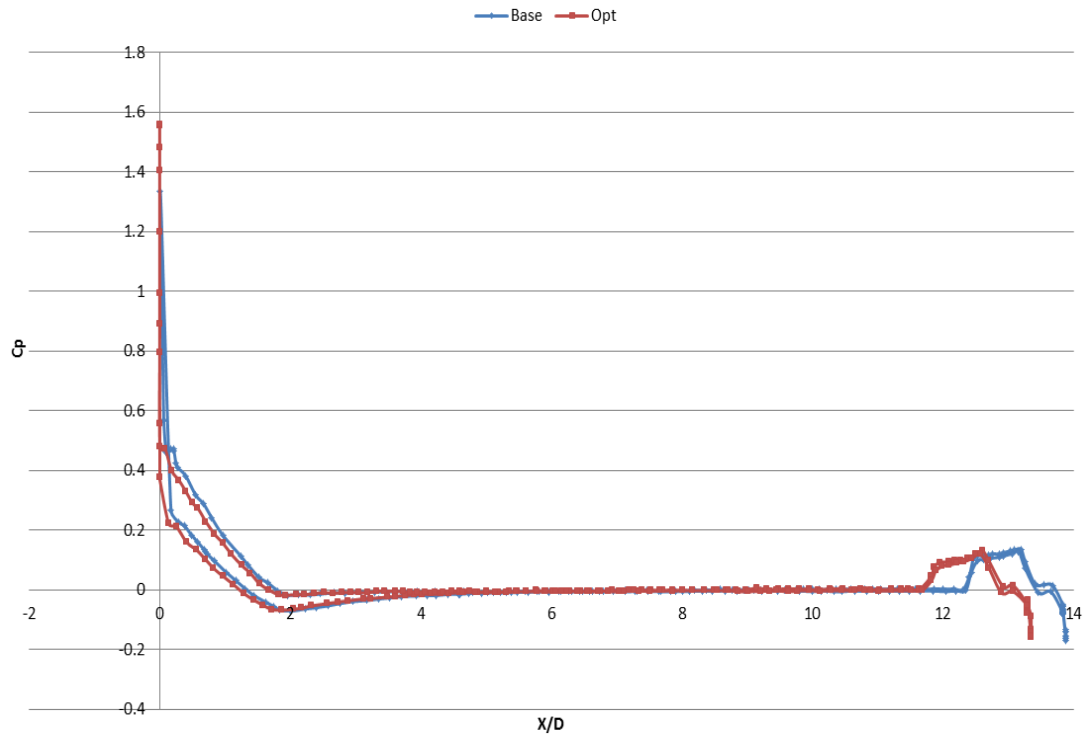
Figure 4.14 Local sensitivity chart

Surface pressure distribution coefficient is also crucial to understand whether the aerodynamic performance is improved or not. Hence, pressure coefficient distribution is presented for missile body missile fin at 1.4, 2 and 2.5 Mach numbers and 4° AoA in Figure 4.15 and 4.16, respectively. From these figures, some comments can be made that fin span and fin length increase while fin thicknesses decrease result of optimization so, fin area increase for optimum missile model. This means that lifting force increases and drag force decrease. It is observed that the length of the missile is effect the drag reduction. Pressure occurring on the tip of the nose for optimum shape is bigger than baseline shape for Mach 2 and 2.5. This is the reason to increase lift force on the front of the missile due to AoA. However, pressure difference on the fin is higher at Mach 1.4 when compared with Mach 2 and 2.5. It is show that the increase of the lift to drag ratio is mostly thanks to fin design at Mach 1.4. Pressure distribution differences between the lower and upper surface is small since solution process is performed at 4° AoA that is small value for the missile however, experimental data is available at 4° AoA for the selected missile.

Consequently, lift to drag ratio improve when compared with baseline model after optimization processes.

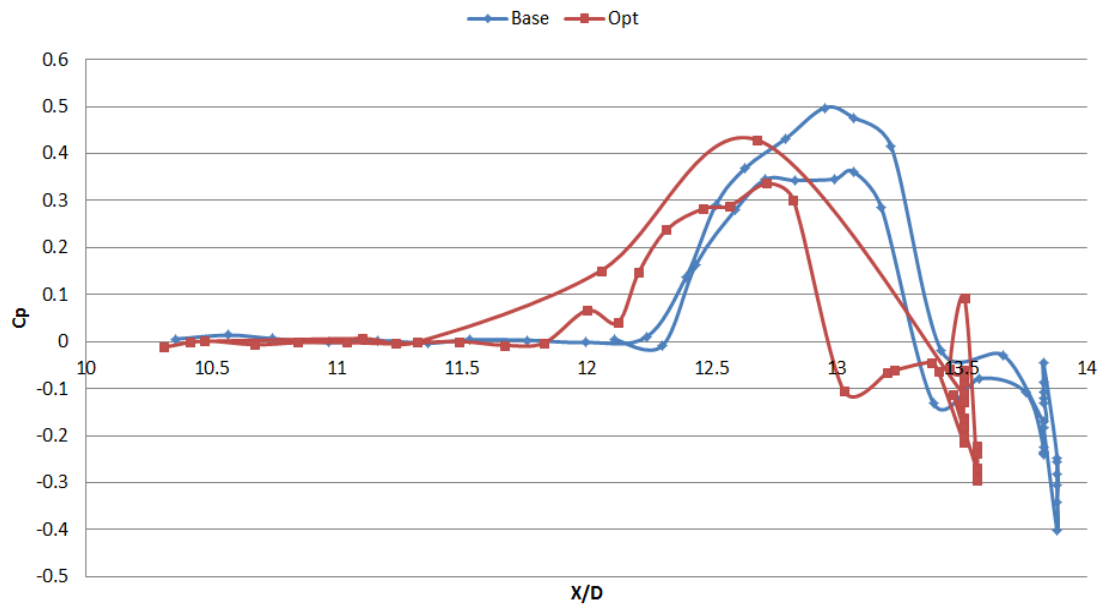


(b)

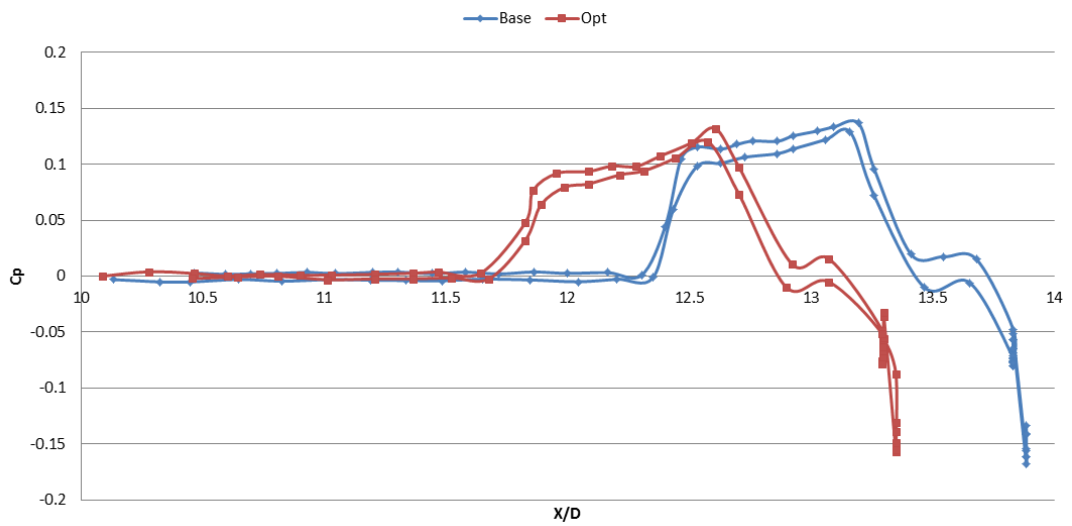
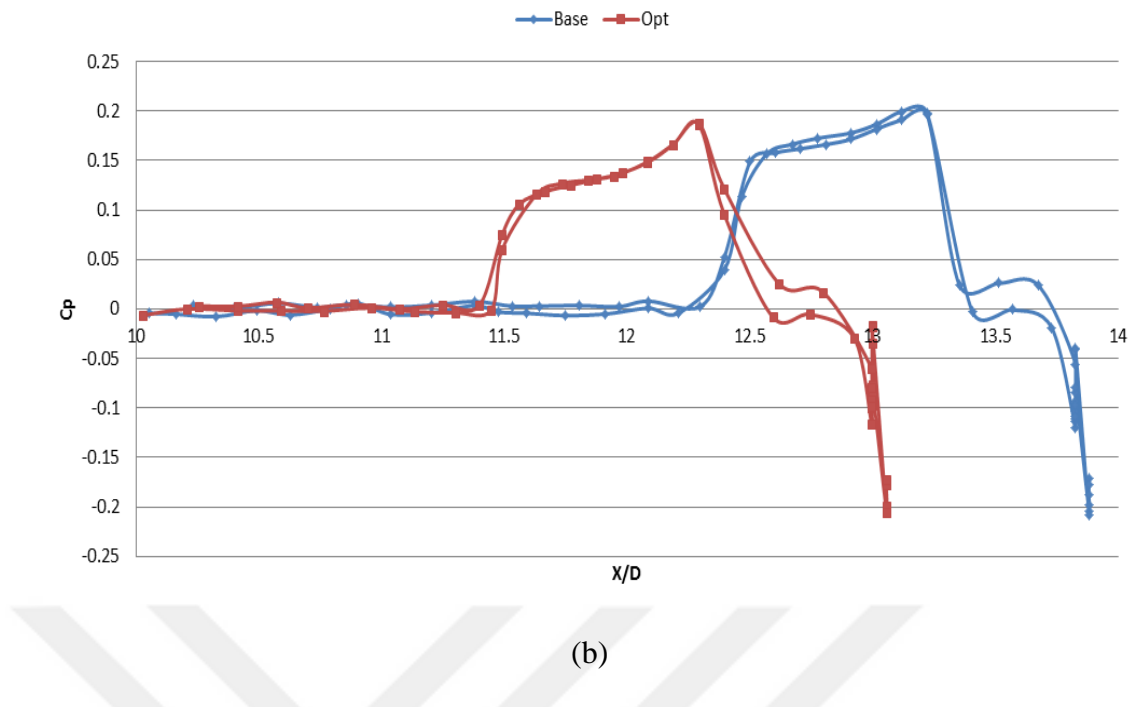


(c)

Figure 4.15 Pressure coefficient distribution for base and optimum missile body at 4° AoA (a: 1.4 Ma, b: 2 Ma, c: 2.5 Ma)



(a)



(c)

Figure 4.16 Pressure coefficient distribution for base and optimum missile fin at 4° AoA (a: 1.4 Ma, b: 2 Ma, c: 2.5 Ma)

CHAPTER V

CONCLUSION

In this thesis, missile aerodynamic analysis with CFD solution using different turbulence models and missile aerodynamic shape optimization were carried out. A missile geometry model was referenced from previous study which was implemented experimental study by Vidanović et al. (2017). The geometry of the missile was selected as N1G missile model. The beginning of the study, the missile geometry was drawn using Designmodeler and three dimensional (3-D) mesh that includes hexahedral and tetrahedral structural geometry was generated using ANSYS Mesh. CFD solution was then performed using SST $k-\omega$, Realizable $k-\epsilon$ and Spalart-Allmaras turbulence models at 1.4, 2, 2.5, 4 Mach numbers and 4° and 6° AoA. It was concluded that an experimental study and CFD solution were good agreement with each other. However, SST $k-\omega$ model gave more accurate results for same number of mesh elements when compared with Spalart-Allmaras and Realizable $k-\epsilon$ turbulence models since SST $k-\omega$ turbulence model provides superior solution performance for thin boundary layer, recirculation and separation. In order to show mesh independency, mesh was generated from course to finer mesh elements (100000 to 4.2 Million) to perform the three-dimensional CFD solution. However, the results of the CFD solutions showed negligible change between 2 million and 4.2 million mesh elements. In addition, lift to drag ratio was also calculated to show missile performance at high AoA. The ratio increased up to 12° AoA and after that, it decreased due to increases drag forces and separation of flow. In addition, pressure contours and streamlines were presented to show the effects of pressure changing on the missile body and separation of the flow at high AoA. It was concluded that low-pressure region is observed at 4° and 8° AoA to be larger than at high AoA around the rear of missile body. So, drag coefficient increased due to pressure differences between the nose and rear of missile. Moreover, drag coefficients increase more than lift coefficients at high AoA since the wake flow appears on missile body and fins.

Optimization step have been performing using DesignXplorer in ANSYS optimization tool which helps to find out the best geometry of the selected missile model. In optimization process, design variables were determined to perform optimization. The missile body and fin parameters need to be estimated in order to design optimum missile geometry. Lift and drag coefficients were considered as objective function for optimization process. Input and output parameters were collected to obtain design points. Multi-Objective Genetic Algorithm (MOGA) was used to optimize missile geometry. Nose, main body and tailfins were improved for each selected Mach numbers. Lift to drag ratio was calculated to observe how much improvement was achieved. Therefore, base and optimum missile geometry were compared each other. The results of the optimization solution problem was shown that lift to drag ratio increase 17.17 %, 16.05 %, and 11.89 % for Mach numbers 1.4, 2, 2.5, respectively. It was concluded that body radius is more effective to reduce the drag coefficients with respect to nose curve radius and nose front radius. In addition, fin thickness, fin root and tip chords lengths are more effective on the lift coefficient when compared with other design variables.

The results of the study can be applied to perform other missile models. SST $k-\omega$ turbulence model is given more accurate results at supersonic speeds. Moreover, multi-objective optimization problem can be solved by using modern computational fluid dynamics (CFD) optimization technique. CFD solution method and the optimization procedure can be applied to design or optimize different geometry. In addition, the aerodynamic modeling is integrated within optimization techniques. The optimum shapes of the missile in terms of aerodynamic performance were found.

5.1 Recommendation for the Future Work

In this study, aerodynamic shape optimization of missile was performed by using Genetic algorithm in ANSYS. This study may be extended to some hybrid algorithm in our code. It may be given more accurate results. Canard or wing can be mounted to improve lift to drag ratio and they can be optimized changing geometry and position. In addition, wing, canard and tailfin can be made from elastic materials to obtain more realistic results.

REFERENCES

- A. Inc., Ansys Fluent User's Guide, 2011.
- Abney, E. J., McDaniel, M. A. (2005). High angle of attack aerodynamic predictions using missile Datcom, *AIAA*, 5086.
- Ageev, N., Pavlenko, A. (2016). Minimization of body of revolution aerodynamic drag at supersonic speeds, *Aircraft Engineering and Aerospace Technology: An International Journal*, **88**, 246-256.
- Ahuja, V., Hartfield Jr, R. J. (2011). Aero-Propulsive Optimization of the Boeing-737 Wing-Engine Integrated Geometry using Smart Panel Approaches and Modified Potential Theory, *In 29th AIAA Applied Aerodynamics Conference*, 3805.
- AL-Doulaimi K. I., Jabur H. M. (2006). Prediction aerodynamic coefficients of missile using panel method, *Journal of Engineering*, **12**, 389-404.
- Anderson, J. D., Wendt, J. (1995). Computational fluid dynamics. New York: McGraw-Hill.
- Anderson, M. B., Burkhalter, J. E., Jenkins, R. M. (2000). Missile aerodynamic shape optimization using genetic algorithms, *Journal of Spacecraft and Rockets*, **37**, 663-669.
- ARSLAN, K. (2014). Aerodynamic optimization of missile external configurations. Doctoral dissertation, Middle East Technical University.
- Azab, M. B., Ollivier-Gooch, C. (2010). Higher Order Two Dimensional Aerodynamic Optimization Using Unstructured Grids and Adjoint Sensitivity Computations, *In 48th AIAA Aerospace sciences meeting 4-7Jan 2010*.
- Bak, K., M. (2010). Experimental investigation and computational fluid Dynamics analysis of missile with grid fin in subsonic flow, *International Journal of Engineering Science and Technology*, **2**, 6214-6220.

- Baysal, O., Eleshaky, M. E. (1992). Aerodynamic design optimization using sensitivity analysis and computational fluid dynamics. *AIAA journal*, **30**, 718-725.
- Bes, P. A. (2006). Numerical Investigation and Flow Interactions of a Mixedcompression Hypersonic Inlet. Bachelor of Science, University of Miami.
- Burgreen, G. W., Baysal, O. (1996). Three-dimensional aerodynamic shape optimization using discrete sensitivity analysis. *AIAA journal*, **34**, 1761-1770.
- Chakravarthy, S., Akdag, V. (2015) Importance of accuracy in CFD simulations, *6th BETA CAE International Conference. Greece*.
- Champigny, P., d'Espiney, P., Bredif, M., Broussard, H., Gillyboeuf, J. P. (2003). Numerical simulation of vortex flows around missile configurations. Nato Research And Technology Organization Neuilly-Sur-Seine (France).
- Chen, S., Lyu, Z., Kenway, G. K., Martins, J. R. (2015). Aerodynamic Shape Optimization of Common Research Model Wing–Body–Tail Configuration, *Journal of Aircraft*, **53**, 276-293.
- Colonna, M. R., Palacios, F., Economon, T., Lonkar, A. K., Alonso, J. J. (2013). An Adjoint-Based Aerodynamic Shape Optimization Methodology for Fairing Systems, *AIAA Paper*, **2649**, 24-27.
- Cronvich, L.L. (1983). Missile Aerodynamics. *Johns Hopkins APL technical Digest*. **4**, 175-186.
- Cui, K., Yang, G. W. (2010). Shape optimization for hypersonic arc-wing missiles, *Journal of Spacecraft and Rockets*, **47**, 694-700.
- Da, R., (2010). Computational Intelligence in Complex Decision Making Systems, *Springer Science & Business Media*, **2**.
- Deck, S., Duveau, P., d'Espiney, P., Guillen, P. (2002). Development and application of Spalart–Allmaras one equation turbulence model to three-dimensional supersonic complex configurations, *Aerospace Science and Technology*, **6**, 171-183.
- DeSpirito, J., Vaughn Jr, M. E., Washington, W. D. (2003). Subsonic flow CFD investigation of canard-controlled missile with planar and grid fins, *In 41 st AIAA*

Aerospace Sciences Meeting & Exhibit, Reno, NV.

DeSpirito, J., Vaughn, E. M., Washington, W. D. (2004). Numerical Investigation of Aerodynamics of Canard-Controlled Missile Using Planar and Grid Tail Fins, Part II: Subsonic and Transonic Flow, *Army Research Laboratory*

Doyle, S., Alston, K., Winter, T. (2011). Developing the aerodynamics module for the integrated multidisciplinary optimization object system, *In 49th AIAA Aerospace Sciences Meeting*, 0008.

Duygu, A. (2014). Bulaşık Makinesi Tasarımı ve CFD analizi. Sakarya University. Undergraduate Thesis.

Dyer, J. D., Hartfield, R. J., Dozier, G. V., Burkhalter, J. E. (2012). Aerospace design optimization using a steady state real-coded genetic algorithm, *Applied Mathematics and Computation*, **218**, 4710-4730.

Dillenius, M. F., Lesieutre, D. J., Hegedus, M. C., Perkins Jr, S. C., Love, J. F., Lesieutre, T. O. (1999). Engineering-, Intermediate-, and High-Level Aerodynamic Prediction Methods and Applications. *Journal of Spacecraft and Rockets*, 36(5), 609-620.

Eberhart, R., Kennedy, J. (1995). A new optimizer using particle swarm theory, In Micro Machine and Human Science, *Proceedings of the Sixth International Symposium*, 39-43.

El-Mahdy, L. A., Ahmed, M. Y. M., Mahmoud, O. K., Abdel-Hameed, O. E. (2016). Experimental computation and empirical evaluation of supersonic missile aerodynamic coefficient, *Proceeding of the 17th Int. AMME Conference*, 28-42.

Feyzioğlu, E. (2014). Roll Characteristics And Shape Optimization of the Free-to-Rotate Tail-Fins on A Canard-Controlled Missile. Doctoral Dissertation, Middle East Technical University.

Fleeman, E. L. (2001) Tactical Missile Design, *American Institute of Aeronautics and Astronautics*. 1801 Alexander Bell Drive, Reston, VA 20191, USA.

Foster, N. F., Dulikravich, G. S. (1997). Three-dimensional aerodynamic shape

optimization using genetic and gradient search algorithms, *Journal of Spacecraft and Rockets*, **34**, 36-42.

Franzuebbers, B. C. (2013). Drag coefficients of inclined hollow cylinders: RANS versus LES. Worcester Polytechnic Institute.

Gaiddon, A., Knight, D. D. (2002). Aerodynamic optimization of the aeropropulsive system of a ramjet powered missile, *In Proceedings of the 2002 Symposium on Multidisciplinary Analysis and Optimization*, 4-6.

Giannakoglou, K. C. (2002). Design of optimal aerodynamic shapes using stochastic optimization methods and computational intelligence. *Progress in Aerospace Sciences*, **38**, 43-76.

Goldberg, D. E. (1989). Genetic algorithms in search, optimization, and machine learning. Reading MA: Addison-Wesley.

Guy, Y., Morrow, J. A., McLaughlin, T. E. (1999). The effects of canard shape on the aerodynamic characteristics of a generic missile configuration, *AIAA Paper 99*, 4256.

Gülay, E., Akgül, A., Isaković, J., Mandić, S. (2011). Computational Fluid Dynamics and Experimental Investigation of Wrap-Around-Fins Missile Rolling Moment, *Scientific Technical Review*, **61**, 8-15.

Gültekin, G. K., Ögücü, M. O., Sayginer, E., Saranh, A. (2012). A genetic algorithm based solution to constrained component placement of a mobile robot, *In 2012 International Symposium on Innovations in Intelligent Systems and Applications*, 1-6.

Güzelbey, İ. H., Şumnu A., Doğru M. H. (2018) Importance of Mesh Accuracy on Aerodynamic of Missile. 3rd International Mediterranean Science and Engineering Congress (IMSEC 2018) October 24-26, 2018, Adana/Turkey.

Hassan, R., Cohanım, B., De Weck, O., Venter, G. (2005). A comparison of particle swarm optimization and the genetic algorithm, *In 46th AIAA/ASME/ASCE/AHS/ASC structures, structural dynamics and materials conference*, 1897.

He, Y., Agarwal, R. K. (2014). Shape optimization of NREL S809 airfoil for wind turbine blades using a multi-objective genetic algorithm, *International Journal of*

Aerospace Engineering.

Hekmat, M. H., Mirzaei, M., Izadpanah, E. (2009). Constrained and non-constrained aerodynamic optimization using the adjoint equations approach. *Journal of mechanical science and technology*, **23**, 2479-2491.

Holland, J. (1975). Adaptation in natural and artificial systems: an introductory analysis with application to biology, *Control and artificial intelligence*.

Honkanen, T., Tuisku, T., Pankkonen, A. (2011). CFD simulations and wind tunnel experiments of a generic split-canard air-to-air missile at high angles of attack in turbulent subsonic flow, *In AIAA Atmospheric Flight Mechanics Conference*, 6335.

Missile Control System. Aerospaceweb.org contributors. <http://www.aerospaceweb.org>, 11.07.2018.

Hu, R., Jameson, A., Wang, Q. (2012). Adjoint-based aerodynamic optimization of supersonic biplane airfoils, *Journal of Aircraft*, **49**, 802-814.

Hutchison, M. G., Unger, E. R., Mason, W. H., Grossman, B., Haftka, R. T. (1994). Variable-complexity aerodynamic optimization of a high-speed civil transport wing, *Journal of Aircraft*, **31**, 110-116.

Jones, K. O. (2005). Comparison of genetic algorithm and particle swarm optimization, *In Proceedings of the International Conference on Computer Systems and Technologies*, 1-6.

Kachitvichyanukul, V. (2012). Comparison of three evolutionary algorithms: GA, PSO, and DE, *Industrial Engineering and Management Systems*, **11**, 215-223.

Kaleeswaran, B., Kumar, S. R. (2013). An Aerodynamic Optimization of Supersonic Flow Over The Nose Section of Missiles, *In International Journal of Engineering Research and Technology*, 2, ESRSA Publications.

Kallrath, J., Milone, E. F., Wilson, R. E. (2009). Eclipsing binary stars: modeling and analysis. 120, New York: Springer.

Khalghani, A., Pasandideh-Fard, M., Djavarehshkian, M. H. (2016). Aerodynamic shape study of supersonic surface to surface missiles with continuous flexible

nose, *Journal of Mechanical Science and Technology*, **30**, 3183-3192.

Khanolkar, N. P., Bhushan, B., Siddharth, M., Borrison, E., Sinha, J. (2017). Analysis of aerodynamic characteristics of a missile configuration, *In 2017 International Conference on Infocom Technologies and Unmanned Systems (Trends and Future Directions) (ICTUS)*, 877-882. IEEE.

Khot, M. T. S. (2012). CFD Based Airfoil Shape Optimization For Aerodynamic Drag Reduction. Doctoral dissertation.

Konak, A., Coit, D. W., Smith, A. E. (2006). Multi-objective optimization using genetic algorithms: A tutorial, *Reliability Engineering & System Safety*, **91**, 992-1007.

Körpe, D. S., Kanat, Ö. Ö. (2019). Aerodynamic Optimization of a UAV Wing subject to Weight, Geometric, Root Bending Moment, and Performance Constraints, *International Journal of Aerospace Engineering*.

Kulkarni, M. N. K., Patekar, M. S., Bhoskar, M. T., Kulkarni, M. O., Kakandikar, G. M., Nandedkar, V. M. (2015). Particle swarm optimization applications to mechanical engineering-A review. *Materials Today: Proceedings*, **2**, 2631-2639.

Lacau, R.G. (1988). A survey of missile aerodynamics, *Nielsen Engineering & Research*.

Le Pape, A., Beaumier, P. (2005). Numerical optimization of helicopter rotor aerodynamic performance in hover, *Aerospace science and technology*, **9**, 191-201.

Lee, D. S., Gonzalez, L. F., Srinivas, K., Periaux, J. (2008). Robust evolutionary algorithms for UAV/UCAV aerodynamic and RCS design optimization, *Computers & Fluids*, **37**, 547-564.

Lesieutre, D. J., Quijano, O. (2014). Studies of Vortex Interference Associated with Missile Configurations, *In Proceedings of the 52nd Aerospace Sciences Meeting, AIAA SciTech (AIAA 2014-0213)*, National Harbor, MD, USA, 13-17.

Lesieutre, D. J., Dillenius, M. F. E., Gjestvang, J. (2002). Application of MISDL/KDA aerodynamics prediction method to Penguin missile.

Lesieutre, D. J., Dillenius, M. F., Lesieutre, T. O. (1998). Multidisciplinary design

optimization of missile configurations and fin planforms for improved performance, *AIAA*, 98-4890,

Lesieutre, D. J., Love, J., Dillenius, M., Blair Jr, A. B. (2002). Recent applications and improvements to the engineering-level aerodynamic prediction software misl3, *In AIAA Aerospace Sciences Meeting and Exhibit, 40th, Reno.*

LeVeque, R. J. (2002). Finite volume methods for hyperbolic problems, **31**, Cambridge university press.

Li, C. C., Tai, C. S., Lai, C. C., Fu, S. M., Tsai, Y. C. (2014). Study of the aerodynamic characteristic and flight trajectories in a tail fin-stabilized projectile with different shapes, *Procedia Engineering*, **79**, 108-113.

López, D., Domínguez, D., Gonzalo, J. (2014). Optimization of air-ejected rocket/missile geometries under validated supersonic flow field simulations, *In 10th International Conference on Mathematical Problems in Engineering, Aerospace and Sciences*, **1637**, 600-606 AIP Publishing.

Mader, C. A., Martins, J. R. (2014). Computing Stability Derivatives and Their Gradients for Aerodynamic Shape Optimization, *AIAA Journal*, **52**, 2533-2546.

Maurice, A. F. (2009). Aerodynamic performance predictions of a SA-2 Missile using Missile Datcom. Naval Postgraduate School Monterey Ca.

McDaniel, M. A., Evans, C., Lesieutre, D. J. (2010). The effect of tail fin parameters on the induced roll of a canard-controlled missile, *In 28th AIAA Applied Aerodynamics Conference*, 4226.

Menter, F. R. (1994). Two-equation eddy-viscosity turbulence models for engineering applications, *AIAA journal*, **32**, 1598-1605.

Misaghian, B., Soltani, M. R., Karimi, A. (2007). Fin shape optimization to minimize aerodynamic heating using genetic algorithm, *HEFAT*.

Morris, A. M., Allen, C. B., Rendall, T. C. S. (2009). Aerodynamic shape optimization of a modern transport wing using only planform variations, *Proceedings of the Institution of Mechanical Engineers, Part G: Journal of Aerospace Engineering*, **223**,

843-851.

Mortazavi, A., Toğan, V. (2016). Simultaneous size, shape, and topology optimization of truss structures using integrated particle swarm optimizer, *Structural and Multidisciplinary Optimization*, **54**, 715-736.

Muñoz-Paniagua, J., García, J., Crespo, A. (2014). Genetically aerodynamic optimization of the nose shape of a high-speed train entering a tunnel, *Journal of Wind Engineering and Industrial Aerodynamics*, **130**, 48-61.

Nguyen, N. V., Tyan, M., Lee, J. W., Byun, Y. H. (2014). Investigations on Missile Configuration Aerodynamic Characteristics for Design Optimization. *Transactions of the Japan Society for Aeronautical and Space Sciences*, **57**, 210-218.

Nikbay, M., Öncü, L., Aysan, A. (2009). Multidisciplinary code coupling for analysis and optimization of aeroelastic systems, *Journal of Aircraft*, **46**, 1938-1944.

Nobahari, H., Nabavi, Y., Pourtakdoust, H. (2006). Aerodynamic Shape Optimization of Unguided Projectiles Using Ant Colony Optimization and Genetic Algorithm, *In 25TH International Congress of the Aeronautical Sciences*, Sharif University of Technology.

Ocokoljić, G. J., Rašuo, B. P., Bengin, A. Č. (2017). Aerodynamic shape optimization of guided missile based on wind tunnel testing and computational fluid dynamics simulation, *Thermal Science*, **21**.

Oktay, E., Alemdaroğlu, N., Tarhan, E., Champigny, P., d'Espiney, P. (2000). Unstructured Euler solutions for missile aerodynamics, *Aerospace science and technology*, **4**, 453-461.

Oktay, E., Merttopcuoglu, O., Sener, C., Ketenci, A., Akay, H. U. (2009). Grid Altyapısı Üzerine bir füzenin paralel şekil optimizasyonu, *1. Ulusal Yüksek Başarım ve Grid Konferansı, ODTÜ KKM, Ankara*.

Öztürk, M. Y. (2009). Multi-objective design optimization of rockets and missile, Master's Thesis, Middle East Technical University, Ankara.

Pankkonen, A. (2011). Method for rapid modelling of missile aerodynamics,

In Proceedings of the AIAA Atmospheric Flight Mechanics Conference.

Queipo, N. V., Haftka, R. T., Shyy, W., Goel, T., Vaidyanathan, R., Tucker, P. K. (2005). Surrogate-based analysis and optimization, *Progress in aerospace sciences*, **41**, 1-28.

Reuther, J., Alonso, J. J., Rimlinger, M. J., Jameson, A. (1999). Aerodynamic shape optimization of supersonic aircraft configurations via an adjoint formulation on distributed memory parallel computers, *Computers & fluids*, **28**, 675-700.

Riddle, D. B., Hartfield, R. J., Burkhalter, J. E., Jenkins, R. M. (2009). Genetic-algorithm optimization of liquid-propellant missile systems, *Journal of Spacecraft and Rockets*, **46**, 151-159.

Runduo, C., Xiaobing, Z. (2018). Multi-objective optimization of the aerodynamic shape of a long-range guided rocket. *Structural and Multidisciplinary Optimization*, **57**, 1779-1792.

Ryan, K. (2011). Trajectory optimization and aerodynamic modeling of long range morphing projectiles. Doctoral dissertation, University of Maryland, College Park.

Sahu, J. (2017). CFD simulations of a finned projectile with microflaps for flow control, *International Journal of Aerospace Engineering*.

Sahu, J., Heavey, K. (2009) Computations of Supersonic Flow over a Complex Elliptical Missile Configuration, *AIAA Paper*, 5714.

Schoene, T. (2011). Step-optimized particle swarm optimization. Doctoral dissertation, University of Saskatchewan Saskatoon.

Schoene, T., Ludwig, S. A., Spiteri, R. J. (2012). Step-optimized particle swarm optimization, *In 2012 IEEE Congress on Evolutionary Computation*, 1-9.

Shi, Y., Xu, M., Wang, Z. M. (2011). Integrated optimization of aerodynamic shape with trajectory for aircraft in conceptual design, *In Electronic and Mechanical Engineering and Information Technology (EMEIT)*, 3808-3811.

Shih, T. H., Liou, W. W., Shabbir, A., Yang, Z., Zhu, J. (1995). A new $k-\epsilon$ eddy viscosity model for high Reynolds number turbulent flows, *Computers & Fluids*, **24**,

227-238.

Silton, S. I. (2005). Navier-Stokes computations for a spinning projectile from subsonic to supersonic speeds, *Journal of Spacecraft and Rockets*, **42**, 223-231.

Smith, K. D. (2009). A Comparison of Two Inviscid Numerical Approaches to Modeling the Flow Field about a Supersonic Ballistic Object: The Method of Characteristics and a Finite Volume Euler Solution. Doctoral dissertation, Rensselaer Polytechnic Institute.

Sooy, T. J., Schmidt, R. Z. (2005). Aerodynamic predictions, comparisons, and validations using missile Datcom (97) and aeroprediction 98 (AP98), *Journal of spacecraft and rockets*, **42**, 257-265.

Spalart, P. R., Allmaras, S. R. (1992). A one-equation turbulence model for aerodynamic flows, *AIAA*, 92-0439.

Tahani, M., Masdari, M., Kazemi, M. (2017). Aerodynamic performance improvement of a canard control missile, *Aircraft Engineering and Aerospace Technology*, **89**, 871-878.

Tanı, Ç., Platin, B. E., Yazıcıoğlu, G. (2009). External configuration optimization of missiles in conceptual design, *AIAA Atmospheric Flight Mechanics Conference At: Chicago, IL, USA*

Taş, O., Başlamışli, U., Küçük, U. C. (2015). Computational study of high angle of attack aerodynamics at supersonic flight condition, *Ankara International Aerospace Conference*.

Teo, H. H. (2008). Aerodynamic predictions, comparisons, and validations using Missilelab and Missile Datcom (97). Naval Postgraduate School Monterey Ca.

Tianyuan, H., Xiongqing, Y. (2009). Aerodynamic/stealthy/structural multidisciplinary design optimization of unmanned combat air vehicle. *Chinese Journal of Aeronautics*, **22**, 380-386.

Usta, E., Arslan, K., Tuncer, İ. H. (2015). Aerodynamic design analysis of missile with strake configuration at supersonic Mach numbers, *8th Ankara International Aerospace*

Conference 10-12 September.

Versteeg H., Malalasekera W. (2007). Classification of fluid flow, *An Introduction to Computational Fluid Dynamic, The Finite Volume Method.* 33-35.

Vidanović, N., Rašuo, B., Damljanovic D. B., Vukovic D. S., Curcic D. S. (2014). Validation of the CFD code used for determination of aerodynamic characteristic of non-standard AGARD-B calibration model, *Thermal Science*, **18**, 1223-1233.

Vidanović, N., Rašuo, B., Kastratović, G., Maksimović, S., Čurčić, D., Samardžić, M. (2017). Aerodynamic–structural missile fin optimization, *Aerospace Science and Technology*, **65**, 26-45.

Vytla, V. V., Huang, P. G., Penmetsa, R. C. (2010). Multi objective aerodynamic shape optimization of high speed train nose using adaptive surrogate model, *In 28th AIAA Applied Aerodynamic Conference.*

Wei, Z., Meijian, S. (2013). Design optimization of aerodynamic shapes of a wing and its winglet using modified quantum-behaved particle swarm optimization algorithm, *Proceedings of the Institution of Mechanical Engineers, Part G: Journal of Aerospace Engineering*, **228**, 1638-1647.

Xia, C. C., Jiang, T. T., Chen, W. F. (2016). Particle Swarm Optimization of Aerodynamic Shapes With Nonuniform Shape Parameter–Based Radial Basis Function, *Journal of Aerospace Engineering*, **30**, 04016089.

Yamazaki, W., Matsushima, K., Nakahashi, K. (2008). Aerodynamic design optimization using the drag-decomposition method, *AIAA journal*, **46**, 1096-1106.

Yang, Y. R., Jung, S. K., Cho, T. H., Myong, R. S. (2012). Aerodynamic Shape Optimization System of a Canard-Controlled Missile Using Trajectory-Dependent Aerodynamic Coefficients, *Journal of Spacecraft and Rockets*, **49**, 243-249.

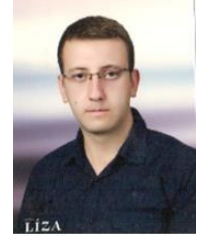
Zhang, M., Rizzi, A., Meng, P., Nangia, R., Amiree, R., Amoignon, O. (2012). Aerodynamic design considerations and shape optimization of flying wings in transonic flight, *In 12th AIAA Aviation Technology, Integration, and Operations (ATIO) Conference and 14th AIAA/ISSMO Multidisciplinary Analysis and*

Optimization Conference, 5402.

Zhang, W. D., Wang, Y. B., Liu, Y. (2013). Aerodynamic study of theater ballistic missile target, *Aerospace science and technology*, **24**, 221-225.



CURRICULUM VITAE (CV)



AHMET ŞUMNU

ahmetsumnu@gantep.edu.tr

GSM: 0506 409 206 61

University of Gaziantep, Faculty of Aeronautics and Aerospace, Aircraft and Aerospace Engineering Department, Gaziantep, Turkey 27310

Education

University of Gaziantep, TURKEY

Mechanical Engineering Doctor of Philosophy, Mechanic Division,
“*Aerodynamic Shape Optimization for Missile*” 2015–2020, GPA:
3.64/4.00

University of Gaziantep, TURKEY

Mechanical Engineering Master of Science, Mechanic Division,
“*Design and Analysis of the Stewart Platform*” 2013–2015, GPA:
3.67/4.00

University of Gaziantep, TURKEY

Mechanical Engineering, September 2008–June 2013, GPA:3.48/4.00

Experience

Research Assistant, University of Gaziantep, Faculty of Aeronautics and Aerospace, Aircraft and Aerospace Engineering Department, January 2014- Ongoing

Projects

Scientific Research Project Governing Unit (BAPYB),
Comprehensive Research Project

Project No: HUBF17.04, Füze için Aerodinamik Şekil Optimizasyonu, 2017-2019

Computer Skills

Microsoft Office Applications:	Excellent
AutoCAD:	Excellent
SOLIDWORKS:	Good
MATLAB:	Good
Ansys :	Good
C++:	Good

Foreign Language

English (Reading: Good, Speaking: Good, Writing: Good)

YÖKDİL: 81.25 (Spring 2017)

YDS: 67,5 (Spring 2017)

Research Topics

- Dynamics of Mechanical Systems
- Mechanics
- Fluid Mechanics
- Aerodynamics

Publications

International Journals (Sci)

- **Journal :** *Journal of Mechanical Science and Technology*
No/Edition: 31/1
Autors: Ahmet ŞUMNU, İbrahim Halil GÜZELBEY, Mehmet Veysel ÇAKIR
Simulation and PID control of a Stewart platform with linear motor. (2017)
- **Journal :** *International Journal of Aerospace Engineering*
Autors: Ahmet ŞUMNU, İbrahim Halil GÜZELBEY, Orkun ÖĞÜCÜ
Aerodynamic Shape Optimization of Missile Using Multi-Objective Genetic Algorithm (2020)

International Journals (TR directory)

- **Journal :** *Journal of Aeronautics and Space Technologies*
No/Edition: 11/2
Autors: İbrahim Halil GÜZELBEY, Müslüm ÖZKESİCİLER, Ahmet ŞUMNU
Design and Modelling of Nano Aerial Vehicle Hummingbird on Hover Flight (2018)

International Scientific Meetings

- 2nd International Conference on Advances in Mechanical Engineering
İstanbul,(ICAME' 16) May 10-13
Autors: Ahmet ŞUMNU, İbrahim Halil GÜZELBEY, Mehmet Veysel ÇAKIR
Analysis and PID Control of the Stewart Platform

- 2nd International Conference on Advances in Mechanical Engineering
İstanbul,(ICAME' 16) May 10-13
Autors: Edip ÖZTÜRK, İbrahim Halil GÜZELBEY, Ahmet ŞUMNU
Simulation of Non-Linear Computed Torque Control on Simulink for Two
Link Scara Type Manipulator
- 3rd International Mediterranean Science and Engineering Congress (IMSEC
2018) October 24-26, 2018, Adana/Turkey
Autors: İbrahim Halil GÜZELBEY, Ahmet ŞUMNU, Mehmet Hanifi
DOĞRU
Importance of Mesh Accuracy on Aerodynamic of Missile
- International Conference on Technology, Engineering and Science
(ICONTES' 18) October 26-29, Antalya/Turkey
Autors: İbrahim Halil GÜZELBEY,Ahmet ŞUMNU, Mehmet Hanifi
DOĞRU
A Review of Aerodynamic Shape Optimization for a Missile